Mapping developmental dynamics of autism spectrum disorder mouse models at single-cell resolution

by

Lena A. Schwarz

April, 2025

A thesis submitted to the
Graduate School
of the
Institute of Science and Technology Austria
in partial fulfillment of the requirements
for the degree of
Doctor of Philosophy

Committee in charge:
Tim Vogels, Chair
Gaia Novarino
Johann Danzl
Fiona Francis



The thesis of Lena A. Schwarz, titled *"Mapping developmental dynamics of autism spectrum disorder mouse models at single-cell resolution"* is approved by:

Supervisor: Gaia Novarino, ISTA, Klosterneuburg, Austria

Signature: _____

Committee Member: Johann Danzl, ISTA, Klosterneuburg, Austria

Signature: _____

Committee Member: Fiona Francis, Institut du Fer à Moulin – IFM, Paris, France

Signature: _____

Defense Chair: Tim Vogels, ISTA, Klosterneuburg, Austria

Signature: _____

Signed page is on file

© by Lena A. Schwarz, April 2025

[CC BY 4.0 The copyright of this thesis rests with the author. Unless otherwise indicated, its contents are licensed under a Creative Commons Attribution 4.0 International License. Under this license, you may copy and redistribute the material in any medium or format. You may also create and distribute modified versions of the work. This is on the condition that you credit the author.]

ISTA Thesis, ISSN: 2663-337X

I hereby declare that this thesis is my own work and that it does not contain other people's work without this being so stated; this thesis does not contain my previous work without this being stated, and the bibliography contains all the literature that I used in writing the dissertation.

I accept full responsibility for the content and factual accuracy of this work, including the data and their analysis and presentation, and the text and citation of other work.

I declare that this is a true copy of my thesis, including any final revisions, as approved by my thesis committee, and that this thesis has not been submitted for a higher degree to any other university or institution.

I certify that any republication of materials presented in this thesis has been approved by the relevant publishers and co-authors.

Signature: _____

Lena A. Schwarz

April, 2025

Signed page is on file

Abstract

Numerous studies have revealed a wide range of genes associated with autism spectrum disorder (ASD), raising critical questions about how mutations across different genes lead to similar clinical presentations. Yet, specific molecular mechanisms underlying most ASD cases remain elusive. Notably, ASD is diagnosed four times more frequently in males than in females, highlighting a substantial sex disparity. This male predominance is among the most recognized but least understood characteristics of the disorder. Thus, uncovering molecular mechanisms involved is crucial for exploring both shared and distinct aspects of ASD.

We utilized single-nucleus multi-omics sequencing to explore these unresolved questions, enabling us to investigate changes in gene expression and chromatin accessibility concurrently. In the present work, we analyzed and compared 251 samples collected from eleven different monogenic mouse models of ASD, incorporating both sexes and two brain regions. Samples span three primary developmental stages, which include prenatal, early postnatal, and juvenile brain development. This comprehensive dataset allowed us to map functional mechanisms specific to cell states, sex, and developmental periods.

We discovered that ASD mutations commonly delay the progression of radial glial cells, temporarily affecting the neural lineage specification. The most notable gene expression changes occurred perinatally, mainly affecting excitatory and inhibitory neurons. These alterations involved a downregulation of genes related to synapses and ion channels, indicating possible homeostatic adaptations. While there were several common molecular changes across all models, each mutant also displayed unique states.
Throughout the perinatal phase, numerous processes of cortical regulation and refinement take place. At this stage, several ASD risk genes exhibit a common set of differentially expressed genes, converging on a subclass of dysregulated mechanisms. However, as cortical development progresses, these shared processes start to diverge. This suggests that the period around P4 represents a critical time window for many converging molecular processes, marking it as the most impacted stage.

Importantly, our study highlighted sex-specific gene expression alterations, with females often showing broader dysregulations and larger effect sizes compared to males.
In contrast to the cerebral cortex, the cerebellum showed fewer gene expression changes across most ASD mutant models, with the exception of one mutant that showed consistent alterations in both brain regions.

Overall, our findings provide a thorough view of the cellular and molecular dynamics in different ASD models, highlighting both common and unique features across different genetic backgrounds. By exploring multiple genetic forms of ASD, we could demonstrate the dynamic nature of ASD-related changes in the brain and emphasize the importance of accounting for sex-dependent factors. In conclusion, this work serves as a valuable multi-omics resource, providing a foundation for future investigations.

Acknowledgments

The work presented in this doctoral thesis was performed at the Institute of Science and Technology (ISTA) and financially supported by a European Research Council (ERC) Consolidator Grant (PR1028ERC02), by SFARI (PR1028SIM02) and by the Austrian Science Fund (FWF) to Gaia Novarino (PE1028W1232). I am very thankful to the Doctoral Program “Molecular Drug Targets” (MolTag) for offering me financial support to perform essential experiments during my PhD studies and to participate in international conferences and courses.

I am very grateful to my supervisor, Gaia Novarino, for supporting me throughout my PhD and being a guiding hand whenever needed. She taught me how to think critically about science and has helped me grow as a scientist and person. I am thankful that Gaia entrusted me with such a huge, incredible project - even when I did not trust my own capabilities. Thank you for supporting me and sharing as much interest and enthusiasm for this project as I do.
Further, I would like to express my gratitude to Fiona Francis and Johann Danzl, my external and internal thesis committee members, for their interest in this project, their feedback, and for taking the time to read and evaluate my PhD thesis.

Many people have contributed to this work, through their collaborative work, sharing data, and supporting me over the last few years.
Specifically, I would like to thank all the scientists and collaborators who have significantly contributed to this project: Bárbara Oliveira, Bernadette Basilico, Gintarė Sendžikaitė, Satish Arcot Jayaram, Peter Koppensteiner, Igor Adameyko, and Christoph Bock. Special thanks go to all the bioinformaticians involved, who did not shy away from analyzing the wealth of my data: Christoph Dotter, Christoph Büschl, Sergey Isaev, and Daniel Malzl. I would also like to especially thank Sabrina Ladstätter and Matteo Barel for their great effort in supporting me in the experiments of this work. In addition, I would like to thank the Imaging and Optics Facility at ISTA for data analysis and technical support. Further, I would like to acknowledge the Biomedical Sequencing Facility at CeMM for assistance with next-generation sequencing. Many thanks also to the team of the Preclinical Facility, especially Angela Stichelberger, Sophie Liegenfeld, Satish Arcot Jayaram, Claudia Gold, and Michael Schunn.

I am beyond grateful for all my present and past colleagues I had the chance to work with. Thank you for all your great input, support, teamwork, and shared laughter over the last few years. Especially, I would like to thank Anna and Viktor for their great technical support.
Special thanks go to all my colleagues in and outside the lab who became close friends over the years, especially Barbara, Bernadette, Jasmin, Lisa, Nathalie, and Verena. Thank you for your endless support and for always having an open ear and heart. My PhD would not have been the same without you.

I want to thank my parents and my family for their unwavering support, for being my personal cheerleaders and biggest fans. Thank you for having my back no matter what – even when deciding to become a crazy scientist. I would not be where I am now without you.
Last but by no means least, I want to thank my partner, Flo. You contributed more to this work than you can imagine. Thank you for being the greatest listener, my scientific sparring partner, and my personal first aider. You are my safe harbor. Thank you for your limitless support and love, for making me laugh, and for reminding me that those who give their best, can always hope for the best. You are the main reason I made it to this point. Thank you for always being there whenever I need you.

Lena
Vienna, Spring 2025

About the Author

Lena A. Schwarz obtained her BSc in Biomedicine and Biotechnology from the University of Veterinary Medicine Vienna in 2018. During her studies, she conducted research for her Bachelor's thesis at the Institute of Molecular Biotechnology (IMBA) under the supervision of Prof. Jürgen Knoblich. Her research focused on cerebral organoids and their potential to establish a vascularized network, which sparked her interest in neuroscience and led her to pursue a PhD at ISTA. In 2019, she joined the group of Prof. Gaia Novarino and became a member of the FWF-funded doctoral program "Molecular Drug Targets" (MolTag) in Vienna. Throughout her PhD studies, Lena focused on deciphering various aspects of convergence in autism spectrum disorders. Her research efforts culminated in a shared first-author publication in *Nature Communications* in 2021 and several co-authorships. Lena presented her research at both international and national conferences and earned the best poster award at the MolTag conference in 2023.

List of Publications

1. Jasmin Morandell*, **Lena A. Schwarz***, Bernadette Basilico, Saren Tasciyan, Georgi Dimchev, Armel Nicolas, Christoph Sommer, Caroline Kreuzinger, Christoph P. Dotter, Lisa S. Knaus, Zoe Dobler, Emanuele Cacci, Florian K. M. Schur, Johann G. Danzl and Gaia Novarino. ***"Cul3 regulates cytoskeleton protein homeostasis and cell migration during a critical window of brain development***". In: *Nature Communications*; 12, 3058, doi: 10.1038/s41467-021-23123-x. (2021)
   * shared first co-authorship

2. Lisa S. Knaus, Bernadette Basilico, Daniel Malzl, Maria Gerykova Bujalkova, Mateja Smogavec, **Lena A. Schwarz**, Sarah Gorkiewicz, Nicole Amberg, Florian M. Pauler, Christian Knittl-Frank, Marianna Tassinari, Nuno Maulide, Thomas Rülicke, Jörg Menche, Simon Hippenmeyer and Gaia Novarino. ***„Large neutral amino acid levels tune perinatal neuronal excitability and survival."*** In: *Cell*; 186, 1950–1967 April 27, 2023; doi: https://doi.org/10.1016/j.cell.2023.02.037

3. **Lena A. Schwarz,** Christoph P. Dotter, Sergey Isaev, Christoph Büschl, Sabrina Ladstätter, Bárbara Oliveira, Matteo Barel, Bernadette Basilico, Gintarė Sendžikaitė, Satish Arcot Jayaram, Igor Adameyko, Christoph Bock and Gaia Novarino. "***Developmental dynamics of the cortical cellular and molecular landscapes in autism spectrum disorder models."*** In: *Nature (in revision),* October 2024

Table of Contents

Abstract v
Acknowledgments vii
About the Author ix
List of Publications x
Table of Contents xi
List of Figures xiii
List of Extended Data Figures xiii
List of Supplementary Tables xiv
List of Abbreviations xiv
1 Introduction 1
1.1 Autism Spectrum Disorder 1
1.1.1 Etiology of ASD *1*
1.1.2 Environmental risk factors and their interaction with genetic components *3*
1.1.3 Skewed gender ratio among ASD patients *4*
1.1.3.1 Can the female protective effect explain gender differences in ASD? 5
1.1.3.2 Gender bias in diagnostic autism screening and women's behavioral adaptations 6
1.1.3.3 Impact of fetal testosterone exposure and X-chromosome association 8
1.2 Critical milestones for cortical development and implications for ASD 10
1.2.1 Neurogenesis and neuronal migration during embryonic corticogenesis *11*
1.2.2 Glial cells and their pivotal functions in the brain *13*
1.2.3 Cerebellar development – more than just the "little brain" *15*
1.2.4 Cortical malformations and disruptions in the context of ASD *17*
1.3 Convergent genes and causal pathways dysregulated in ASD 21
1.3.1 Synapse development, signaling, and plasticity: Implications for treatment *22*
1.3.2 Transcriptional regulation, epigenetic layers, and chromatin modifiers shape ASD *24*
1.3.3 Balancing protein synthesis and degradation in ASD *28*
1.4 Conclusion and open questions 31
2 Results 33
2.1 Single-nucleus multi-omics profiling of 251 mouse brain samples 33
2.2 ASD mutants show radial glia lineage progression defects 35
2.3 ASD mutants converge on altered gene expression at early postnatal stages 36
2.4 Common pathway disruptions in ASD mutant mice 40
2.5 Unique synaptic states and gene expression changes in ASD mouse models 42
2.6 Chromatin accessibility analysis reveals regulatory dynamics in ASD mutants 47
2.7 Sex-specific gene expression alterations in ASD mutants 48
2.8 ASD mutant effects in the cerebellum are restricted to Bckdk mutant mice 53
3 Discussion 57
4 Concluding remarks, limitations, and future directions 62
5 Methods 64

5.1 GENERATION OF EXPERIMENTAL MODELS 64
5.2 METHOD DETAILS 65
6 Supplementary Information 74
6.1 EXTENDED DATA FIGURES 74
6.2 SUPPLEMENTARY TABLES 90
References 94

List of Figures

Figure 1. Various etiologies contribute to the risk of ASD 2
Figure 2. Schematic model of the female protective effect 5
Figure 3. Hormonal fluctuations in females and males throughout life 8
Figure 4. Developmental milestones of brain development in mice and humans. ... 10
Figure 5. Cellular mechanisms driving cortical expansion and the formation of a six-layered structure 11
Figure 6. Inhibitory neuron migration to their designated cortical location 13
Figure 7. Scheme illustrating key processes of gliogenesis throughout mouse pre- and postnatal development 15
Figure 8. Conserved cerebellar architecture in humans and mice. 17
Figure 9. ASD risk genes impact synaptic signaling, transcription, chromatin regulation, and protein balancing. 21
Figure 10. Large-scale multi-omics profiling of high-risk ASD genes 38
Figure 11. Differential gene expression highlights stage-specific convergent mechanisms. 43
Figure 12. Distinct transcriptional profiles and unique biological processes identified in ASD mutant mice 46
Figure 13. Chromatin differential accessibility analysis in ASD mutants 49
Figure 14. Sex-specific effects across ASD mutants 52
Figure 15. Multi-omics sequencing of perinatal cerebellar tissue. 55

List of Extended Data Figures

Extended Data Figure 1. Expression of the selected ASD risk genes and sequencing quality statistics. 74
Extended Data Figure 2. Cell type classifications and distribution across individual time points. 76
Extended Data Figure 3. Analysis of the cellular composition and transcriptome correlations across mutants. 77
Extended Data Figure 4. Network of the biological processes affected in ASD mutant mice 79
Extended Data Figure 5. Biological processes impacted in excitatory cells and inhibitory neurons at postnatal stages. 81
Extended Data Figure 6. Biological processes affected in neural lineage cells at E14.5, and glial cells at postnatal stages. 83
Extended Data Figure 7. Gene Set Enrichment Analysis of individual cell types at P4. 85
Extended Data Figure 8. Differential gene expression analysis and quality control of female and male mice. 86

Extended Data Figure 9. Gene expression analysis of female and male ASD mutants, bulk RNA-seq results confirm sex-specific gene expression changes. 88
Extended Data Figure 10. Correlation of snRNA- and snATAC-seq. 89

List of Supplementary Tables

Supplementary Table 1. List of barcodes used for sequencing, oligonucleotides, and cell type references used (related to Methods section). 90

List of Abbreviations

AAV	Adeno-Associated Virus
ADHD	Attention-Deficit Hyperactivity Disorder
ASD	Autism Spectrum Disorder
ASO	Antisense Oligonucleotides
ATS	Antisense Transcript
BG	Bergmann Glia
CGE	Caudal Ganglionic Eminence
CMOs	Cholesterol-Modified Oligos
CNV	Copy Number Variation
CP	Cortical Plate
DARs	Differentially Accessible Regions
DEGs	Differentially Expressed Genes
DS	Dravet Syndrome
DUB	Deubiquitinating Enzyme
E	Embryonic Days
E/I imbalance	Excitation/ Inhibition Imbalance
E1	Ubiquitin-Activating Enzymes
E2	Ubiquitin-Conjugating Enzymes
E3	Ubiquitin Ligases
EGL	External Granule Layer
EMP	Erythromyeloid Progenitors
fbDEGs	Female-Biased DEGs
FCD	Focal Cortical Dysplasia
FDR	False Discovery Rate
FMR1	Fragile X Mental Retardation
FMRP	Fragile X Mental Retardation Protein
fsDEGs	Female-Specific DEGs
FXS	Fragile X Syndrome
GCL	Granule Cell Layer

GE	Ganglionic Eminence
GO	Gene Ontology
GoC	Golgi Cells
GrC	Granule Cells
GSEA	Gene Set Enrichment Analysis
GW	Gestational Week
HDAC3	Histone Deacetylase 3
HECT	Homologous To E6AP C-Terminus
ID	Intellectual Disability
IGF-1	Insulin-Like Growth Factor 1
IPC	Intermediate Progenitor Cell
iSVZ	Inner Subventricular Zone
KI	Knock-In
KO	Knock-Out
LGE	Lateral Ganglionic Eminence
MGE	Medial Ganglionic Eminence
ML	Molecular Layer
mTORC1	Mammalian Target Of Rapamycin Complex 1
MZ	Marginal Zone
NDD	Neurodevelopmental Disorder
NLGN	Neuroligin
NPC	Neural Progenitor Cell
NRXN	Neurexin
ODC	Oligodendrocyte
OPC	Oligodendrocyte Precursor Cell
oRGC	Outer Radial Glial Cell
oSVZ	Outer Subventricular Zone
PAF1	Polymerase-associated factor 1
PCL	Purkinje Cell Layer
PC	Purkinje Cell
PN	Projection Neuron
PV	Parvalbumin
RG	Radial Glial Cell
RNA Pol II	RNA Polymerase II
RTT	Rett Syndrome
snRNA-seq	Single-Nucleus RNA-Seq
SST	Somatostatin
SVZ	Subventricular Zone
TADA	Transmission And De Novo Association
TCA	Tricarboxylic Acid Cycle
TF	Transcription Factor
UBC	Unipolar Brush Cell
UPS	Ubiquitin-Proteasome System
VZ	Ventricular Zone

1 Introduction

1.1 Autism Spectrum Disorder

Autism spectrum disorder (ASD) is a heterogeneous group of neurodevelopmental disorders characterized by stereotyped behaviors along with difficulties in communication and social interaction. The prevalence of ASD has risen steadily over the years, affecting 1 in 44 children nowadays[1]. Individuals diagnosed with ASD display varying degrees of its core symptoms and often present comorbidities, including epilepsy, motor deficits, or intellectual disability (ID), broadening the phenotypic heterogeneity of the disorder even further[2].

Early signs of ASD emerge most often between 18 and 24 months of age; however, on average, the diagnosis tends to be after four years of age[3,4]. Diagnosing ASD is a challenging task because of the spectrum's diverse manifestations. Some individuals exhibit only mild symptoms, and frequently, children are diagnosed with related conditions such as ID, epilepsy, or attention-deficit hyperactivity disorder (ADHD) instead[5,6]. Remarkably, over the past decades, the prevalence of ASD has increased dramatically. While 20 years ago, 1 in 150 children received an ASD diagnosis, nowadays, the rate has risen to 1 in 36 children[1]. This steady rise may not be directly linked to etiological reasons but rather could be attributed to advancements in the early detection of ASD, increased public awareness of the disorder, and changes in reporting and diagnostic criteria[7,8].

1.1.1 Etiology of ASD

ASD is a highly heritable disorder, with genetic risk factors accounting for 65-70% of ASD heritability. 50% due to common variations and 15-25% due to *de novo* mutations, with the remaining risk factors still unidentified[9–11] (Fig. 1). Due to its large heritability, ASD is considered one of the most heritable among complex disorders and leads to a broad spectrum of phenotypes, now affecting more than 1% of the population[12]. In addition to genetic risk, environmental factors may also play a role in the etiology of ASD. Nutritional deficiencies, parental age, maternal diabetes, or chemicals are thought to contribute to the risk of ASD, among others. Some environmental factors could interact with genetic components and, in turn, might affect neurodevelopment through epigenetic mechanisms, which in turn may also lead to an increased risk of ASD[13] (Fig. 1).

The etiology of ASD is highly multifactorial and cannot be attributed to a single cause. Investigating the various causes is challenging due to the substantial genetic complexity, as well as the interactions and influences of environmental factors that occur during critical developmental periods.

Furthermore, understanding the specific time windows during which disruptions occur is crucial in determining the impact on neurodevelopmental processes. While prenatal insults are likely to impact cell cycle progression, neurogenesis, neuronal migration,

and positioning, later disturbances tend to affect neuronal differentiation, synaptogenesis, myelination, and neuronal network formation[14–16].

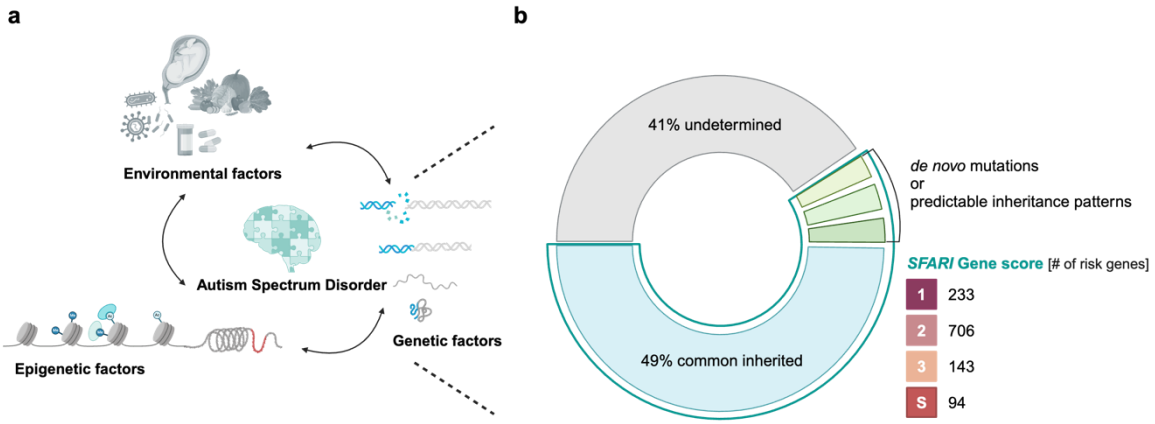


Figure 1: Various etiologies contribute to the risk of ASD (adapted from Gaugler et al.[10]).
a, Genetic factors are the primary factor contributing to the risk of ASD. Similarly, environmental and epigenetic components can have an impact. **b**, Genetic risks comprise around 50% common variations and 15-20% due to *de novo* mutations, with the remaining risk factors still unidentified. To date, over 1000 ASD risk genes have been identified based on their link to ASD. They can be categorized in "Category 1" showing high confidence, "Category 2" being strong candidate risk genes, "Category 3" having suggestive evidence, and "Syndromic (S)" genes (Version Q1 2024).

Rapid methodological and technological advances in genomics underscored a strong genetic component of ASD by identifying a large number of causative mutations in recent years[17–20]. Currently, hundreds of genes encoding proteins belonging to a multitude of functional classes have been associated with ASD. The SFARI Gene database* compiles various types of genetic data and organizes them into distinct categories. The classification into specific sub-categories is based on the evidence linking genes to ASD, with each gene assigned a score ranging from 1 (highest confidence) to 3 (suggestive evidence)[21]. The wide range and diversity of genes impacted by *de novo* mutations in ASD suggests that a broad array of biological functions is involved in the disorder's pathology.
In fact, this genetic variety raises the question of how aberrations in these diverse molecular pathways result in the same core set of symptoms. It has become clear that a multitude of risk genes control different neurodevelopmental processes. Accordingly, genetic mutations impacting balanced cellular programs of neural cell proliferation, differentiation, and migration have all been implicated in ASD[22,23]. Additionally, mutations in ASD risk genes affect molecular systems, including synaptic functioning, chromatin remodeling, or protein homeostasis[15].

* https://gene.sfari.org/ [Version used: Q1 2024]

1.1.2 Environmental risk factors and their interaction with genetic components

Environmental exposures are considered as risk factors for ASD, with several exogenous agents linked to an increased ASD risk. For example, advanced parental age is associated with higher autism rates, suggesting that children of older parents are more likely to develop ASD[24–27]. While parental age per se can be considered an environmental risk factor, it also interacts with and influences genetic risk substantially. Several studies evaluating the rate of *de novo* mutations and their relationship with parental age have shown that mutation rates increase with the age of either parent[24–29]. Notably, the paternal background has a more substantial effect on mutation rates than maternal age, with higher maternal age increasing the risk by 41% and a higher paternal rate corresponding to a 55% increased risk[24].
Commonly suggested mechanisms for the elevated risk associated with higher paternal age highlight that men undergo more germline cell divisions than women, continuing throughout adulthood. Furthermore, this difference grows as men age, which provides a plausible explanation for the observed sex differences and the effect of paternal age[40]. This implies that the older the father, the greater the number of potential mutations passed on through sperm, thereby increasing the risk for neurodevelopmental disorders such as ASD.

While major advances have been made in identifying new ASD-related genes through detecting rare *de novo* mutations from exome sequencing studies[25,30,31], the heterogeneity of identified risk genes is substantial and further complicated by their interactions with environmental risk factors. Another layer of complexity in ASD risk arises from the interplay between genetic and environmental influences, which result in epigenetic modifications that are not apparent in the DNA sequence alone.
Epigenetic modifications, such as methylation, acetylation, and phosphorylation, alter the conformational arrangement of nuclear structures, adding epigenetic marks on DNA or histones, thereby influencing intracellular activities. For example, changes in chromatin structure or the modulation of gene expression are direct consequences of epigenetic modifications[32–34]. As a result, the role of epigenetic regulation in ASD has received increased attention in recent years[35–39].
Many genes linked to ASD are involved in chromatin remodeling and transcriptional regulation; among many others, *ADNP, CHD8, MECP2*, and *KMT5B* are strongly associated with and often studied in ASD (for further information, refer to **1.3.2**)[30,40,41]. Here, epigenetic modifications of a gene can trigger abnormal transcription or translation, leading to altered activity of its encoded protein, which may potentially affect the function of all downstream genes it regulates.

Altogether, significant progress has been made in understanding ASD etiologies, particularly in the complex aspects of autism genetics and ASD-related pathways. However, deciphering and linking the various causes and their roles in the disorder's pathophysiology remains challenging due to the extensive number of genetic risk factors, potential environmental influences, and their dynamic interplay.

1.1.3 Skewed gender ratio among ASD patients

Males are diagnosed with ASD four times more frequently than females, resulting in a notable sex disparity (4:1 ratio)[42–45]. The male predominance in ASD is one of the most recognized yet least understood aspects of this condition. Various hypotheses have been proposed to explain this diagnostic imbalance, however definitive evidence clarifying the higher susceptibility of males remains elusive.

Among these hypotheses, the “female protective effect” is frequently discussed. This theory suggests that multiple genetic factors contribute to the susceptibility to developing ASD, however, females require a higher threshold of genetic liability or more penetrant mutations to manifest the disorder compared to males[46–48]. Diagnostic biases are another substantial factor contributing to the ASD sex disparity, which may stem from differing clinical or phenotypical presentations of autistic traits between females and males. They could also be related to the tendency of women to ‘camouflage’ or the ability to conceal their autistic behaviors to blend in more effectively according to societal norms[49–52]. Another prominent hypothesis addressing the observed gender bias suggests the involvement of fetal testosterone exposure, whereby higher levels of testosterone during fetal development may influence the emergence of ASD traits[53,54]. Lastly, susceptibility factors encoded on the X or Y chromosomes may impact males differently than females due to males having only one X chromosome. This results in males being more frequently affected when an X-linked gene is mutated, as there is not another X chromosome to compensate for effects[55].

1.1.3.1 Can the female protective effect explain gender differences in ASD?

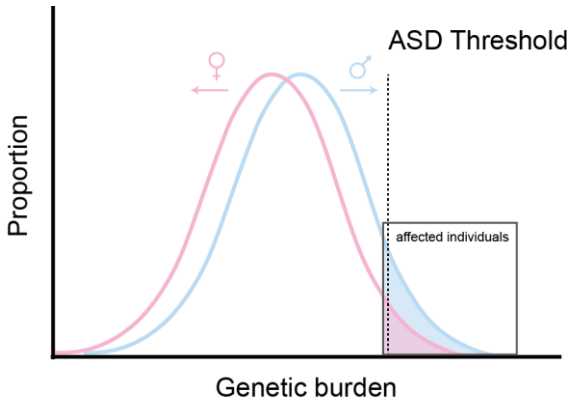


Figure 2: Schematic model of the female protective effect (adapted from Dougherty et al.[59]).
Considering that both sexes have the same threshold for an ASD diagnosis (dashed line), the genetic burden in males is shifted closer to this threshold. Consequently, more males exceed the threshold, resulting in a skewed gender ratio.

Females are considered 'protected' from autistic traits relative to males. It is suggested that females need a higher level of genetic risk to exhibit the same degree of autistic characteristics (Fig. 2)[46–48,50]. Compelling evidence supporting this theory stems from family and twin studies[56–58]. Recent research suggests that siblings of autistic girls are more likely to receive an ASD diagnosis than siblings of autistic boys. This may imply that females require a higher familial etiologic load to develop ASD as compared to males. Alternatively, it could indicate that males are more prone to exhibit autistic traits and need fewer familial risk factors to reach a similar threshold of impairment[56,57]. Interestingly, in families showing a history of the disorder, female family members exhibit a lower risk compared to their male familial counterparts. Recurrence rates are also significantly lower among later-born girls and female co-twins in such families, suggesting a potential protective effect despite the genetic predisposition for ASD[56]. Additionally, it was demonstrated that family members of female probands with autistic impairments tend to have higher autistic trait scores compared to the family members of male probands with a similar level of impairment. This suggests that females require a greater familial etiological load to manifest observable autistic impairments[57]. In that regard, females require a higher mutational burden to exhibit clinical manifestations of ASD compared to males. Intriguingly, females are found to carry more rare mutations and are three times more likely to carry copy number variations (CNVs) that comprise risk genes for neurodevelopmental disorders (NDDs)[48,58]. Similarly, mothers tend to have an increased mutational burden compared to fathers, suggesting that inherited mutations are more likely to be passed down from unaffected mothers than from fathers[58].

A recent study[48] utilized the Transmission and *de novo* association (TADA) model[59], which integrates data of *de novo* mutations, inherited variants, and variants identified in ASD cases and controls. Here, ASD risk genes were categorized according to their sex-specific expression, i.e., genes with *de novo* mutations found exclusively in either females or males and those present in both. Interestingly, gene co-expression analysis across multiple brain regions revealed that all three gene subclasses (i.e.: *de novo* mutations, inherited variants, and variants identified in ASD cases and controls) were more frequently co-expressed in female brain regions during prenatal development,

even though the co-expressed genes showed higher variabilities in standard deviations across most of the analyzed brain regions in females.
These findings suggest that compensatory mechanisms may explain the lower prevalence of ASD in females. Specifically, mutations in ASD candidate genes could be counterbalanced by a greater number of co-expressed genes in females during critical developmental stages. This compensation may, therefore, contribute to the reduced incidence of ASD observed in females.

The complex interplay of genetic factors that affect the manifestation of ASD differently in females and males is still in its early stages of thorough understanding, and many open questions remain to be answered.

1.1.3.2 Gender bias in diagnostic autism screening and women's behavioral adaptations

While boys are diagnosed with ASD four times more frequently than girls, this sex disparity might not accurately reflect the disorder's actual prevalence. The skewed male-to-female ratio could potentially be a consequence of mis- or underdiagnosing females. In fact, the sex differences in ASD prevalence could arise from phenotypic or symptomatic divergences between females and males, potentially leading to a diagnostic bias that favors identifying more males with the condition. One fundamental issue with current diagnostic criteria is that behavioral characterizations are based on conceptions of autistic behaviors that have been developed mainly on male behaviors[60,61]. As a result, current diagnostic assessments of autistic females often focus on areas where symptoms overlap with those of males. Consequently, females who do not display male-characteristic symptoms are more likely to be overlooked[62]. Additionally, it has been noted that the clinical presentation of females with ASD differs from that of males, including variations in core symptoms and cognitive and behavioral outcomes. While autistic females exhibit greater social interaction and communication skills[63,64], their intellectual performance is reported to be worse[65,66]. On the other hand, males are reported to show more severe communication impairments and repetitive, stereotyped behaviors[67–69]. Intriguingly, autistic females without comorbid intellectual disability tend to perform similarly to unaffected females and better than affected males in social cognition tasks and language abilities[70,71]. This seemingly neurotypical social functioning of autistic females is often linked to their ability to mask their behaviors and adapt to social norms[64,72–74].

Autistic individuals, especially females, adopt behaviors and strategies to adapt to and manage socially accepted norms, thereby 'camouflaging' their intrinsic difficulties[49,52,72–74]. Camouflaging allows affected individuals to hide autistic behaviors, minimizing the visibility of appearing 'autistic' and enabling them to mimic neurotypical behavior[49]. Affected individuals accomplish this either through mimicry or by developing strategies to compensate for social difficulties associated with ASD symptoms[49,50,75]. Several studies have observed differences in camouflaging

behaviors among affected females and males. Females tend to establish eye contact during conversations, mimic facial expressions and gestures, actively suppress repetitive behaviors, and learn to follow appropriate behaviors during social interactions[49,50,73]. Regarding the latter, for instance, autistic girls often stay closer to their peers than boys and copy their peers' mannerisms and interests[49,76]. Camouflaging seems to occur in both genders but is generally executed more successfully by females than males[73,75].

Overall, camouflaging is a complex behavior often used by autistic patients to compensate for intrinsic deficits and is particularly prevalent among affected girls and women. Furthermore, it is essential to adjust the diagnostic criteria for ASD to consider female-specific representations and not solely rely on male-oriented standards. Since females present with varying degrees of the core symptoms of ASD, they may frequently go unnoticed in the diagnostic process.
The implications of the diverse manifestations of female behavior are far-reaching, contributing to increased gender discrepancies in ASD and resulting in mis- and underdiagnoses or delayed diagnoses for females. Moreover, being undiagnosed for ASD will prevent women from accessing health support. Further research is necessary to study the presentation of ASD in females and understand the associated symptomatology. Generally, the perspective from a "male-centered" disorder must shift toward a more equal and balanced gender representation. This would present a crucial step towards establishing more accurate and tailored diagnostic approaches for autistic females.

1.1.3.3 Impact of fetal testosterone exposure and X-chromosome association

A prevailing hypothesis regarding the etiology of ASD and its male predominance points to hormonal dysregulation during prenatal development, which may predispose males to ASD while developing in the womb. Generally, starting from 8 weeks post-conception, males exhibit higher testosterone levels until approximately 24 weeks of gestation, with a hormonal peak around week 16 (Fig. 3a). Beyond this prenatal hormonal burst, males experience two additional periods of elevated testosterone, one shortly after birth, peaking around 3-4 months of age. The second spike occurs around puberty (Fig. 3a). In contrast, while females typically have low levels of testosterone throughout prenatal development and childhood, their hormonal levels are constantly fluctuating (Fig. 3b)[77,78].

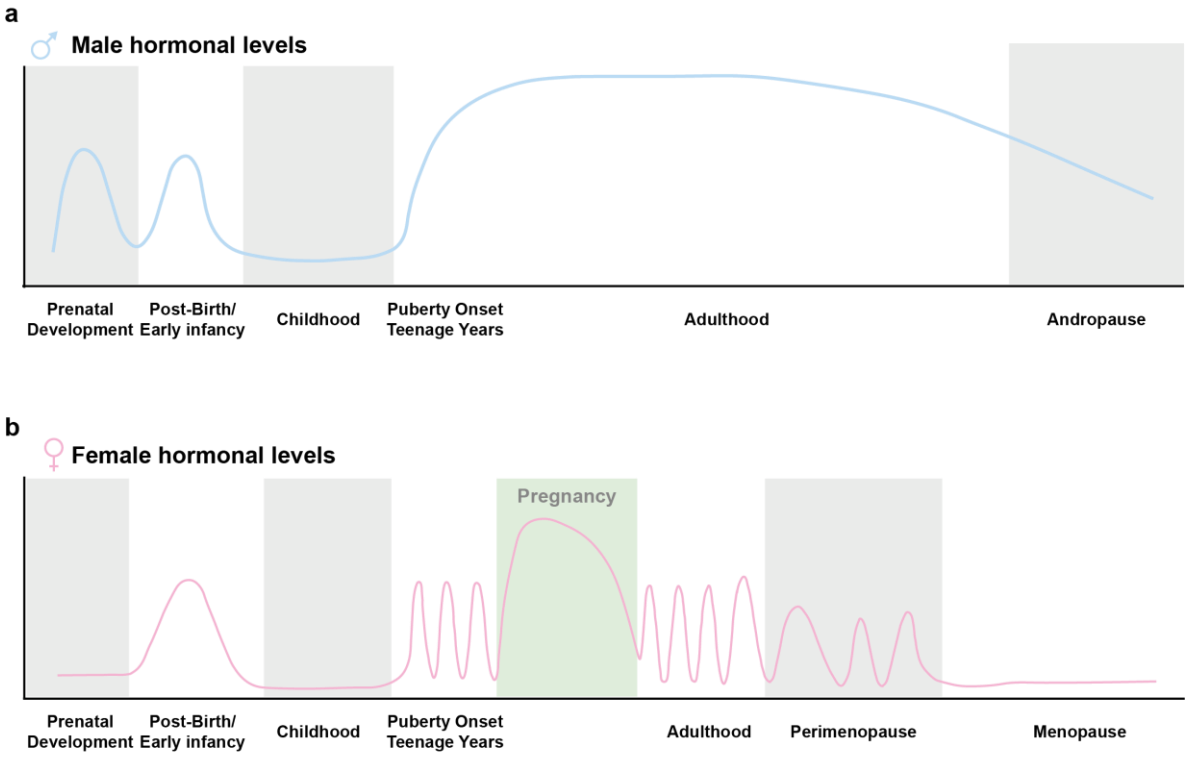


Figure 3: Hormonal fluctuations in females and males throughout life (adapted from Ocañas et al.[90]).
a, Males undergo several hormonal bursts throughout life, the first already happening during fetal development initiating sex differentiation. Another substantial hormonal increase occurs during infancy, stabilizes during childhood, and reaches a nearly constant level after puberty and throughout adulthood. **b,** Females experience numerous hormonal fluctuations, particularly during puberty with the menstrual cycle. Pregnancy temporarily halts the hormonal cycle, maintaining elevated levels throughout. With the beginning of the perimenopause, hormonal cycling becomes irregular and stops upon entering menopause.

Linking elevated prenatal testosterone to sex differences was first proposed by Norman Geschwind and Albert Galaburda in 1985[79]. Their theory suggested that lateralization of brain function accounts for sex differences, with circulating testosterone in males delaying the maturation of the left hemisphere. As such, this delay could impact left-sided brain areas, leading to, for example, reduced language

processing abilities. However, this hypothesis was primarily based on observational studies lacking supportive empirical evidence. Simon Baron-Cohen and colleagues proposed a similar theory[77,80], testing it experimentally by analyzing steroid levels in amniocentesis samples[54,81–83]. Based on several studies exploring sex differences in ASD-related behaviors, their theory posits that exposure to high levels of male sex hormones during pregnancy could lead to a higher prevalence of autistic traits later in life[81]. It was shown that fetal testosterone exposure is associated with poorer sociability, increased restricted interests[82], and a lack of empathy in males[84].

Taken together, there are several limitations associated with these theories. Hormonal levels tested from amniotic fluid are used as a proxy for those in the fetus's brain. Given that fetal brains are, of course, inaccessible for direct investigations, it remains questionable whether androgen levels measured through amniocentesis truly mirror the conditions affecting the prenatal brain. Moreover, research led by Baron-Cohen and his colleagues has predominantly shaped the understanding of excessive fetal testosterone exposure. Independent replications of these findings are currently falling short, which need to be addressed in further studies. Additionally, elucidating the molecular mechanisms through which fetal testosterone influences brain development during critical time windows represents an important step toward clarifying how hormonal influences contribute to the observed male predominance.

Another plausible mechanism contributing to the observed sex differences in ASD could be genetic risks encoded on the X or Y chromosomes. While females, having two X chromosomes, might be able to compensate for deleterious effects if one X chromosome carries a truncating variant, males with only one X chromosome cannot counterbalance in the same way. Conversely, genetic risks encoded on the Y chromosome would not affect females due to the lack thereof. Although some ASD risk genes have been identified on the X and Y chromosomes, such as *MECP2, FMR1, NLGN3, NLGN4X, NLGN4Y,* and *USP9Y*, there is limited evidence to suggest that common risk factors with a strong effect for ASDs are located on either of these chromosomes[47,55,85–87].

1.2 *Critical milestones for cortical development and implications for ASD*

ASD is a prime example of a neurodevelopmental condition. Considering its significance as a neurodevelopmental disorder, it is essential to discuss the aspects of (patho-)physiological cortical development in both humans and mice since mice are the preferred animal model to study NDDs and ASD. The human brain consists of approximately 170 billion cells, roughly half of which are neurons. The other half comprises non-neuronal (e.g., glial) cells. Interestingly, the cerebellum, which accounts for only about 10% of the brain's mass, contains 80% of all neurons (~ 69 billion) in the human brain, which will be discussed in **1.2.3**[88]. In contrast, the mouse brain consists of approximately 100 million cells, of which 71 million are neurons[89]. Many of the brain's key features are common across mammals, including the regionalization in motor, sensory, and cognitive association areas, as well as a multi-layered cortical organization[90,91].

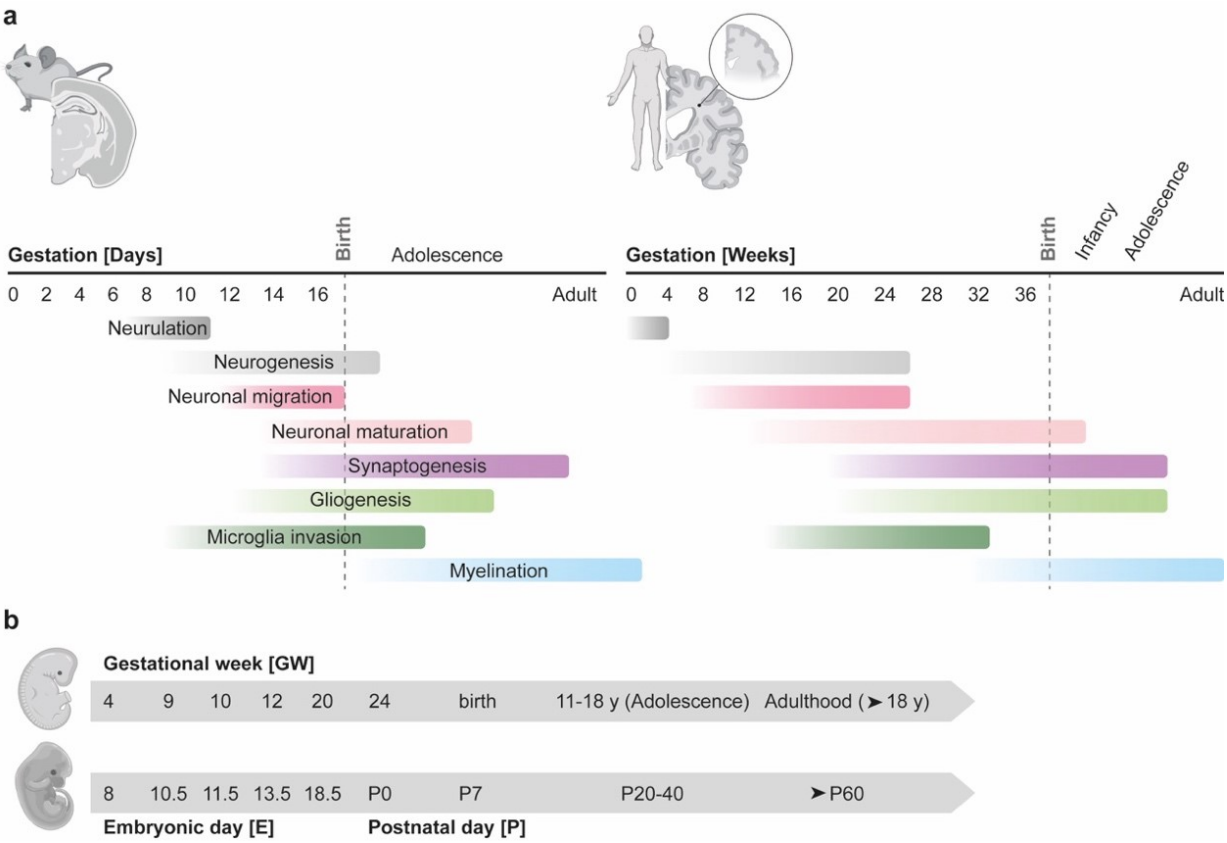


Figure 4: Developmental milestones of brain development in mice and humans.
a, Brain development begins around E6.5 and GW3-4 with neurulation. Neurogenesis and neuronal migration start after neural tube closure, peaking around E14.5 to E16.5 and the mid-fetal stage. Shortly after, gliogenesis occurs with astrocytes forming first, followed by oligodendrocytes, which initiate axonal myelination shortly after birth. **b,** Comparison of developmental timing in humans (top) and mice (bottom).

Human brain development spans a prolonged period, beginning at gestational week (GW)3 and extending into early adolescence[92], with neurogenesis potentially continuing into adulthood (Fig. 4a, right)[93,94]. Corticogenesis in mice starts between

embryonic days (E)9.5 and 10.5, extending until birth (Fig. 4a, left)[95–97]. Remarkably, the key stages of cortical development are largely conserved between mammalian species. Common processes shared between humans and mice include neurogenesis, myelination, synaptogenesis, and pruning of neurons and synapses (Fig. 4)[98]. Although the length of the individual biological processes varies, their developmental timing is generally comparable (Fig. 4b)[99]. Disruptions, such as environmental insults or genetic mutations occurring during these intricate processes can have profound effects on corticogenesis, leading to pathological consequences in brain development and structure.

1.2.1 Neurogenesis and neuronal migration during embryonic corticogenesis

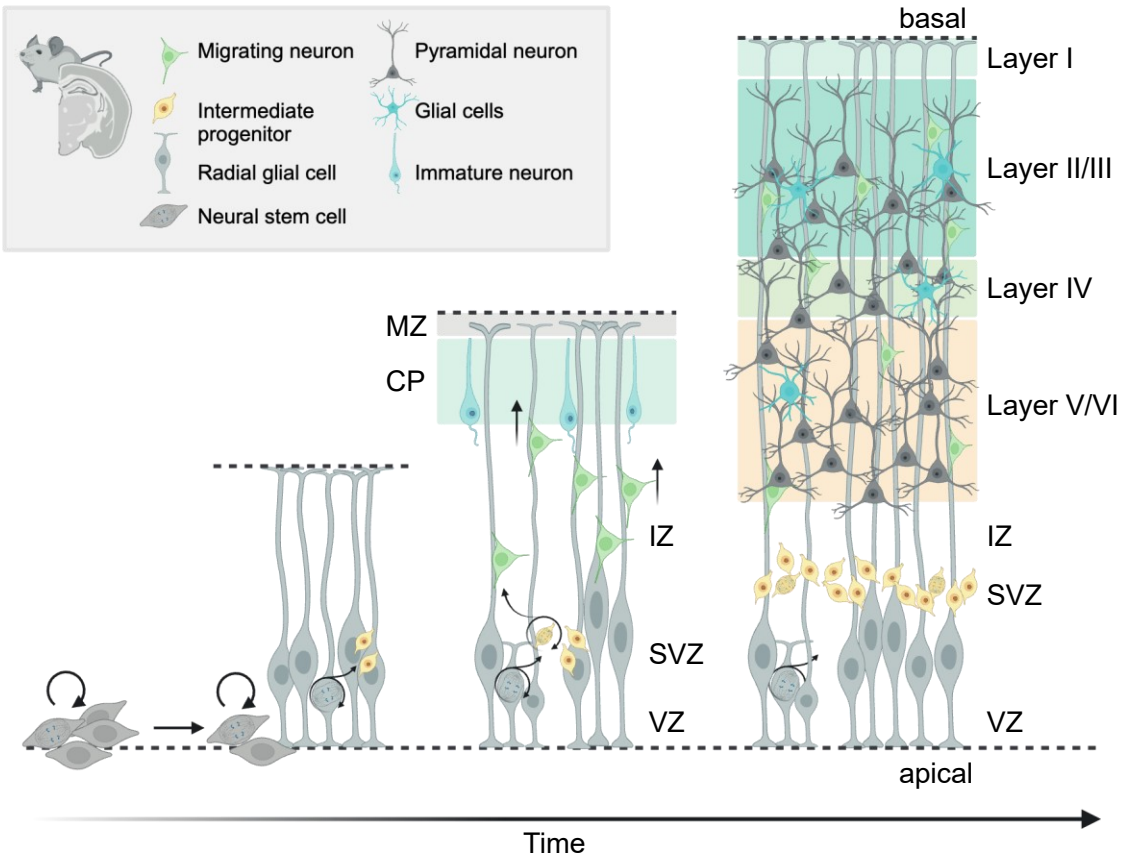


Figure 5: Cellular mechanisms driving cortical expansion and the formation of a six-layered structure.
CP: Cortical Plate, IZ: Intermediate Zone; MZ: Marginal Zone; SVZ: Subventricular Zone; VZ: Ventricular Zone. Initially, neural stem cells undergo symmetrical divisions, producing radial glial cells (RGs). RGs divide asymmetrically in the VZ, producing intermediate progenitor cells populating the SVZ and post-mitotic neurons that migrate along radial glial processes and through the IZ into the CP. Immature neurons differentiate and eventually mature into layer-specific pyramidal neurons. The six-layered cerebral cortex is formed with early-born neurons forming the deep-layer pyramidal neurons, while later-born neurons migrate along RG basal processes to establish superficial cortical projection neurons.

The initial stage of corticogenesis involves the expansion of a neural progenitor cell (NPC) pool, which originates from neural stem cells that undergo symmetrical divisions to expand the number of progenitors. Upon the start of neuronal production, cell divisions transition to asymmetrical divisions, thereby allowing the maintenance of a proliferative cell pool while simultaneously generating post-mitotic neurons (Fig. 5). Throughout this process, more specialized NPCs, known as radial glial cells (RGs), are produced. Typically, RGs expand in the ventricular zone (VZ), a neuroepithelial layer lining the brain's ventricles. As they shift to neurogenic divisions, RGCs generate either cortical projection neurons (PNs) or intermediate progenitor cells (IPCs). IPCs then divide symmetrically within the subventricular zone (SVZ) to form neurons (Fig. 5). Thereby, a substantial fraction of the cortical neuronal population is generated, accounting for up to ~80% of all excitatory PNs across all cortical layers[91]. During neurodevelopment, the transition from symmetric to asymmetric cell division occurs around E11.5-E12.5 in mice and GW8 in humans[100,101].

A remarkable but subtly distinct feature of human and mouse cortical development involves outer RGCs (oRGCs). While these cells are barely present in mice, they largely contribute to the late-stage (i.e., from GW16 onward) cortical expansion in human brains[102–104]. In humans, the SVZ is subdivided into an inner and outer SVZ (iSVZ and oSVZ, respectively). oRGCs are located in the latter (i.e., oSVZ) and retain their basal processes but lack apical junctions. Nonetheless, oRGCs can self-renew and undergo multiple proliferative divisions to expand the neural precursor cell pool and differentiate into neurons. Presumably, this ensures a progressive accumulation of neurons during corticogenesis, contributing to higher numbers of cortical neurons in humans compared to mice[103,105].

During this period of neurogenesis, the large number of excitatory neurons generated subsequently migrate to their final location. The migration of neurons happens in an inside-out fashion – with early-born neurons forming deeper cortical layers, and later-born neurons forming superficial layers[92]. Here, immature neurons utilize the processes of RGs, which extend to the basal pial surface, to migrate radially to reach the developing cortical plate (CP; Fig. 5). These processes act as scaffolding, essential for the migration of neurons and their correct laminar positioning within the cortex[90,92]. Interestingly, once excitatory neurons reach their final destinations, they project to various brain areas. While neurons in layers 5 and 6 send long-range projections to subcortical targets, layer 2/3 neurons primarily project locally to other cortical regions. In contrast, layer 4 neurons receive most of the monosynaptic connections from the thalamus carrying sensory information[96]. While the migratory phase lasts from E12.5 to E18.5 in mice, it peaks between GW12-20 in humans and is largely complete by GW26[100,106,107]. In early cortical development, RGs initially produce neurons; however, after the neurogenic period, their morphology changes, leading to a gliogenic fate. Consequently, RGs generate cells from the macro-glial lineage, such as astrocytes and oligodendrocytes. The neurogenic-to-gliogenic switch is primarily influenced by internal mechanisms and molecular signals[108,109].

In contrast to cortical PNs, interneurons are generated outside the developing cortex, specifically within the ganglionic eminences (GEs). Here, cortical inhibitory neurons populate the cortex by tangential migration, passing through the SVZ and marginal zone (MZ). Interneurons are primarily produced in the caudal, lateral, and medial GEs (CGE, LGE, and MGE, respectively; Fig. 6), from where they navigate along distinct migratory routes to reach their final positions in the cortex[91,95]. Once interneurons have reached the cortex via MZ or SVZ streams, they migrate radially within the cortex to settle in the respective cortical layers[95,110]. While the CGE produces interneurons migrating to the cerebral cortex, the LGE generates interneurons with olfactory bulb fate, and precursors of striatal medium spiny neurons. The MGE serves as the main source of interneurons for the cortex, hippocampus, and striatum[111–113]. The migratory routes of interneurons are partly correlated to their temporal origin and designated cell fate, and are encoded in their distinct genetic programs[114].

Moreover, these migratory paths are also shaped by permissive and chemoattractant cues that guide neurons to specific brain regions[110]. The expression of regulatory genes during GE development is crucial in contributing to the regional cell diversity and migration of interneurons. These regulatory mechanisms, in part, ensure that interneurons are properly diversified and guided to their final positions within the brain[112]. Approximately 20% of cortical neurons in mice are interneurons, while in humans, this proportion is increased to roughly 25-30%[111,115,116].

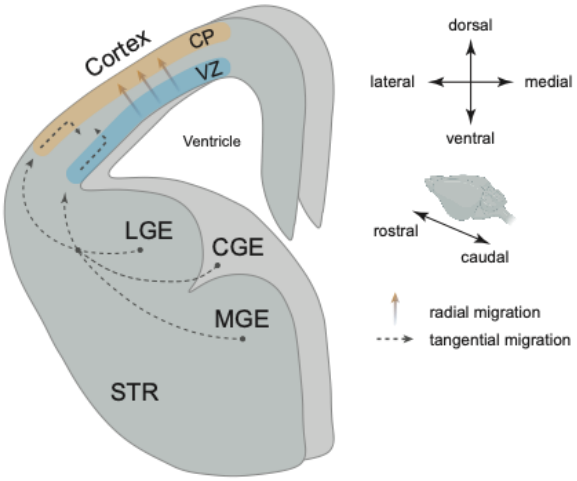


Figure 6: Inhibitory neuron migration to their designated cortical location **(adapted from Guo et al.)[126]**
CP: Cortical Plate; CGE: Caudal Ganglionic Eminence; LGE: Lateral Ganglionic Eminence; MGE: Medial Ganglionic Eminence; VZ: Ventricular Zone; Primary migratory routes of inhibitory neurons originating from the CGE, LGE, and MGE. Initially, inhibitory neurons migrate tangentially toward the cortex before transitioning to radial migration to reach their final cortical positions.

1.2.2 Glial cells and their pivotal functions in the brain

Beyond excitatory and inhibitory neurons, the brain is populated by various types of glial cells that support the cortical network, each with distinct functions. These include astrocytes, microglia, and oligodendrocytes. During cortical neurogenesis, the precursors that initially generate neural progenitors (i.e. RGCs) switch from a neurogenic to a gliogenic differentiation program around E18.5, initiating the production of astrocytes. Oligodendrocytes are similarly derived from RGCs after birth. Instead, microglia have a distinct origin, arising from erythromyeloid progenitors (EMPs) in the yolk sac[117,118]. Notably, the human brain consists of approximately 50%

neurons and 50% glial cells. In contrast, in mice, glial cells constitute around 35% of cells within the brain[89,119].

Astrocytes are crucial in promoting synapse formation, thereby supporting the cortical neuronal network. Additionally, they support synaptic functioning and communication, provide metabolic support, and contribute to forming and maintaining the blood-brain barrier[120,121]. Astrocytes begin to develop around E18.5 in mice and around GW16-18 in humans[122–124]. In mice, astrocyte development spans a period of 3 weeks of proliferation and maturation. During the first postnatal week (P0-P7), glial progenitors expand and migrate within the cortical layers and proliferate to expand their cell pool. This is followed by a differentiation and maturation phase, characterized by elevated arborization, increased cell volume, and greater complexity of their morphology (Fig. 7; green)[121,122,125].

Oligodendrocytes (ODCs) are the myelinating cells of the central nervous system, originating from oligodendrocyte precursor cells (OPCs). OPC generation in the mouse forebrain happens in three temporally distinct waves. The first wave occurs around E12.5 starting from the MGE, with OPCs migrating tangentially to populate the forebrain. In the second wave, originating from the LGE at E15.5, OPCs migrate dorsally to the cortex. Lastly, the third wave of OPC production occurs around birth, with OPCs migrating radially from the SVZ to populate the corpus callosum and cortical layers.
Interestingly, it was shown that early OPCs originating from the first two waves are largely displaced by those originating from the SVZ[126].
In humans, the population of OPCs expands between GW16-23. Pre-myelinating ODCs peak between GW20-30, while myelination primarily occurs during the first years of life but continues throughout an individual's lifetime[123,127–129]. Generally, OPCs transform first into pre-myelinating ODCs and afterward into myelin-producing ODCs[130,131]. The central function of ODCs involves myelination during development and adulthood, as well as remyelination following damage. Myelin is essential for the saltatory conduction of action potentials along axons, acting as an electrical insulator and enabling rapid transmission of neural signals (Fig. 7; blue)[132].

Microglia are fundamental to brain homeostasis as the resident macrophages and immune "guardians" of the central nervous system. Unlike astrocytes and ODCs, which are derived from neuroectodermal tissue, microglia are of mesodermal origin and originate from the yolk sac. Around E8.5 of murine development, early primitive macrophages and erythrocytes, along with erythromyeloid progenitors (EMPs), emerge from the yolk sac[118,133]. A subset of EMPs become microglial progenitors that migrate tangentially toward the brain from E9.5-10.5, continuing until E14.5, when the blood-brain barrier forms. Subsequently, microglial cells proliferate locally and migrate radially to colonize all cortical areas, continuing their expansion until after birth[134,135]. Microglia fulfill versatile roles in maintaining brain homeostasis, including removing apoptotic cells and debris, synaptic pruning, and supporting processes such as myelination, oligodendrogenesis, and neurogenesis[136,137]. Synapses are produced in excess during brain development, creating too many synaptic connections. Here, microglia contribute to the activity-dependent elimination of surplus synapses, aiding the formation of mature and functional synaptic networks (Fig. 7; orange)[135].

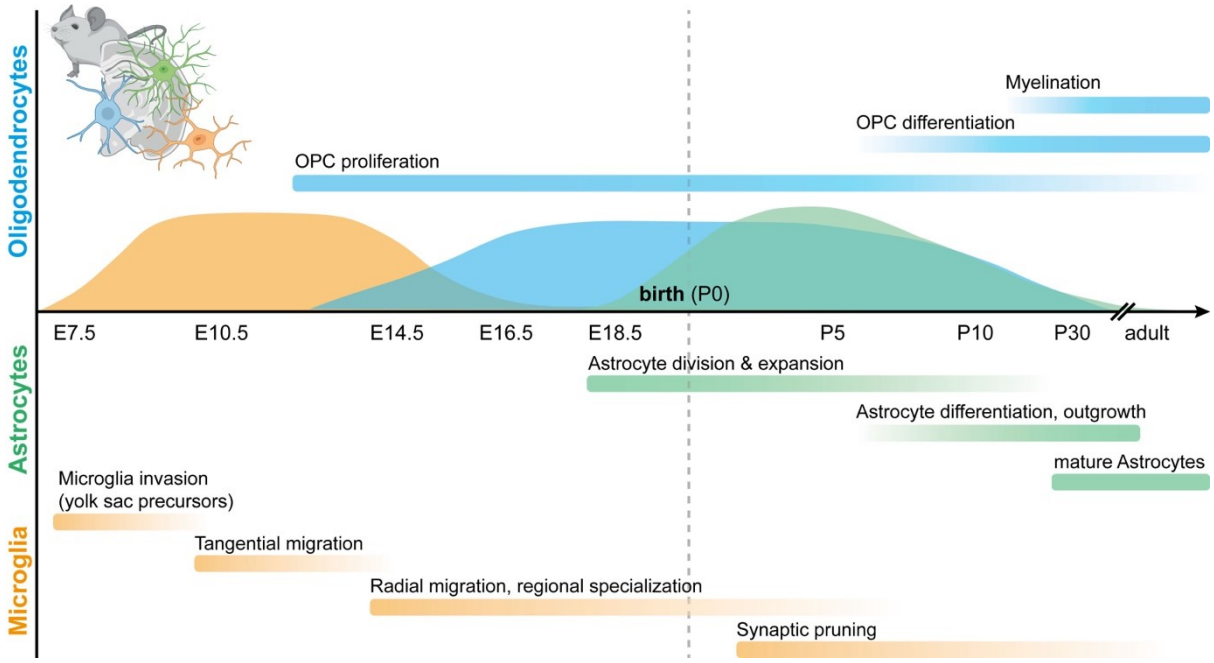


Figure 7: Scheme illustrating key processes of gliogenesis throughout mouse pre- and postnatal development.
Timeline of key developmental processes involved in astrocyte (green), microglia (orange), and oligodendrocyte (blue) generation in mice.

1.2.3 Cerebellar development – more than just the "little brain"

Despite being termed the "little brain", the cerebellum contains the majority (~80%) of all neurons present in the human brain, even though it accounts for approximately 10% of the total brain mass[88]. While it was originally thought to be involved solely in motor functions, it has become clear in recent years that it also participates in cognition, reward, and sensory contexts[138–141]. Generally, cerebellar development differs between humans and mice. In humans, development already starts around GW7 and

continues until the age of 2, whereas, in mice, cerebellar development starts around E13.5 and is largely complete by P20[142,143].

Neurons in the cerebellum originate from the cerebellar VZ, neuroepithelia that form the roof of the 4th ventricle, or the rostral rhombic lip. GABAergic neuronal cells, including Purkinje cells, Golgi cells, stellate cells, and basket cells, are derived from the VZ. In contrast, cerebellar glutamatergic neurons, such as granule cells and unipolar brush cells, originate from the rhombic lip[144]. Cerebellar neuronal subtypes are generated at distinct developmental stages. Purkinje cells are generated early, between E10.5 and E13.5. Granule cell progenitors begin to migrate from the rhombic lip at E13.5 and undergo extensive clonal expansion to form the vast population of granule cells, which will eventually outnumber the total neuronal population of the cerebral cortex[144,145].

Post-mitotic Purkinje cells migrate via the cerebellar plate to aggregate into clusters until E18. These clusters are spatially organized domains that are molecularly distinct and can be distinguished through different cell type markers. They also serve as a scaffold around which other cerebellar cell types organize[145,146]. By P20, Purkinje cell clusters reorganize into a monolayer of parasagittal stripes[144,145,147].
Simultaneously, granule cells migrate from the rhombic lip to form a secondary germinal zone known as the external granule layer (EGL), where they extensively proliferate to increase their cell numbers. After exiting the cell cycle around P0, post-mitotic granule cell progenitors migrate radially and settle in the granule cell layer by P20, located beneath the Purkinje cell layer[145,147].
Although the developmental timing is different between humans and mice, the overall cerebellar architecture is relatively conserved[148]. The mature cerebellum is organized into three layers (Fig. 8), from the deepest to the most superficial layer: the granule cell layer (GCL), Purkinje cell layer (PCL), and molecular layer (ML). The GCL contains excitatory granule and unipolar brush cells, along with inhibitory Golgi cells. The PCL is made up of inhibitory Purkinje cells and Bergman glia. The uppermost layer, the ML, consists of inhibitory basket and stellate cells, along with the Purkinje dendritic trees and parallel fibers of granule cells (Fig. 8)[149,150]. Granule cells have a single ascending axon that bifurcates into the ML, forming T-shaped parallel fiber structures.

Purkinje cells extend their dendritic tree into the ML, forming synapses with the parallel fibers of granule cells and the axons of stellate cells[149]. Given the cerebellum's extended developmental period - being one of the first brain structures to develop and among the last to fully mature - it is particularly susceptible to genetic and epigenetic risk factors as well as environmental insults.

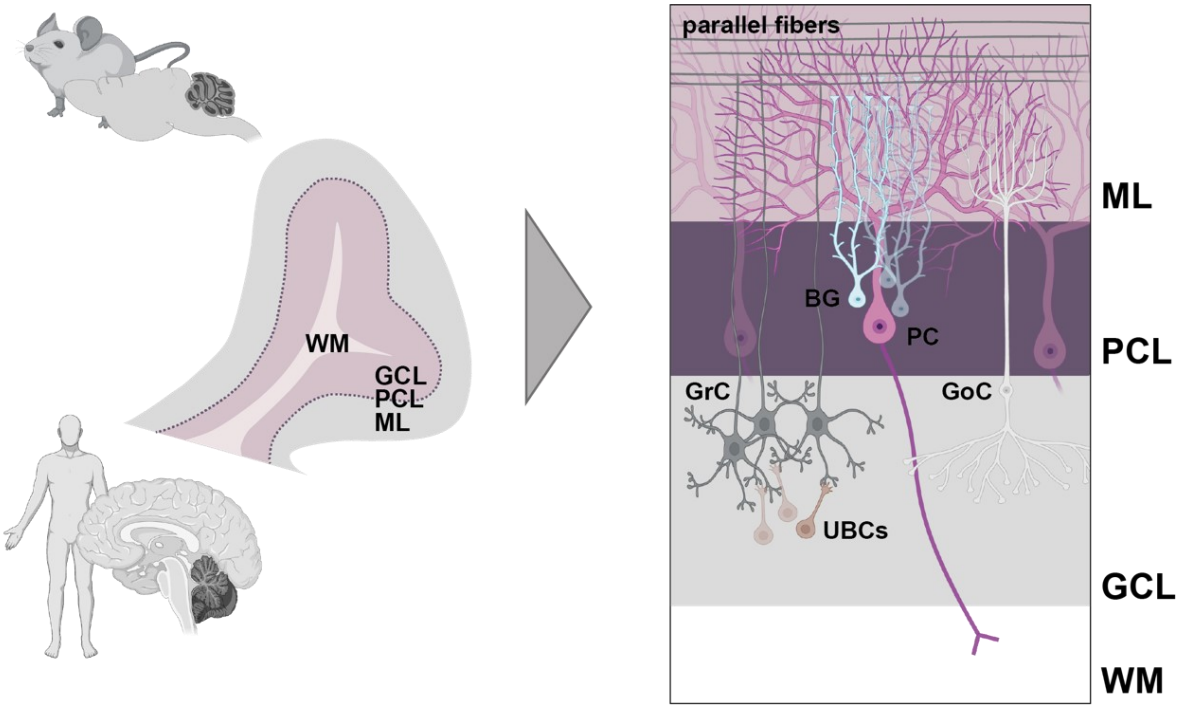


Figure 8: Conserved cerebellar architecture in humans and mice.
The cerebellum presents a deeper white matter (WM) and an outer gray matter with a three-layered structure, from deepest to most superficial layer, the granule cell layer (GCL), the Purkinje cell layer (PCL), and molecular layer (ML). GrC: Granule cells; UBCs: unipolar brush cells; GoC: Golgi cells; PC: Purkinje cell; BG: Bergman glia.

1.2.4 Cortical malformations and disruptions in the context of ASD

The formation of the six-layered cortex is driven by tightly orchestrated cellular and molecular processes, broadly categorized into proliferation, migration, and differentiation/maturation (as described in **1.2**). Disruptions at any of these sequential events can lead to cortical malformations, which encompass a wide range of morphologies, etiologies, and, consequently, clinical manifestations[151–154]. The timing of insults during corticogenesis is critical in determining the severity of these cortical malformations[151]. Depending on the occurrence of disruptions, different processes and subsequent steps may be altered, including:

(a) Progenitor proliferation and differentiation into early-born neurons during neurogenesis,
(b) Migration of newborn neurons to their designated cortical layers,
(c) Cell specification, defining cortical lamination,
(d) Neuronal morphogenesis and synaptogenesis, and
(e) Migration and maturation of GABAergic interneurons[155].

Disruptions in any of these steps can affect cortical development at multiple levels, altering the intricate balance of processes required for proper cortical formation. Neurodevelopmental disorders emerge when one or more of these critical steps are affected. Although numerous causal genes and associated characteristics have been identified, the order of events linking molecular disruptions to clinical manifestations remains largely unclear.
Cortical malformations, particularly concerning head size, are of particular interest in ASD research due to their frequent occurrence in various combinations and offer valuable insights into non-invasive brain development. Macrocephaly (enlarged head size) or microcephaly (reduced head size), classified as more than two standard deviations above or below the mean head size based on age and sex, are often seen in ASD patients[151,152,155,156]. About 20% of individuals with ASD exhibit macrocephaly, while around 15% are identified with microcephaly[151,152].

Alterations during neurogenesis can often manifest as microcephaly or macrocephaly. Based on its onset, **microcephaly** can be categorized into two forms: congenital (occurring before birth) and postnatal (developing after birth). In the latter case, patients fall within the normal head range at birth but develop subsequent microcephaly due to halted or decelerated brain growth[157].
Postnatal microcephaly is linked to mutations in ASD risk genes such as *SLC7A5, DYRK1A, CDKL5,* and *FOXG1*[153,158–161]. At a cellular level, microcephaly is often caused by abnormal neuronal or glial cell proliferation and apoptosis[153,162].
Macrocephaly may be attributed to increased neuronal size or elevated neuronal numbers, often resulting from abnormalities in molecular pathways that impact cell proliferation, differentiation, cell cycle regulation, and apoptosis or cellular survival[163,164]. For example, mutations in *CHD8, PTEN, POGZ*, and *FOXP1* are linked to alterations in neurogenesis and are ultimately associated with the development of macrocephaly[155,165].

Cortical malformations associated with abnormal cell migration include lissencephaly, heterotopia, and polymicrogyria. While a smooth brain characterizes **lissencephalic brains** due to primarily absent gyri and a thickened neocortex, **polymicrogyria** describes an excessively folded cortex with small folds of the brain surface[153,155,162].
Heterotopia is marked by abnormal clusters of neurons along the ventricles or packaged band-like formations of neurons[166,167].

Lissencephaly, polymicrogyria, and band heterotopias have been viewed as distinct disorders for a long time. Nonetheless, recent research suggests that lissencephaly and polymicrogyria formations could be associated with mutations in the same genes, especially those related to tubulin, which is essential during the early stages of neuronal proliferation, migration, differentiation, and axonal guidance. This subgroup of cortical malformations is often referred to as tubulinopathies[153,168–170]. Microtubules are essential during corticogenesis, as developing neurons rely on the cytoskeleton to proliferate, migrate, and differentiate. They are involved in a wide range of processes,

including mitosis, centrosome formation, dendritogenesis, synapse formation, and axon specification[168]. Mutations in tubulin genes *TUBA1A, TUBB2B, TUBB3, TUBB4A, TUBB5, TUBA8*, and *TUBG1* contribute to this group of heterogeneous cortical malformations, many of which are also associated with an increased risk of ASD[153,171–174]. Deletions and mutations in *LIS1* account for the majority of lissencephaly cases. *LIS1* is critical in the neuronal cytoskeleton, interacting with microtubule-associated proteins to regulate cell migration[153,175,176]. Interestingly, mutations in the DCX gene, located on the X chromosome, result in heterotopia in women, while in men, these mutations are linked to lissencephaly, indicating a dose-dependent relationship[167,177].

Focal cortical dysplasia (FCD) is similarly attributed to neuronal migration defects, failing to form cortical layering properly. FCD refers to limited focal areas of abnormal neuronal cytoarchitecture, organization, and morphology, usually restricted to one or two brain lobes[178]. The pathology of FCD is heterogeneous, with several subclassifications, though all forms are generally classified as malformations resulting from abnormal proliferation, differentiation, and cell growth to abnormal cortical layering[153,162,178].

While many ASD-associated genes affect excitatory neurons, some significantly impact GABAergic interneurons. For example, *ARID1B* plays a critical role in the birth and migration of Somatostatin (SST)- and Parvalbumin (PV)-positive interneurons. Interestingly, haploinsufficiency of *Arid1b* in mice results in decreased cortical interneuron numbers both in *vivo* and in *vitro* due to decreased proliferation and promoted apoptosis of medial ganglionic eminence progenitors. This effect was specific to PV^+ neurons[179].
Interestingly, cell type-specific knockouts of *Arid1b* in PV and SST neurons revealed distinct ASD-relevant traits. PV-specific *Arid1b*-knockout mice exhibited deficits in sociability and social recognition, along with anxiety and depression-like behaviors. In contrast, SST-specific knockouts displayed learning and memory impairments as well as stereotyped, repetitive behaviors.

Cortical malformations are frequently associated with abnormalities in axonal guidance and tract extension, often shown by atrophy or agenesis of the corpus callosum, the largest axonal commissure in the brain that connects both hemispheres[180,181]. Similar to neuronal migration, axonal guidance and extension processes rely on proper cytoskeletal function. Consequently, synaptic dysfunction and disrupted synaptic connectivity may arise together with neuronal migration defects. Disruptions in neuronal positioning, changes in cell signaling cues, or the presence of atypical neurons can substantially influence developmental processes that contribute to physiological cortical synaptic connectivity. These alterations can result in abnormal connectivity, worsening the functional deficits linked to cortical malformations[155,167,181].

Altered neuronal morphogenesis and synaptogenesis have emerged as critical factors contributing to the risk of ASD. Various genes associated with ASD have been linked to defects impacting synaptic structure, excitability, and functionality, ultimately altering the neural network and influencing behavioral outcomes. Likewise, disruptions in ion channel function or expression, improper localization, or trafficking of synaptic proteins can lead to imbalances in excitatory/inhibitory signaling[19,182,183]. The following sections (**chapter 1.3**) will explore in more detail the key processes affecting synaptogenesis and circuit formation and their effects on ASD.

1.3 Convergent genes and causal pathways dysregulated in ASD

The etiological complexity of ASD has hampered efforts to identify treatments targeting the core cause of the disorder. Currently, treatment focuses primarily on managing symptoms and addressing comorbid conditions like epilepsy, language delay, and gastrointestinal problems. Or, more generally, supporting patient development through specialized education and training to help with challenges related to developmental delay. In recent years, multiple studies have revealed the heterogeneous landscape of ASD risk by identifying numerous risk genes. Although these findings are essential for understanding the biological processes involved, a key question remains: How do such differing sets of risk genes result in essentially similar behavioral and cognitive traits?

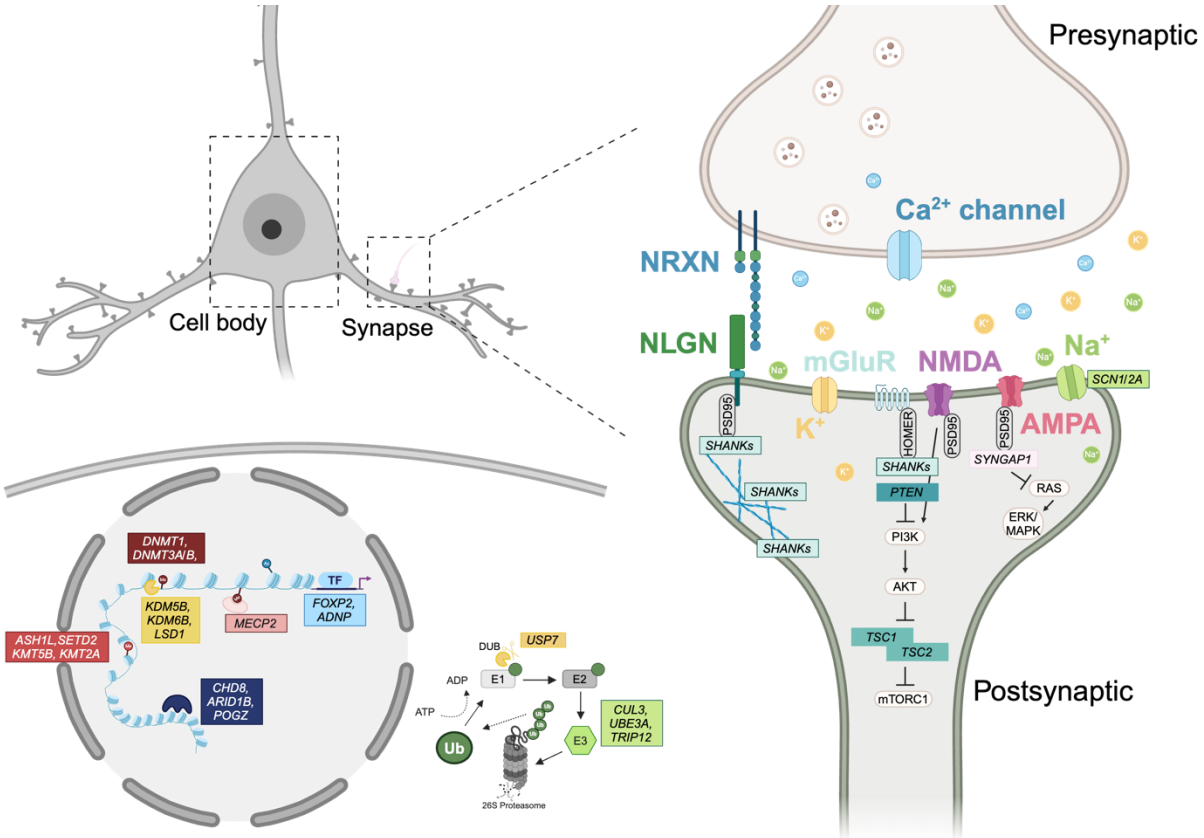


Figure 9: ASD risk genes impact synaptic signaling, transcription, chromatin regulation, and protein balancing.

Interestingly, it became increasingly evident that many ASD risk genes converge on shared molecular pathways. Common points of overlap include a substantial fraction of genes involved in synaptic signaling and structure[15,184,185], protein synthesis and degradation[186,187], transcriptional regulation, and chromatin modification (Fig. 9)[188–190]. Frequently implicated biological pathways include neurogenesis, neuronal migration, and WNT signaling[15,20,190,191]. Identifying commonalities among a wide array of ASD risk genes may help to guide therapeutic strategies by focusing on a set of shared pathways rather than attempting to treat individual mutations. This approach could streamline the development of treatments by targeting key molecular processes

affected across various forms of ASD. The diverse range of genes associated with ASD suggests that multiple pathways may independently lead to autism characteristics or that functionally distinct ASD risk genes can produce effects that converge on a few shared ASD pathways involved in the ASD pathogenesis. At the same time, it is essential to highlight that whether convergence indeed exists in the pathophysiology of ASD remains largely unknown. Alternatively, it is possible that no common impairments are involved in the disorder's etiology, and ASD may instead represent a broad spectrum of pathophysiologically distinct conditions.

1.3.1 Synapse development, signaling, and plasticity: Implications for treatment

A prevalent hypothesis suggests that ASD may emerge from disruptions in neuronal network activity caused by an imbalance between excitatory and inhibitory neurotransmission. In fact, the frequent comorbidity of epilepsy has further fueled speculation that an excitation/inhibition (E/I) imbalance may, in part, contribute to ASD[192]. A neuronal E/I imbalance reflects altered regulation at either the synaptic level or within higher circuits. In individual pyramidal neurons, the overall number of excitatory and inhibitory synapses is tightly regulated to maintain a stable E:I synapse ratio within dendritic segments. At the circuit level, maintaining a balance is essential for ensuring a stable global circuitry[193,194]. Disruptions in physiological synaptic mechanisms and circuit refinement, vital for balancing excitation/inhibition (E/I), may significantly contribute to cognitive and behavioral abnormalities.
Genetic factors may play a significant role in this imbalance, as many mutations related to ASD risk are linked to synaptic scaffolding proteins, as well as glutamatergic and GABAergic receptors. These elements influence neuronal activity, synaptic strength and number, and ultimately, synaptic plasticity[30,190,192,195,196].

Among these are the family of neurexins (NRXNs), presynaptic cell-adhesion molecules, and their postsynaptic counterparts, neuroligins (NLGNs; Fig. 9, right). Neuroligins function as postsynaptic receptors for neurexins, modulating synapse formation and transmission[196]. Mutations in *NRXN1, NLGN3*, and *NLGN4* have been linked to ASD, further highlighting the importance of these proteins in synaptic function[197].
In addition, mutations in *SHANK3,* an intracellular scaffolding protein that indirectly binds to NLGNs, have also been frequently associated with ASD[198]. To explore the underlying cellular and molecular pathways in greater detail, several different mutant mouse lines of NRXN and NLGN have been generated, providing an amenable system for studying these mechanisms.

To recapitulate the R451C mutation of *NLGN3* found in patients, knock-in (KI) mice were generated and characterized for both behavioral and synaptic changes. Interestingly, *NLGN3* R451 KI mice showed social interaction deficits but improved

spatial learning abilities – mirroring some clinical features observed in ASD patients. Although no changes were observed in the number of excitatory or inhibitory synapses, the mice showed an increase in inhibitory synaptic transmission, suggesting an imbalance in excitation and inhibition (E/I imbalance). Notably, these behaviors were absent in *NLGN3* knock-out (KO) mice[199]. Interestingly, several studies have demonstrated that genetic re-expression of *NLGN3* in juvenile and adult mice can restore both social deficits and synaptic abnormalities[200–202]. Similarly, transgenic Nrxn1β (βNrx1ΔC) mice present with autistic-like traits, including repetitive behaviors, sociability issues, and synaptic deficits such as impairment of glutamatergic synaptic transmission. Interestingly, upon inactivating βNrx1ΔC transgene expression, these behavioral deficits were reversed in juvenile and adult mice, restoring autistic traits to control levels[203].

SHANK genes, such as *SHANK1, SHANK2*, and *SHANK3*, are frequently associated with ASD and encode essential scaffold proteins of the excitatory postsynaptic density (Fig. 9, right). These proteins interact with glutamate receptors and are critical for facilitating synaptic transmission[204,205]. Interestingly, KO mice with mutations in *Shank* genes present behaviors similar to those observed in ASD patients. For instance, *Shank1* KO mice exhibit increased anxiety-like behavior, impaired contextual fear memory, reduced motor functions, and enhanced working memory but impaired long-term memory[206–208]. *Shank1* KOs exhibit smaller dendritic spines and reduced basal synaptic transmission, though long-term potentiation and long-term depression remain unaffected[206,208].
Similarly, *Shank2* KO mice show increased anxiety-like behavior, repetitive behaviors, and sociability issues. The protein composition at synapses, particularly those of NMDA-type glutamate receptors, was altered in *Shank2*$^{-/-}$ mice. Depending on the location of the gene knock-out, heterogeneity in synaptic neurotransmission was observed[208–210].
Shank3 is among the best-characterized mutations within the *SHANK* family associated with ASD and is considered a core genetic cause of Phelan-McDermid syndrome[211,212]. *Shank3* KO mice exhibit ASD-like traits, including repetitive behaviors and deficits in social interaction[213–215]. Several studies have reported alterations in the E/I ratio in mouse models of *Shank3*, with most effects seen at the level of excitatory synaptic transmission[183]. Depending on the specific mutation and brain region targeted, *Shank3* mutant mice displayed, for example, reduced excitatory postsynaptic currents[213,214], decreased glutamatergic transmission, and impaired long-term potentiation in the hippocampus[216,217]. Interestingly, several studies have investigated the possibility of alleviating some of the observed autistic traits in *Shank* mutant mice, either by restoring the gene expression to physiological levels[218–220] or through pharmacological intervention[210,221–224]. Remarkably, the latter has fostered clinical trials for clinical intervention in patients. As such, subcutaneous treatment with Insulin-like growth factor 1 (IGF-1) has beneficial effects on ASD symptoms, such as improved repetitive behaviors, sensory reactivity, and hyperactivity[225].

Although *Shank1*, *Shank2*, and *Shank3* mutant mice show specific molecular and functional differences, they all share behavioral phenotypes relevant to ASD and a commonly altered E/I balance. This E/I imbalance may stem from changes in glutamatergic synaptic transmission and composition[205].

Another example of ASD risk genes frequently implicated in synaptic signaling and plasticity are mutations in voltage-gated sodium channel genes, such as *SCN1A* (encoding $Na_V1.1$) and *SCN2A* (encoding $Na_V1.2$), which greatly impact different aspects of neuronal connectivity (Fig. 9, right)[28,186,226]. Interestingly, *SCN1A* and *SCN2A* are clinically among the most relevant sodium channel genes as they pose a major genetic cause of epilepsy, which is frequently comorbid with ASD[227–229]. Haploinsufficiency of the *SCN1A* gene causes Dravet Syndrome (DS), a childhood disorder including recurrent seizures, cognitive deficits, and ASD[230]. *Scn1a*$^{+/-}$ mice present with E/I imbalances, impairing cortical and hippocampal GABAergic inhibitory neurotransmission, which can be restored by a positive allosteric modulator of the $GABA_A$ receptor, clonazepam[230]. Similarly, KO of *Scn2a* results in altered neuronal excitatory transmission[231,232].

Overall, the exact origins of an E/I imbalance, its variability among patients, and the specific brain regions affected remain unclear. The causes of this imbalance are likely multifaceted, involving a complex interplay between genetics, structural brain alterations, and potential compensatory mechanisms that influence its severity.

1.3.2 Transcriptional regulation, epigenetic layers, and chromatin modifiers shape ASD

More than half of the genes linked to ASD are involved in gene regulation, indicating that transcriptional regulation and chromatin dynamics significantly contribute to the etiology of ASD. Disruptions in any of these ASD-related transcriptional regulators may, in fact, lead to similar neurodevelopmental outcomes by affecting common genomic targets[20,30].

Epigenetics refers to DNA modifications that can modulate gene expression without altering the underlying genetic sequence. Chromatin regulation can act at different scales: it can involve direct methylation of genomic DNA at promotors and enhancers, functional modification of histones, or broader changes in chromosome structure within the nucleus[233,234].
DNA methylation controls transcriptional access to genomic locations; for instance, methylation of gene promoters is associated with repression or reduced gene transcription[235]. Additionally, enhancer activation is closely linked to DNA methylation, as it directly controls the occupancy of transcription factors[236].

Common histone modifications encompass acetylation, methylation, phosphorylation, and ubiquitination of different residues across histones[237]. Epigenetic modulators can

be directly implicated in diseases. However, they also serve as adjustable “knobs” that can either worsen or ameliorate disease phenotypes by modulating gene expression.

Brain development is inherently dependent on dynamic shifts in gene expression patterns. In recent years, susceptibility loci including genes encoding chromatin and histone modifiers (e.g., *ARID1B, CHD8, KDM6B, KMT5B, MECP2, POGZ, SETD5, UBE3A*) or involved in DNA methylation (e.g., *DNMT1, DNMT3A, DNMT3B*) have been frequently identified in ASD patients (Fig. 9, left)[19,30,38,185]. Furthermore, studies examining global DNA methylation and histone modifications have uncovered altered epigenetic signatures in patients with idiopathic ASD[238–241]. The downstream targets of these proteins or their reversible modifications can vary tremendously, spanning from a handful to several hundreds. These targets often encompass biological processes previously noted in ASD, including areas like synaptic formation, protein degradation, and broader processes such as neuronal migration and differentiation. Notably, a recent study examining the Gene Ontology (GO) enrichment of high-risk ASD genes highlighted "Chromatin Binding" as a relevant process closely ranked after terms related to synaptic and channel functions[242].

MECP2 was one of the initial genes examined in the early research into ASD*. MECP2*, also known as methyl CpG binding protein 2, functions as a chromatin modifier. The MECP2 protein can recognize DNA and histone methylation marks, thereby acting as a methylation-dependent transcriptional modulator. Loss-of-function mutations in *MECP2* result in Rett Syndrome (RTT), a neurodevelopmental disorder similar to ASD, which was among the first genes to be studied in early ASD research years. RTT predominantly affects females as it is inherited in an X-linked dominant manner without following a pattern of epigenetic inheritance[243].
RTT is a postnatal progressive neurodevelopmental disorder that emerges after birth, typically becoming evident in early childhood. Although most symptoms are not initially noticeable, they gradually develop as the child ages. Patients with RTT usually develop normally until about 6 to 18 months of age, when their development begins to plateau. An early indicator of neurological effects is the onset of postnatal microcephaly by the age of two. Subsequently, patients start to display autistic traits, such as stereotypic, repetitive behaviors, social withdrawal, and a drastic loss of motor coordination[244].

Interestingly, the expression levels of *MECP2* correlate with neuronal maturation. While levels are low during embryonic development, they progressively increase during postnatal neuronal maturation[245,246]. Utilizing an inducible RTT model, which specifically deletes *Mecp2* in adult mice, reproduces the phenotypes seen in germline KO mice and highlights the gene’s significant neurological function in adulthood[247]. These insights are particularly important for understanding the therapeutic potential in treating RTT, as the disorder likely requires lifelong treatment to address MECP2 loss and dysfunction.

In 2007, Adrian Bird's lab successfully restored endogenous *Mecp2* expression in hemizygous male and heterozygous female adult mice, thus reversing many RTT-related phenotypes[248]. This paved the way for the development of RTT gene replacement therapies. However, pre-clinically tested therapies often led to *MECP2* overexpression, causing severe off-target defects[249,250]. Consequently, several novel strategies have been employed to find suitable delivery vectors that could accurately transduce *MECP2* primarily in brain cells without causing harmful side effects. A recent study employed *Toxoplasma gondii*, leveraging its ability to cross the blood-brain barrier and its specific secretory system to deliver Mecp2 into neurons in the brain[251].

While *MECP2* was among the first genes identified in connection with ASD; more recently, an increasing number of genes involved in chromatin modeling have been discovered, including *CHD8*. Mutations in *CHD8* are highly penetrant risk factors for ASD and have been recognized as such for over a decade[28]. *CHD8* is now known as one of the most frequently mutated loci in individuals with ASD[226,252,253]. *CHD8* belongs to the ATP-dependent chromatin remodeling family, which influences gene expression, chromatin dynamics, and cell survival through interacting with transcriptional complexes, transcription factors, and histone-modifying complexes[254,255]. Individuals carrying *CHD8* mutations exhibit a distinctive phenotype, characterized by one prominent feature of a significantly enlarged head size (macrocephaly). Additionally, patients with *CHD8* mutations often present with ID, cognitive impairments, delay in speech development, and social interaction deficits[256]. Multiple KO mouse models of *CHD8* have been generated to explore the molecular consequences of *CHD8* deficiency. Complete loss of *CHD8* results in embryonic lethality[257]; *CHD8* haploinsufficient mice, however, recapitulate several of the characteristics and phenotypes observed in affected patients. Notably, *Chd8* haploinsufficient mice exhibit macrocephaly, anxiety, and atypical social behavior, aligning with findings in patients[258–261].

Several studies have explored the downstream effects of *Chd8* deficiency, showing that most differently expressed genes are primarily associated with chromatin and histone modifications and cell-cycle regulation[262]. The latter aspect may be connected to the observed macrocephalic phenotypes. Moreover, given that macrocephaly may arise due to increased proliferation and migration during neurodevelopment, several studies have investigated this possibility, though results remain inconsistent. Durak and colleagues reported defective neural progenitor proliferation and differentiation, with an increase in cell cycle exit, largely due to impaired Wnt signaling[261]. In contrast, Gompers et al. reported enhanced proliferative capacities in RGs and intermediate progenitors[260]. These discrepancies may indicate cell-autonomous and non-cell-autonomous mechanisms, effects that are specific to certain time points, and variations based on gene knockouts.

While delineating the cellular and molecular functions for the above-described classes of genes was relatively straightforward, there are other intriguing cases with puzzling functions. One such example is *SETD5*. *SETD5* loss-of-function variants are highly common in individuals with ID. Patients often exhibit stereotypical and repetitive behaviors, along with symptoms of obsessive-compulsive disorder and ASD[263–265]. Using KO mouse models of *Setd5* demonstrated that *Setd5* homozygous mice are embryonically lethal around E10.5, showing failure of neural tube closure, defects in cardiovascular development, and increased cell cycle arrest[266]. Instead, *Setd5*$^{+/-}$ haploinsufficient mice recapitulate ASD-relevant behavioral traits and show impaired learning and memory. Along this line, *Setd5*$^{+/-}$ mice exhibit abnormal synaptic plasticity and connectivity[267–269].

SETD5 is a SET-domain-containing protein and functions as a histone methyltransferase[270]; however, it has been reported to actually lack this enzymatic activity[266,267,271,272]. Instead, Setd5 contributes to epigenetic regulation and indirectly controls gene expression by binding to chromatin-regulating complexes, such as the Paf1 (polymerase-associated factor 1) and Hdac3 (histone deacetylase 3) complexes[266,267]. PAF1 regulates various histone modification cascades and interacts with RNA polymerase II (RNA Pol II), thus influencing, for example, transcriptional elongation[273]. HDAC3 serves as a histone deacetylase and plays a crucial role in chromatin remodeling, functioning as a transcriptional regulator[274].
In summary, Setd5 regulates RNA Pol II levels, most likely due to its interaction with the Paf1 complex. Although the recruitment of Hdac3 is not directly influenced by the loss of *Setd5*, it was shown that Setd5 preferentially targets transcription start sites occupied by Hdac3. Thereby, it potentially modulates chromatin states by synchronizing RNA Pol II recruitment with Hdac3-mediated deacetylation[267]. Notably, considering the impaired memory formation seen in *Setd5*$^{+/-}$ mice, histone deacetylation could be an important mechanistic factor. Similarly, *Hdac3* has been identified as a negative regulator of long-term memory formation[275].

In conclusion, a large part of ASD-associated genes encode proteins that function as transcriptional regulators, including transcription factors, histone modifiers, and chromatin remodelers. Their broad regulatory roles make it challenging to identify their specific genomic targets and to determine their transcriptomic consequences. These genes are broadly involved throughout brain development and are influenced by several factors such as cell type, brain region, and developmental stage. For example, transcriptional regulators are crucial during early neurodevelopment, a period characterized by highly dynamic chromatin changes. Overall, the complexity in gene function and timing complicates the development of therapeutic interventions and underscores the need for a more thorough understanding of the involved regulatory cascades.

1.3.3 Balancing protein synthesis and degradation in ASD

Proteostasis, involving both protein biogenesis and protein breakdown, requires the coordination of several interconnected pathways, including protein synthesis, proper folding, and protein clearance[276,277]. Cellular proteostasis is a dynamic process influencing the fate of a protein from synthesis to degradation. The latter is primarily facilitated by the ubiquitin-proteasome system (UPS), which is pivotal in maintaining protein homeostasis in eukaryotic cells[187,278]. Genes that encode regulators of protein synthesis, including *FMR1, TSC1/2*, and *PTEN*, as well as those involved in degradation, like *UBE3A, TRIP12*, and *CUL3*, are significant contributors to ASDs.

Fragile X Syndrome (FXS) represents a prominent link between abnormal protein synthesis and ASD, stemming from mutations in the *fragile X mental retardation (FMR1)* gene. Notably, 15%-30% of patients with FXS are also diagnosed with ASD, and conversely, up to 6% of those presenting with ASD are found to have FXS[279,280]. Patients with FXS frequently have ID, anxiety, ADHD, and sensory processing deficits, with more severe manifestations commonly observed in males than in females due to the syndrome's X-linked inheritance[281]. The transcriptional silencing of *FMR1* leads to a deficiency of the Fragile X mental retardation protein (FMRP), which is a critical regulator of protein translation. FMRP serves as mRNA binding proteins, responsible for localization, stabilization, and translation of approximately 4% of mRNA in the fetal brain[282]. Upon absent FMRP expression, basal protein synthesis increases due to FMRP's role as a repressor. *In vivo* studies with *Fmr1* KO mice showed increased signaling through the mammalian target of rapamycin complex 1 (mTORC1). Furthermore, several targets of FMRP encode mTORC1 repressors, such as *TSC1* and *PTEN*. Therefore, the silencing of FMRP may indirectly affect protein synthesis by hindering the translation of mTORC1 signaling components[283,284].

Currently, numerous studies have connected alterations in protein degradation to ASD, highlighting mutations in genes that encode components of the UPS[15,187,278,285]. Protein degradation in the UPS occurs through a cascade involving three classes of enzymes: ubiquitin-activating enzymes (E1), ubiquitin-conjugating enzymes (E2), and ubiquitin ligases (E3): E1 enzymes activate ubiquitin, which subsequently gets transferred to an E2 enzyme, conjugating ubiquitin to an E3 ligase[187,286]. Following this conjugation step, an E3 ligase catalyzes the covalent attachment of ubiquitin to the target protein. Repeated cycles of ubiquitination result in the formation of a polyubiquitin chain that is essential for the target protein to be recognized and degraded by the 26S proteasome[187,286]. Conversely, deubiquitinating enzymes (DUB) can reverse the ubiquitination process, enabling the reuse of ubiquitin moieties for subsequent targeting[287].

While E2-conjugating enzymes can interact with several E3 ligases, substrate specificity and target recognition are primarily determined by ubiquitin ligases. Moreover, all E2 enzymes interact with one E1 and one or more E3's, although no

universal rule applies on how E2 enzymes specifically recognize their cognate binding partners[288,289].

The role of the UPS in neurons makes it indispensable for maintaining physiological functioning. Protein synthesis and degradation balance numerous neuronal processes, including dendritic morphogenesis[290,291], axon guidance[292,293], synaptic maturation and plasticity[187], and neurite outgrowth[294]. Abnormalities in the UPS can cause proteins to accumulate, leading to an excess of aggregated deposits that disrupt this homeostatic system. A common hypothesis suggests that mutations in the UPS alter protein levels, resulting in an excess of protein substrates that interfere with a usually balanced system[295].

Considering the extensive number of proteins involved in the UPS and its importance for neurons, it is unsurprising that some have been genetically associated with neurodevelopmental disorders, such as ASDs[187,278,286]. While the UPS is well-studied for its essential function in degrading brain proteins related to neurodegenerative disorders[296], its role in neurodevelopmental conditions remains less understood. Notably, 10-15% of newly identified genes linked to ID, frequently comorbid with ASDs, are ubiquitin-modifying proteins and their substrates[297].

Notably, Angelman Syndrome is a significant neurodevelopmental disorder associated with proteasome function, caused by mutations in the *Ubiquitin Protein Ligase E3A (UBE3A)* gene. *UBE3A* selectively targets proteins for ubiquitination and subsequent degradation[285]. Affected patients present severe cognitive impairments, ID, seizures, and excessive laughter[295,298]. Moreover, copy number variations of *UBE3A*, resulting in duplication or triplication of the maternal copy, cause a similar range of defects, including core features of autism spectrum disorders[299]. A compelling treatment strategy involves restoring *UBE3A* expression by activating the otherwise silenced *UBE3A* gene from the paternally inherited chromosome[300]. Notably, both humans and mice have a functional copy of paternal *UBE3A* in the brain, which remains silenced due to a long non-coding antisense transcript (*UBE3A-ATS*)[300–302]. In order to activate the silenced paternal gene, several approaches have been explored, such as using antisense oligonucleotides (ASO)[303], delivery through adeno-associated virus (AAV)[302], or employing CRISPR/Cas9 approaches[304]. Nevertheless, gene therapy still faces substantial challenges in human applications. Moreover, identifying the optimal timing for treatment is essential, as restoring gene function during early development or around birth improved many of the characteristics linked with Angelman syndrome in mice[305].

A protein with a similar function is TRIP12. *De novo* missense, frameshift, and loss-of-function mutations, impacting distinct protein domains of *TRIP12*, were identified in patients with childhood-onset ASD. In addition to the core symptoms of ASD, carriers of *TRIP12* mutations exhibit several comorbidities, including ID and developmental delay, ADHD, and facial dysmorphic features[306,307]. Its significance during

neurodevelopment may stem from its crucial function in regulating the cell cycle, as *Trip12*$^{-/-}$ knock-out mice show reduced cell growth due to the abnormal activation of the cyclin-dependent kinase inhibitor p16[308].
TRIP12 is part of the HECT (homologous to E6AP C-terminus) family of E3 ligases and is crucial in targeting proteins for degradation. Overall, E3 ligases, including HECT, RING, and RBR ligases, differ mainly in their mechanisms of ubiquitin transfer[309,310]. HECT ligases attach ubiquitin through an intermediate process, where ubiquitin is initially transferred from the E2 to the ligase, followed by its conjugation to the target protein. In this process, substrate specificity is primarily enforced by the HECT ligase itself[309]. Thus, a deubiquitinase eliminates the ubiquitin moiety to avoid auto-degradation of TRIP12 and supports the attachment of ubiquitin to the target protein. Here, *USP7*, also a high-risk gene for ASD within the UPS, facilitates the reversal of TRIP12's self-ubiquitination, underscoring an essential interaction in the system[309,311,312].

Recently, we[313] and others[314,315] have demonstrated that *Cullin3* (*Cul3*), a high-risk ASD gene and crucial component of the UPS, plays a role in regulating cytoskeletal proteins. Patients with *de novo* loss-of-function mutations in *CUL3* exhibit a range of comorbidities, such as varying degrees of ID, ADHD, motor deficits, epileptic seizures, and dysmorphic facial features[316].
Cytoskeletal proteins are crucial for maintaining structural integrity and stability during the complex processes of cell division, proliferation, and migration. We could show that Cul3 is essential during early neurodevelopment, and its diminished function can lead to defects in neural cell migration, resulting in the accumulation of neuronal cells in lower cortical layers. The impaired neural migration is largely due to Cul3 regulating actin cytoskeleton dynamics and adhesion protein levels[313]. Loss of *Cul3* results in a disordered actin structure in protruding neural progenitor cells *in vitro*, likely correlating with the observed migration defects. Interestingly, inducing *Cul3* deletion in juvenile animals did not reveal behavioral abnormalities observed in animals with germline haploinsufficiency, highlighting Cul3's critical role during neurodevelopment[313].
Moreover, through proteomic analyses, we identified specific targets of Cul3 that mediate the migration defects observed both *in vitro* and *in vivo*. Surprisingly, we found a direct correlation between Cul3 and Pls3 levels[313]. With reduced Cul3 protein, Pls3 levels were increased. Pls3 influences cell migration in a cell-autonomous manner by controlling actin cytoskeleton organization, and its protein levels may act as a determining factor of migration properties. Interestingly, by restoring *Cul3* to wild-type levels, we could effectively rescue the altered cellular traits *in vitro,* thereby adjusting the protein levels of its identified targets[313].

In summary, protein homeostasis in the central nervous system is carefully maintained by balancing protein synthesis and degradation. Together, these findings suggest that the UPS could play a significant role in the etiology of ASD, influencing downstream processes like neurogenesis, neural cell migration, proliferation, and apoptosis. Thus, focusing on this key pathway could be a promising strategy for developing treatments

for ASD. However, despite our understanding of key genetic elements within these pathways and their direct targets, complementary approaches are required to capture subsequent changes in downstream cascades. For instance, UPS enzymes typically target multiple proteins. Consequently, adjusting these protein levels to restore gene function or physiological processes may inadvertently trigger complex compensatory reactions. Therefore, a nuanced approach is needed to manage and predict the outcomes of such interventions.

1.4 Conclusion and open questions

Studies on whole exome sequencing of ASD have identified over 100 high-risk genes associated with ASD susceptibility. Each gene has a significant impact, as protein-truncating mutations result in a marked increase in ASD risk. The extensive list of identified risk genes has resulted in numerous studies focusing on converging aspects of the disorder. Rather than examining a wide array of genes and conditions, this approach may allow centering on a selected group of genes that share similar biological functions and downstream effects. Indeed, it clarified the overall characteristics of the disorder, highlighting common pathways related to synaptic function, chromatin regulation, and protein synthesis and degradation[18,317]. On a cellular level, it was recognized that several processes are associated with impairments in neurogenesis, neuronal migration, synaptic functioning, and activity-dependent transcription and translation[15,16,30].

While these discoveries are crucial for understanding the biological processes underlying ASD, fundamental questions remain: How do mutations in numerous genes lead to phenotypically analogous disorders? How closely related are genetically defined ASDs? Moreover, at what biological level do distinct ASDs converge into common themes?

Additionally, current research often focuses on single monogenic models of ASD instead of screening a broader spectrum of risk genes for a comparative analysis. Such investigations make it challenging to determine the shared pathways among various genes that presumably form important core aspects of ASD. While several studies have tried to address this shortcoming by integrating data from multiple sources[17,18,318–320], this often has the downside of comparing various brain regions, cell types, and developmental stages that were experimentally different from each other. Procedural biases can arise when experiments are carried out in multiple batches instead of systematically addressing multiple variables at once. As such, most studies utilizing sequencing technologies require concurrent series of experiments involving various animals or subjects to tackle scientific questions across different scales (e.g., on transcriptomic and epigenomic levels).

Furthermore, the impact of sex remains largely unexplored up to now. This neglect of a balanced representation may stem from inherent experimental biases that typically

involve only male subjects. Such biases could mask important variations and outcomes relevant to both sexes. Consequently, this imbalance may limit the applicability and accuracy of research findings across different populations.

In conclusion, significant steps have been made to stratify affected biological processes contributing to ASD. The concept that various ASD-risk genes could converge on systemically smaller molecular functions holds the potential to refine patient treatments by identifying commonalities. However, this effort may be challenged since several ASD genes serve as crucial regulatory elements in various developmental processes with varying temporal expression across different stages.

2 Results

Note: At the time of this thesis submission, the results were simultaneously in revisions at Nature*. Therefore, excerpts or figures from this work are expected to be published and will be available in their current or slightly revised form in the future.*

Prior studies have compared human brain tissue from individuals with ASD to control subjects, underscoring some common features[18,317]. However, such investigations are often limited by the rarity of available samples, undefined genetic causes, and a lack of developing tissue. To address some of these limitations, broader genetic screenings in murine and human stem cell-derived brain tissue models have been used. However, these models often employ mosaic mutants, where less than 0.1% of cells are affected, complicating the interpretation of genetic consequences[321,322].

Given the complexity of ASD's etiology and the emerging evidence suggesting developmental commonalities along with shared cellular and molecular pathways, this work aimed to systematically evaluate monogenic mouse models of ASD at key developmental stages. With the advent of multi-omics sequencing technologies, we could simultaneously explore gene expression and chromatin states from the same animal, tissue, time point, and nuclei. This approach aimed to uncover dynamic shifts in cellular and molecular landscapes naive to given hypotheses. Additionally, we set out to examine differences between females and males without introducing specific biases by conducting identical experiments for both sexes and analyzing them simultaneously at an unbiased genetic level. Ultimately, this project sought not only to identify dynamically affected processes during brain development but also to explore points of divergence and convergence.

2.1 Single-nucleus multi-omics profiling of 251 mouse brain samples

Here, we employed single-nucleus multi-omics sequencing to analyze and compare 251 samples collected from mouse lines carrying mutations in high-risk ASD genes, sampled at different developmental stages in males and females and from two brain regions (Fig. 10a). Specifically, we analyzed mice carrying constitutive mutations in *Ash1l*, *Bckdk*, *Cul3*, *HnrnpU*, *Kdm6b*, *Kmt5b*, *Ptchd1*, *Setd5*, *Trip12*, *Usp7* or *Wac,* together with wild-type mice serving as controls (Extended Data Fig. 1a). The rationale behind selecting these mouse models of ASD was multilayered; we aimed to include genes representing a variety of functional pathways, different inheritance modalities, and displaying ubiquitous expression (Extended Data Fig. 1b, c). All selected genes are categorized by the SFARI database as high-confidence ASD risk genes (SFARI Gene Score 1, V2023 Q4), except *Usp7,* which is listed as a strong candidate (SFARI Gene Score 2). In all cases, except for *Bckdk* and *Ptchd1*, we studied mice carrying heterozygous mutations to model *de novo*, heterozygous, loss-of-function mutations in patients[30,306,307,323–328]. For *Bckdk*, we studied homozygous mice as this gene is

found in an autosomal recessive form of ASD[329,330], and for *Ptchd1,* we studied hemizygous males as the gene is located on the X chromosome, and primarily male patients have been reported so far[331,332].

From all these mouse strains, we profiled cells obtained from the cerebral cortex of mice at three different developmental stages: embryonic day (E)14.5, postnatal day (P)4, and P14 (Fig. 10a). To study potential sex-specific effects, we analyzed all time points and genotypes in both females and males. Finally, to evaluate differences across brain regions, we additionally profiled the cerebellum obtained from male P4 mice (Fig. 10a). These data provide a thorough view of cell states across ASD-associated mutants and allowed us to uncover converging as well as diverging phenotypes across genotypes, sexes, and brain regions.
Gene expression and chromatin accessibility provide complementary information about cell states, capturing the cells' transcriptional profiles and epigenetic states. With the advent of droplet-based single-cell multi-omics profiling, it is now possible to obtain matched gene expression and chromatin accessibility profiles for thousands of single cells in one experiment. However, existing methods suffer from high costs and low scalability of sample numbers. Here, we optimized a method for multiplexing samples for combined single-nucleus RNA-seq and ATAC-seq (snRNA-seq and snATAC-seq).

Specifically, we utilized a multiplexing approach employing cholesterol-modified oligos (CMOs)[333] as sample-specific barcodes (Fig. 10a). In this way, we performed single-cell multi-omics profiling across a total of 45 conditions and 251 samples, allowing us to monitor changes in transcriptional and chromatin states with single-cell resolution across a broad range of genetic ASD mouse models (Fig. 10a, and Methods).

In total, we collected the molecular profiles of 200,787 nuclei (forebrain: 66,969 at E14.5, 56,260 at P4, 59,974 at P14; cerebellum: 17,584 at P4) and detected an average of ~3,900 transcripts, ~2,000 genes, and ~4,200 fragments per cell at a median sequencing depth of ~25,000 reads/cell (Fig. 15a, Extended Data Fig. 1d), aligning with standard recommendations for these types of analyses.
We performed Leiden clustering separately for each brain region and time point, followed by algorithm-assisted and manual cluster annotation, which identified 12 (E14.5), 22 (P4), 26 (P14; cortex), and 16 (P4; cerebellum) major cell types (Fig. 10b-d, 15b, and Methods). All samples and genotypes were similarly distributed across clusters (Fig. 15c, Extended Data Fig. 2a-c). Each cluster was annotated according to established cell type specifications using the expression of canonical cell type markers of various regions of the mouse brain (Fig. 15d, Extended Data Fig. 2d-g). The earliest stage (Fig. 10b) was primarily composed of cortical plate neurons (CP, expressing *Bcl11b, Satb2*), radial glia (RG; *Pax6, Gas1*) and intermediate progenitors (*Mki67, Top2a, Unc5d*). Additionally, we detected a small fraction of medial-ganglionic eminence (MGE)-derived interneurons (*Nxph1*). At postnatal stages (Fig. 10c, d), we were able to differentiate between upper (Layer II-IV and Layer II/III; *Cux1, Cux2, Bcl11a*) and lower cortical layers (Layer V/VI DLCPN; *Bcl11b, Ldb2, Pex5l*) including

cortico-thalamic projection (Layer V/VI CThPN and Layer IV - VI; *Gse1, Tle4 Zfpm2)* and near-projecting neurons (Layer V/VI NP; *Epha6, Lingo2*). Since our samples included the hippocampus, we distinguished between hippocampal cells (*Cacna2d3, Nr3c2, Epha6*) and adjacent CA1-Subiculum PN (*Tshz2, Tshz3*). Glial cells were first observed at P4, including oligodendrocyte precursor cells (OPCs; *Pdgrfa, Cspg4*) and their maturation stages (postmitotic; *Itpr2, Plp2*, pre-myelinated; *Mpb*), astrocytes (*Ptprz1, Slc1a3, Apoe*), and microglia (*Hexb, Cx3cr1, Csf1r*). In line with the timely cortical positioning of interneurons, we identified several interneuron populations from P4 onwards, including caudal-ganglionic eminence (Int CGE (Vip), Int. Sncg (Vip); *Adar2b, Gad2, Vip, Synpr*) and MGE-derived interneurons (Int MGE (Pvalb), Int. Sst, Int. Lamp5; *Erbb4, Lamp5, Nxph1, Sst*). Our dataset thus provides a comprehensive view of the cellular landscape of the mouse cerebral cortex at different developmental stages (Fig. 10b-d). This cellular classification is consistent with previous reports[334–337] and serves as a reference against which we can examine the effects of ASD mutations in each analyzed mouse model.

2.2 ASD mutants show radial glia lineage progression defects

To explore how ASD mutations affect cortical development, we initially compared the relative proportion of each cell type in all mutant animals, collectively, to wild-type controls (Extended Data Fig. 3a-c). While the cell type abundance was generally comparable across the two groups, the clusters of cortical plate and oligodendrocyte progenitor cells (OPCs) were significantly depleted in mutants at E14.5 and P4 (Extended Data Fig. 3a, b), respectively. Separating the data by genotype, we confirmed that these changes were consistent across all mutants, revealing a high degree of convergence in the affected cell types (Fig. 10e-g). Nevertheless, some mutants, such as *Cul3*, *HnrnpU*, *Kdm6b,* and *Ptchd1*, showed larger trends. In all mutants, the reduction of cortical plate cells observed at E14.5 was concurrent with an increased proportion of radial glial cells (Fig. 10e). At P4, neuronal cell numbers were similar between mutants and wild types; however, at this stage, mutants displayed a reduction of immature astrocytes and OPCs (Fig. 10f). This independently suggests a delay in the radial glial cell lineage progression, potentially impacting the gliogenic switch at later stages. This delay was particularly pronounced in the mutants exhibiting larger differences in RG and CP cell numbers at E14.5, as, for example, observed in *Cul3*, *HnrnpU*, *Kdm6b*, *Ptchd1*, and *Setd5* mutants. At P14, OPC numbers continued to be lower across all ASD mutants, while the number of other cell types had normalized (Fig. 10g).

To gain insights into the source of the observed alterations, we investigated the radial glia cell lineage progression by performing a pseudo-time analysis on the E14.5 dataset (Fig. 10h). We identified two subpopulations of radial glial cells (RG1 and RG2, Fig.10h). RG1 cells were distinguished from RG2 by the expression of proliferation markers, such as *MKi67*, indicating that RG1 cells were in a state of active cell division.

Analysis of these two cell populations revealed that mutant RG cells tend to remain in the proliferating RG1 state (Fig. 10i) at the cost of delayed differentiation.
Next, we investigated differentially regulated genes in RG1 cells that were shared across mutants by analyzing differences in gene expression between all the mutants and the wild-type RG1 cells. Here, shared differentially regulated genes could be candidates for contributing to the observed common cellular phenotype. In mutants analyzed collectively, we observed a significantly lower expression of two genes, *Rsrp1* and *Galnt17* (Fig. 10j). *Rsrp1* encodes a protein interacting with members of the spliceosome. Although its function is mostly unknown, recent studies suggest a role for this protein in regulating splicing and the cell cycle[338]. *Galnt17* is an N-acetylgalactosaminyltransferase whose loss of function was associated with global developmental delay, neurodevelopmental phenotypes, and neural differentiation defects[339]. While these two genes are potential candidate biomarkers for neurodevelopmental delays, they are unlikely to be the sole cause of the observed RG progression phenotype. Thus, we further dissected the molecular differences between mutant and control RG1 by analyzing the single mutants separately. Different mutants showed largely different amounts of differentially expressed genes (DEGs, false discovery rate, FDR < 0.1) in RG1 cells, with some mutants showing none, suggesting that the delay originated earlier during development in some cases. *HnrnpU* stood out as the most affected mutant, with over 150 differentially expressed genes. Intriguingly, while other mutants showed fewer DEGs, some DEGs were detected in multiple mutants. For example, *HnrnpU, Kdm6b,* and *Kmt5b* mutant mice showed significant downregulation of *Setbp1*, a gene found to be mutated in ASD and implicated in neural differentiation and cortical fate commitment[340]. Similarly, *Nrcam*, another ASD gene encoding for a cell adhesion molecule and associated with neurodevelopmental delay[341], was found to be significantly downregulated in both *Kdm6b* and *Kmt5b* mutant RG1 cells.
Altogether, our data indicate a common trend of delayed radial glia lineage progression across all ASD mutants. However, our analysis suggested a limited convergence in the potential underlying mechanisms.

2.3 ASD mutants converge on altered gene expression at early postnatal stages

Differences in the abundance of specific cell types are critical for the proper wiring of the cortex, just as their functional properties are closely tied to gene expression patterns. To investigate the impact of the selected ASD mutations on gene expression across developmental stages and cell types, we conducted a comparative analysis between control and mutant samples.
First, we focused on identifying potential common changes across all mutants. Thus, we performed pseudo-bulk differential gene expression analysis (Fig. 11a). In this method, cells of a particular cluster were aggregated into a single pseudo-bulk gene expression profile. We then compared the gene expression profiles of each cell type across all mutants collectively against those of the wild-type controls (Fig. 11a, *all*

mutants). This analysis revealed a large number of DEGs at P4 in Layer II/IV (715 DEGs, adjusted p-values, *p-adj.*<0.05) and Layer V/VI DLCPN (600 DEGs) neurons. Of these, the majority were downregulated in mutants. We found either a minor number or no DEGs in the other cell types and time points when considering all mutants together. Given the nature of the pseudo-bulk analysis, the number of sequenced cells per cluster was not expected to influence these findings. In agreement, we did not observe a linear relationship between the total number of sequenced cells and the number of DEGs (Extended Data Fig. 3d). Nevertheless, we repeated the analysis by performing pseudo-bulk analysis aggregating cell types into cell subclasses (e.g., aggregating all excitatory neurons, Extended Data Fig. 3e), thus increasing cell numbers for each comparison. This analysis confirmed that excitatory neurons at P4 were the main cell subclass showing shared DEGs across mutants (Extended Data Fig. 3e').

Next, we analyzed each mutant separately by comparing them to wild types. For most of the genotypes, we identified over 700 DEGs distributed across cell subclasses and time points, where repeated DEGs were counted only once (Extended Data Fig. 3f). At E14.5, we observed few changes except for *HnrnpU* and *Kdm6b* mutants, which exhibited a considerable number of DEGs impacting CP, RG, and SVZ migrating cells (Fig. 11a, left). Conversely, at P4, our analysis revealed a substantial number of DEGs across genotypes and multiple cell types (Fig. 11a, center). Neurons were the most profoundly impacted cells, with most DEGs identified in excitatory neurons.

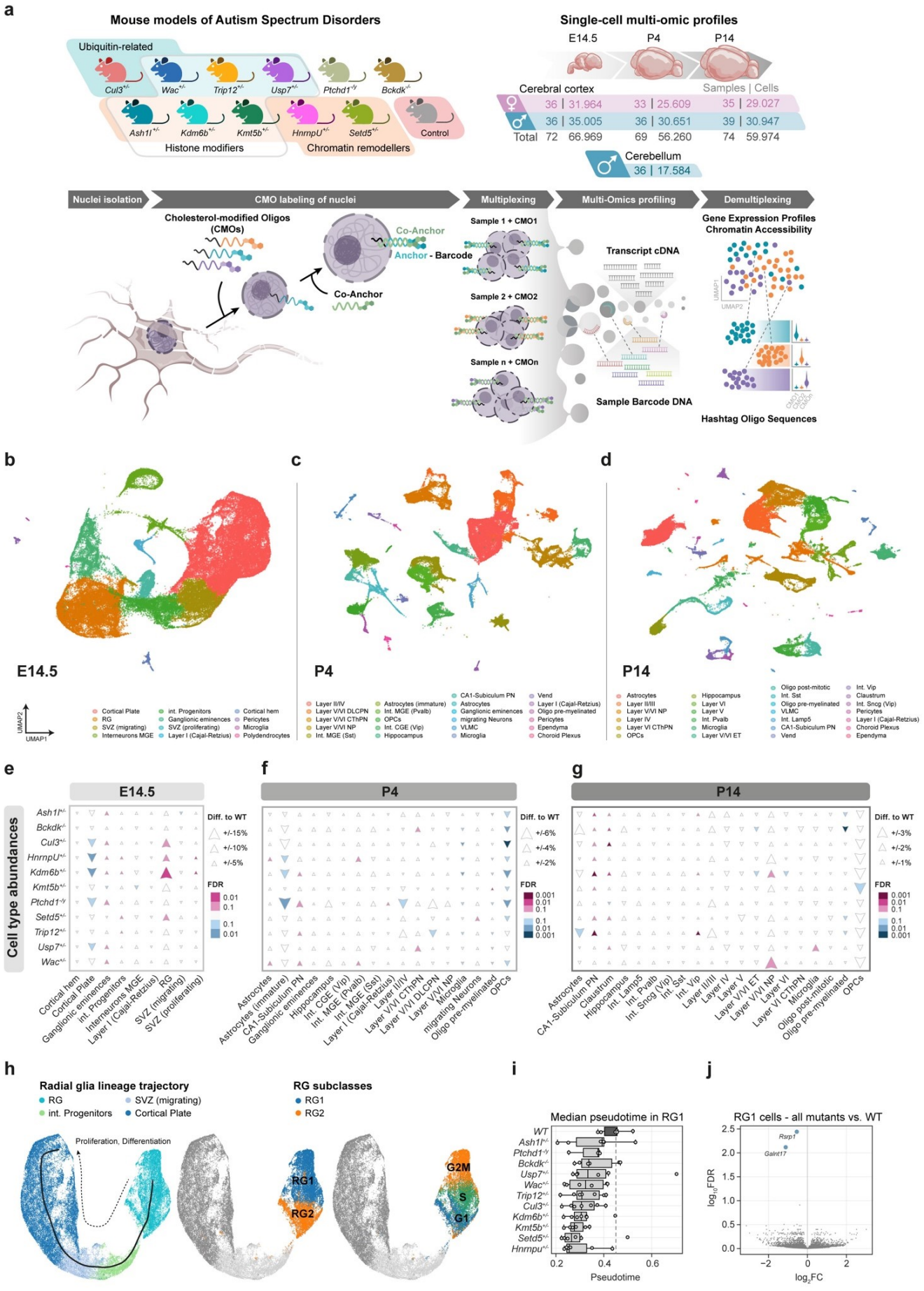


Figure 10: Large-scale multi-omics profiling of high-risk ASD genes.

a, Simultaneous analysis of the transcriptome and chromatin accessibility profile of brain samples obtained from 11 monogenic mouse lines, carrying each a mutation in one high-risk ASD gene. Overview of the experimental design with the total number of samples and cells analyzed per time point indicated. **b-d**, UMAP visualization of integrated snRNA-seq and snATAC-seq data from individual time points. Cell clusters are colored based on cell type assignment. **e-g**, Changes in cell type abundances in individual ASD mutants across the analyzed time points. Arrows represent the relative difference in percentage compared to wild-type (WT) controls. Nominal p-values are shown. **h**, Pseudo-time analysis of the radial glia lineage in ASD mutants at E14.5. (**h**, left) The root is the radial glial (RG) cell cluster progressing towards cells of the cortical plate (arrow). (**h**, center and right) Two sub-populations of RG cells, termed RG1 and RG2, were distinguished; RG1 cells are in G1 and S phase, and RG2 cells are in G2 phase. **i**, Median pseudo-time analysis of ASD mutant RG1 cells demonstrating a consistent delay in ASD mutants compared to WT. **j**, Differential gene expression analysis between all mutants collectively and wild-type RG1 cells highlights two significant downregulated genes, associated with cell cycle, neuronal maturation, and differentiation.

Additionally, several mutants showed a substantial number of DEGs in inhibitory neurons and glial cell types. At P14, the number of DEGs was lower in comparison (Fig. 11a, right). Importantly, despite having more statistical power when analyzing all mutants together, the results for individual mutants (aggregating all replicates of the same genotype) almost always showed more DEGs, indicating the presence of many genotype-specific changes. Additionally, the distribution of up- and downregulated DEGs was more balanced in individual mutants than in the collective analysis. However, some mutants showed a small number of DEGs across all analyzed time points. These include mice with mutations in histone modifier genes, such as *Kmt5b, Setd5,* and *Wac* (Fig. 11a, Extended Data Fig. 3f). This suggests that mutations in this class of genes, at least at these time points and under resting conditions, may have subtle effects on altering gene expression, impacting only a few genes or causing small changes in transcript levels that are challenging to capture with traditional DEG analysis. With respect to the number of DEGs, we noticed no obvious difference between heterozygous, homozygous, and hemizygous mutants, i.e., *Bckdk* and *Ptchd1*.

Numerous mutants exhibited a significant overlap of DEGs across time points (Extended Data Fig. 3g), independently validating these DEGs and indicating that multiple molecular processes are affected throughout development. For example, *HnrnpU* animals showed a marked overlap during early and perinatal development with a high proportion of genes associated with the cell cycle (e.g., *Ccnd2, Cdk4, Mef2c*), axonogenesis (e.g., *Dscam2, Sema5a, Robo2*) and transmembrane transporters (e.g., *Cacnb3, Gabra4, Gria4)*. *Trip12* mutants shared several DEGs related to metabolic processes (e.g., *Eef1a1* and *Nceh1*) and synaptic signaling (e.g., *Nrxn3, Syt5, Rims1*) at P4 and P14 (Extended Data Fig. 3g).
Neuronal subclasses shared large proportions of DEGs, even across mutants (Extended Data Fig. 3h). This trend was particularly pronounced in excitatory neurons at P4, where about 10% of DEGs were shared by at least four of the analyzed mouse models (Extended Data Fig. 3i). In contrast, we observed minimal DEG overlap between neuronal and non-neuronal cells within the same mutant (Extended Data Fig. 3h).

To gain insight into the genes most commonly affected in mutants, we compiled a list of the most frequently identified DEGs across mutants and cell types (Fig. 11b). Notably, this list included a large proportion of ASD genes (34%) and was enriched for genes encoding synaptic-related proteins (*q-value* 1.03^{-15}) (Extended Data Fig. 3j). The corresponding proteins localize both in the pre- and post-synaptic compartments and are connected to processes such as synaptic translation, actin cytoskeleton, synapse organization, and the functioning of membrane channels and receptors (Fig. 11b, Extended Data Fig. 3j). Remarkably, the directionality of the alterations in these sets of DEGs were largely consistent across mutants. Specifically, several mutants showed a broad upregulation of microtubule-related transcripts, including *Tubb5*, *Tubb3*, *Tub1a* and *Tubb2b*. The corresponding proteins are known for their role in the correct positioning and morphology of neurons. Loss-of-function mutations in several of these genes have previously been linked to brain developmental disorders[172,174,342,343]. Conversely, transcripts related to potassium ion channels, such as *Kcnh7*, *Kcnip4*, *Kcnma1*, and *Kcnt2*, were frequently downregulated in mutants, primarily affecting excitatory neurons and thereby potentially impacting their intrinsic excitability.
Overall, these results pinpoint critical periods while highlighting variations in developmental trajectories across ASD mutants, with some having greater impacts in earlier and others in later stages. Furthermore, we have identified shared DEGs across ASD mutants, underscoring the presence of convergent mechanisms potentially influencing cortical development in disease conditions.

2.4 Common pathway disruptions in ASD mutant mice

To identify biological processes affected by ASD mutations, we employed Gene Set Enrichment Analysis (GSEA). GSEA relies more on the expression patterns of gene groups rather than strictly depending on DEG cutoffs of individual genes, thereby offering a broader perspective on cell states.
Initially, we performed GSEA in the individual mutants at the cell subclass level. This analysis further indicated that the effects of ASD mutations were most pronounced at P4, aligning with the results of the DEG analysis. However, GSEA also highlighted a few differences, especially at E14.5 and P14 (Fig. 11c, Extended Data Fig. 4-6a). For example, we identified enrichment for some gene sets in neural lineage cells at E14.5 in *Cul3*, *Kmt5b,* and *Setd5* in addition to *HnrnpU* and *Kdm6b* mutants.

To gain insights into pathways commonly affected across multiple genotypes at the three different developmental stages, we generated networks based on GO terms affected in at least 50% of the mutants displaying molecular phenotypes. In this analysis, we focused on analyzing the excitatory cell lineage, the cell subclass with the majority of the changes. Our results indicate that at E14.5, most of the affected mutants exhibited changes in pathways associated with cell cycle regulation and neuronal projection development (Fig. 11d left, Extended Data Fig. 4a). At P4, mutants

displayed a marked convergence on pathways related to synaptic and ion channel functions (Fig. 11d, bottom). Synapse-related transcripts were also largely affected at P14 (Fig. 11d, right), however, at this stage, we observed more genotype-specific changes and a weaker convergence than for P4 (Extended Data Fig. 4b, c).

Although inhibitory neurons generally showed a slightly lower number of enriched gene sets than excitatory neurons, they were also similarly impacted, with mostly terms related to synaptic transmission, intracellular signaling, ion channels, and transmembrane transporters (Extended Data Fig. 5a, b). Glial cells were generally less affected than neurons, with the exception of *Cul3* and *Ptchd1* mutants, which showed higher numbers of affected GO terms (Extended Data Fig. 6a). While certain gene sets were observed in excitatory and inhibitory neurons at P4 and P14, in some mutants, those pathways were orthogonally regulated at the two time points (Extended Data Fig. 5). For instance, while processes associated with synaptic transmission and organization were downregulated in *Kdm6b* mutant neurons at P4, they were upregulated at P14.

We further refined our GSEA to identify cell type-specific variations. For example, while both RG and CP showed similarly affected processes related to neurogenesis, they also showed distinct features. For instance, mutations in *HnrnpU* and *Kdm6b* altered cell cycle-relevant transcripts, predominantly in RG cells, likely contributing to the developmental delay observed through pseudo-time analysis. Conversely, processes related to synaptic signaling and development were predominantly impacted in CP cells (Extended Data Fig. 6b). Furthermore, effects were more pronounced in excitatory neurons of Layer II/IV, corticothalamic- and near-projecting Layer V/VI, as well as PV^+ interneurons, while hippocampal and Sst^+ neurons showed milder changes (Extended Data Fig. 7).
Several mutant lines showed deregulation of axogenesis and dendrite morphogenesis-related genes, with the directionality of these changes varying between mutants. DEGs associated with these processes were upregulated in PV^+ and Vip^+ interneurons in most ASD mutants, while they were downregulated in excitatory Layer II/IV neurons. *Cul3* and *Ptchd1* mutants were an exception, showing a significant upregulation in the latter. *Cul3* and *Ptchd1* mutants also stood out for an increase in the expression of genes relevant to synaptic functions in immature astrocytes and Vip^+ interneurons and more scattered or milder effects in other neuronal cell types (Extended Data Fig. 7). Finally, *Ptchd1* and *Setd5* mutants had very limited effects on synaptic gene expression in excitatory neurons of the individual cortical layers. This aligns with previous findings showing that *Setd5* mutations do not impair synaptic protein expression in the hippocampus under naïve conditions[267]. Moreover, hippocampal neurons and interneuron cell types exhibited an upregulation of processes related to protein secretion, whereas these processes were downregulated in excitatory neurons of individual cortical layers (Extended Data Fig. 7).

Finally, due to the link between ASD and excitation/inhibition imbalances[344–347], we further explored the changes in ion channels observed in our ASD mutants across the different time points. Specifically, we analyzed the differential expression of calcium, potassium, and sodium channels in excitatory neurons (Fig. 11e). One of the most commonly affected ion channels in ASD mutants was *Scn1a*. *Scn1a* encodes a sodium channel involved in the generation of action potentials and mutated in patients with Dravet syndrome, a form of intractable epilepsy with autistic features[348]. Intriguingly, mouse mutants showing downregulation of *Scn1a* also frequently exhibited downregulation of *Scn8a* and upregulation of *Scn9a*. The latter is known to physically and genetically interact with *Scn1a*[349,350], suggesting a potential compensatory mechanism. Similarly, several potassium and calcium channels were systematically affected in mutant excitatory neurons (Fig. 11e). These included, for example, *Kcnv1*, a modifier subunit of voltage-gated potassium channels, and *Kcnq3*, which forms channels mediating neuronal M-currents involved in regulating neuronal excitability and mutated in familial epilepsy syndromes[351–353].
Overall, these results reveal the complex and especially dynamic gene expression changes occurring in the cerebral cortex of ASD models, pinpointing pathways and transcripts that may play common roles at different developmental stages of these disorders.

2.5 Unique synaptic states and gene expression changes in ASD mouse models

While we observed striking similarities in the patterns of gene expression and pathway alterations, our analysis also underscored genotype-specific changes. Indeed, at least 50% of the DEGs identified in each cell type were unique to a single mutant (Extended Data Fig. 3i). To investigate these findings further, we enhanced the granularity of our analysis to elucidate genotype-specific cell states. Particularly, we employed SynGO (Fig. 12a), a curated database of synaptic-related genes, to define the specific synaptic changes occurring in each mutant. Despite some commonalities, each mutant showed a unique combination of affected processes, suggesting that every mutation leads to a distinct synaptic state (Fig. 12a'). Specifically, our analysis showed that mutations in the majority of the selected ASD genes affected both post- and presynaptic processes, including synapse organization and cytoskeleton, vesicle release, signaling, and neurotransmitter receptor organization (Fig. 12a'). Interestingly, none of the mutants we studied showed enrichment for transcripts related to axon or dendritic transport, processes often linked to neurodegenerative conditions. Metabolic processes and protein translation at the synapse were impacted in only three mutants: *Bckdk*, *Cul3,* and *Trip12*. This finding is noteworthy as these genes have been linked to functions related to proteostasis[308,310,313,354,355]. Several other differences were noted; for example, both *Ash1l* and *Cul3* mutants showed changes in genes related to the synaptic actin cytoskeleton.

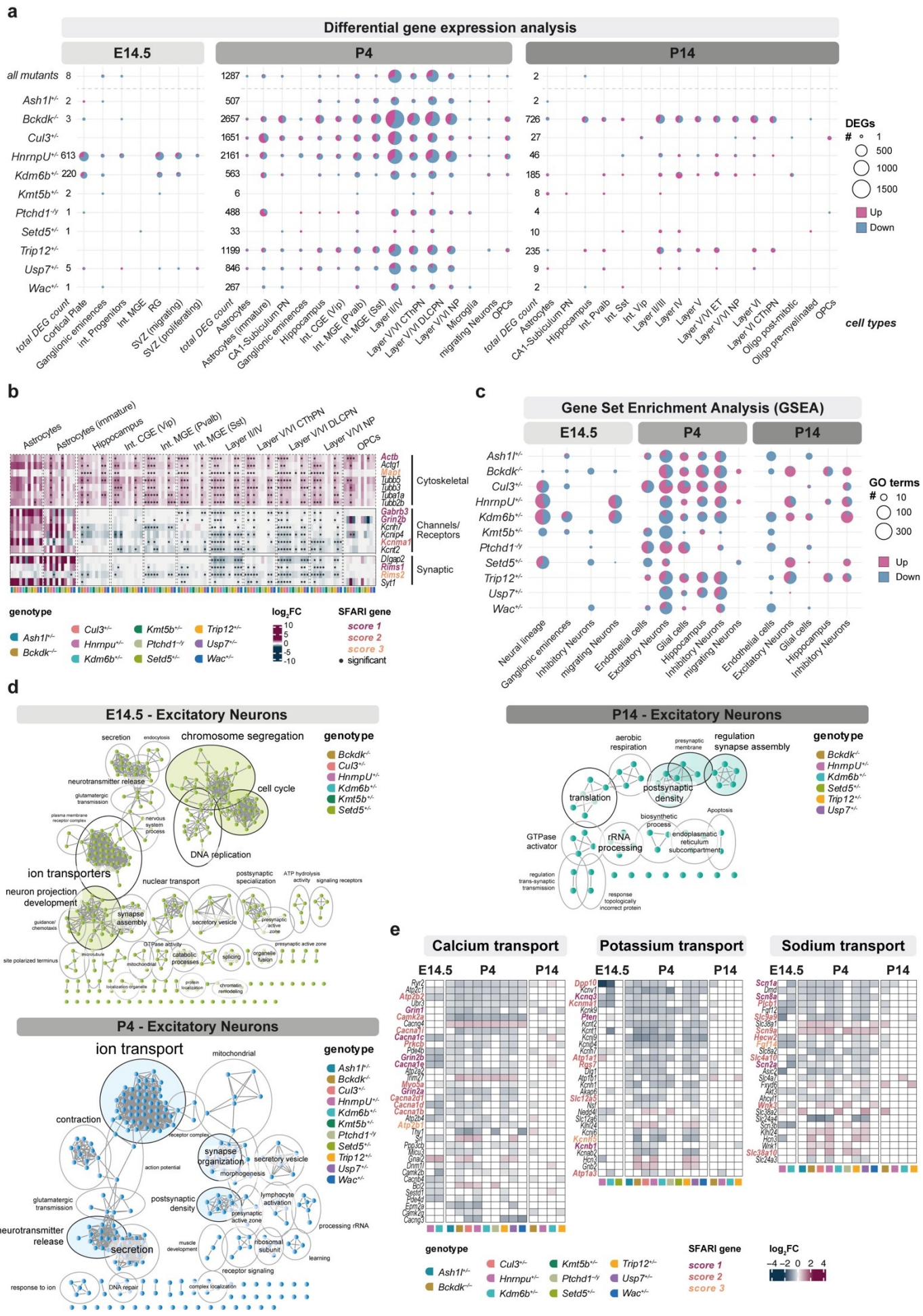


Fig. 11: Differential gene expression highlights stage-specific convergent mechanisms.

a, Number of differentially expressed genes (DEGs; *p-adj.* < 0.05) across mutants and cell types. "*All mutants*" refers to the mutants analyzed collectively compared to wild-type controls. Total number of DEGs are summarized across cell types and per time point, with repeated DEGs counted only once. **b**, Heatmap of fold changes of a representative subset of the most commonly shared DEGs across cell types at P4. DEGs were organized into functional groups such as cytoskeleton, channels/receptors, and synaptic processes. ASD risk genes are highlighted with their respective SFARI gene score. **c**, Number of GO terms identified by the Gene Set Enrichment Analysis (GSEA, FDR < 0.05) across the analyzed time points. Colors indicate the direction of the normalized enrichment score (NES). GO terms were simplified (see Methods) to remove redundancy; all three sub-ontologies (BP, MF, CC) are shown. **d**, Networks of GO terms identified in the excitatory neuronal lineage across time points. GO terms were automatically clustered using the EnrichmentMap plugin of Cytoscape. Nodes represent functionally related gene sets enriched in at least 50% of the indicated mutants, pointing to a high degree of convergence in various biological processes. Cluster size (circles) corresponds to the total number of gene sets; colored clusters are mentioned in the results. **e**, Heatmaps of the fold changes of DEGs identified in the excitatory neuronal lineage and associated with ion transporters (GO:0006813, GO:0006814, GO:0006816) demonstrate a high level of convergence across ASD mutants and time points. DEGs are arranged from top to bottom based on their common identification as DEGs. The heatmaps display only transcripts belonging to the above GO terms that were identified as DEGs in multiple ASD mutants. ASD risk genes are highlighted and colored based on their respective SFARI scores.

However, these mutants present with an enrichment of different sets of DEGs, with changes in *Ash1l* mutants being more related to the dynamics of the actin cytoskeleton and alterations in *Cul3* mutants with its assembly. Additionally, *Ash1l* mutants showed enrichment for DEGs related to synaptic vesicle priming and release, terms absent in the SynGO analysis of *Cul3* mutants.

These subtle differences in synaptic states across mutants were further highlighted by examining the impact of the selected ASD mutations on the expression of specific neurotransmitter receptors and glutamatergic synaptic transmission (Fig. 12b, c). Notably, while nearly all genotypes showed changes in transcripts related to these synaptic functions, thus converging on these pathways, many changes were unique to one of the mutants. Moreover, each mutant exhibited a unique combination of these changes (Fig. 12b, c). Among the transcripts related to neurotransmitter receptors and synaptic transmission, six stood out as exceptions, being altered in the majority of the mutants. These include the upregulation of *Cacng4*, a modulator of AMPA receptors, and the downregulation of *Camk2a*, a calcium/calmodulin-dependent kinase involved in neuronal and glutamatergic synaptic functions. *Rims1* and *Rims2*, which encode proteins essential for the organization of the presynaptic compartment, were downregulated across many genotypes and throughout all analyzed time points. Additionally, *Stxbp5l,* a Syntaxin-binding protein relevant for vesicular trafficking and neurotransmitter release, associated with a form of childhood neurodegeneration[356] was also downregulated in most ASD mutants.

Next, we explored biological processes uniquely affected in each genotype. Thus, we compared each mutant against all others and highlighted the GO terms characteristic for each genotype (Fig. 12d). We further confirmed these changes in the mutants versus wild-type comparison. For example, *Cul3* mutants showed enrichment for DEGs related to cell migration (Fig. 12d), aligning with previous results[313].

The latter was particularly interesting as we independently showed migration deficits associated with changes in cytoskeletal organization in a previous study[313]. We found that the loss of *Cul3* leads to alterations in the actin cytoskeleton at the leading edge of migrating neural progenitor cells. Notably, *Cul3* haploinsufficiency results in neuronal migration deficits both *in vitro* and *in vivo*, likely due to changes in actin cytoskeleton dynamics and adhesion proteins. An analysis of cell density in the cortical layers V/VI of P0 wild-type and heterozygous cortices revealed a marked increase in cell nuclei, indicating an accumulation of neurons in the lower layers. This could directly result from the findings discussed here regarding defects in neural lineage progression and delayed differentiation.
By performing proteomic analyses, we identified specific targets of *Cul3*, including proteins associated with microtubules, actin bundling, and cytoskeleton interaction, which contribute to the observed migration defects[313]. However, our prior study neglected transcriptomic consequences following *Cul3* loss. Notably, Ina, a neuronal intermediate filament protein that was significantly upregulated and a direct target of Cul3 in our previous work, also appeared among our upregulated DEGs in Layer II/IV neurons at P4.

Bckdk and *Trip12* mutants showed broad upregulation of genes related to metabolism and energy production. In *Bckdk* mutant animals, genes implicated in amino acid-related processes, such as *Bcat1, Cars,* and *Slc7a5*, showed significant alterations across multiple cell types and time points but were unaltered in all the other mutants. This corroborates existing literature, indicating that *Bckdk* mutations lead to a deficiency in branched-chain amino acids[329]. Interestingly, our new data suggest that these changes predominantly impact neuronal cells and less glial cells (Extended Data Fig. 12h). While the effects in *Bckdk* mutants align with existing literature and were specifically linked to amino acid-related processes, the function of *Trip12* in the brain remains largely unexplored. We found that *Trip12* mutation impacted processes related to cellular respiration and energy production, such as glycolysis (e.g., *Pdk3, Mpc2*), the tricarboxylic acid (TCA) cycle (e.g., *Mdh1, Mdh2*), and lipid metabolism (e.g., *Lactb*).
Furthermore, *HnrnpU* mutant mice showed changes in transcripts related to secretion and cilium development (Fig. 12d). The latter was independently associated with *HnrnpU* and supported using iPSC from mutant *HnrnpU* patients[357]. Finally, it was interesting to observe that changes in Wnt-related signaling, a pathway often associated with ASD[358,359], were found just in *Kdm6b* mutant samples (Fig. 12d).

In summary, our analysis also underscores unique aspects of gene expression changes in ASD mutant mice. While most of the analyzed ASD mutants exhibited common dysregulations related to synaptic transmission and ion channel functioning, specific mutants showed uniquely affected processes, such as cytoskeleton dynamics, cilium function, or metabolism. Furthermore, we could provide deeper insights into the molecular perturbations of synaptic functions in different genetic contexts.

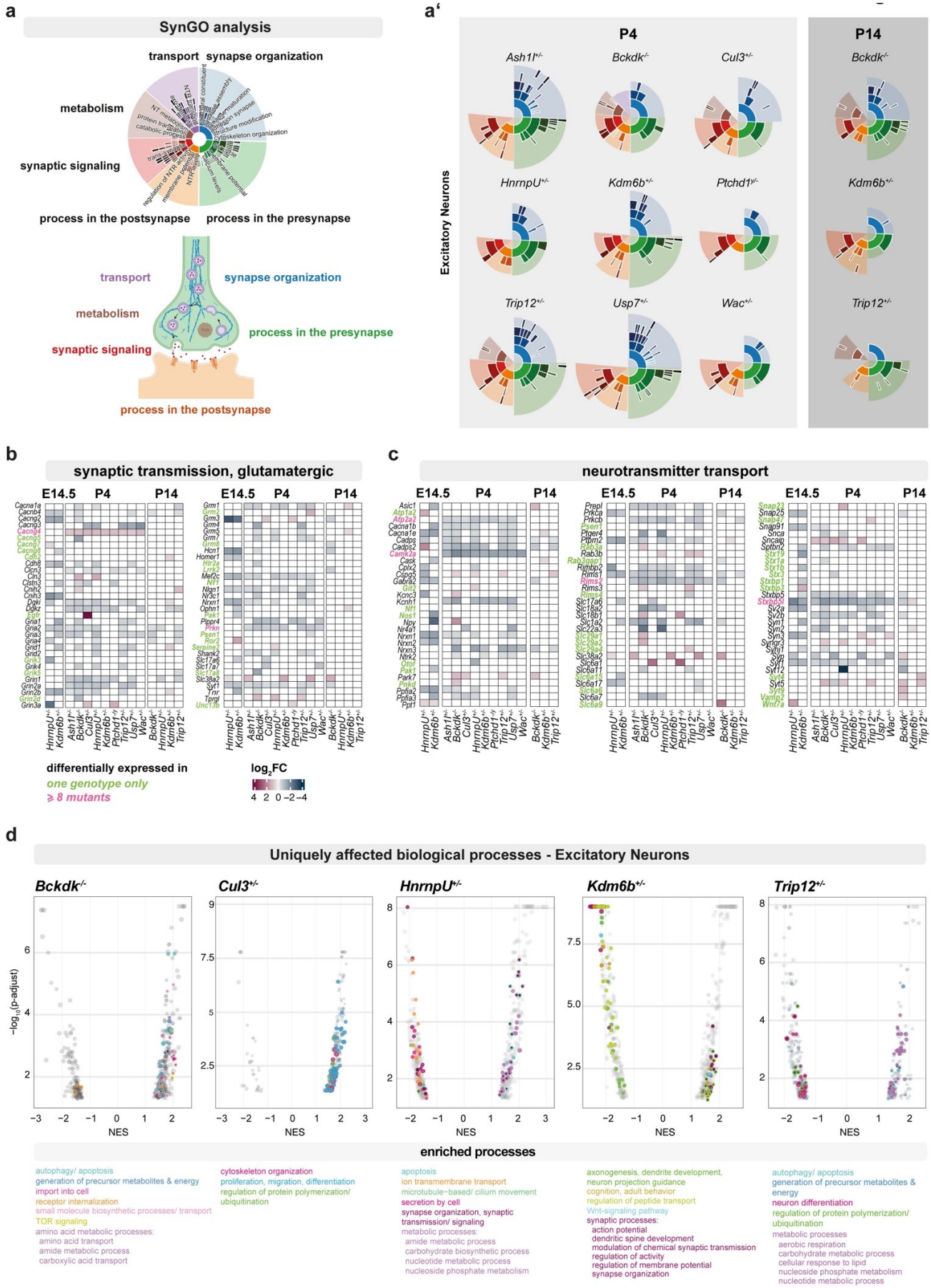


Figure 12: Distinct transcriptional profiles and unique biological processes identified in ASD mutant mice.

a, Annotation of synaptic processes based on SynGO. **a'**, Representation of the synaptic-related DEGs identified in excitatory neurons of each ASD mutant. All the DEGs were used as input for the SynGO analysis. Only SynGO terms identified as significantly enriched in the respective mutant were retained for the generation of the heatmap. Heatmaps are colored based on the SynGO terms. Each ASD mutant shows a unique combination of affected synaptic processes. **b**, **c**, Heatmaps of fold changes of DEGs related to the GO terms 'synaptic transmission' (GO:0035249) and 'neurotransmitter transport' (GO:0006836) highlight distinct synaptic states. **d**, Volcano plots of the biological processes enriched in the selected ASD mutants across the analyzed time points. Colored GO terms were identified uniquely in one ASD mutant. The circle size represents the gene count ratio. E14,5, colored filled circles; P4, gray filled circles; P14, black filled circles.

2.6 Chromatin accessibility analysis reveals regulatory dynamics in ASD mutants

While snRNA-seq revealed transcriptional variations across time points and mutants, it offers a limited understanding of upstream regulatory elements. A strength of our dataset is its single-nucleus multi-omics approach, matching chromatin (snATAC-seq) profiles for each single-nucleus transcriptome (snRNA-seq) profile, thus allowing us to investigate the gene-regulatory landscape underlying the observed ASD mutant changes in gene expression.

Similar to our snRNA-seq analysis, we analyzed the snATAC-seq results considering mutants both collectively and individually. The snATAC-seq results varied from transcriptional profiling in certain aspects. First, we detected the highest number of differentially accessible regions (DARs) at E14.5. While at this stage, all the cell types showed DARs, RG cells were the most impacted, exhibiting the most shared DARs (Fig. 13a). At later developmental stages, the number of DARs declined considerably, with the exception of excitatory neurons at P4, which still showed a high number of DARs comparable to other cell types at E14.5. In general, the collective comparison of all mutants versus wild-type controls (Fig. 13a, *all mutants*) primarily highlighted a reduction in accessible regions (Fig. 13b). This is similar to the observed transcriptomic profiles, where most DEGs were downregulated when analyzing all mutants together.

Next, we correlated the snRNA-seq results with the snATAC-seq data by aggregating peaks across gene bodies. When analyzing all mutants collectively, we found a strong correlation in Layer II/IV neurons at P4 (Extended Data Fig. 10a). This could be explained by the fact that these cells have the highest number of shared changes at the transcriptomic level.

Next, we analyzed each mutant individually after aggregating biological replicates. Generally, the number of DARs was lower when analyzing the single mutants separately compared to all of them collectively (Fig. 13a, b). Two exceptions were *HnrnpU* and *Kdm6b* mutants, which showed the highest number of DARs.

Specifically, at E14.5, *HnrnpU*$^{+/-}$ and *Kdm6b*$^{+/-}$ RG cells showed 801 and 335 DARs, respectively. Interestingly, while *HnrnpU* and *Kdm6b* mutants had fewer DEGs in RG cells at E14.5, RG cells exhibited the highest number of differences at the chromatin accessibility level in these mutants. While the other mutants had fewer DARs overall,

most still showed a larger number of DARs in CP and RG cells at E14.5 than in any other cell type at later stages. *Bckdk* mutants were an exception, with the largest number of DARs found in Layer II/IV at P4, matching the mutant- and cell type-specific transcriptomic profile. The general decrease in DARs over time aligns with previous literature, suggesting that as neural cells differentiate, chromatin gets locked in specific states[360,361].

When comparing snATAC-seq and snRNA-seq results, *HnrnpU*$^{+/-}$ RG and CP cells showed a particularly good correlation between the two modalities (Extended Data Fig. 10a). In fact, GO term enrichment analysis performed on differentially accessible genes of RG cells resulted in GO terms overlapping with those identified at the transcript level in the same cell types (Fig. 13c). Specifically, processes were connected to progenitor proliferation and forebrain development, corresponding to the affected processes identified on a transcriptomic level. Interestingly, we identified Wnt-signaling and BMP activity as recurring impacted processes in both *HnrnpU* and *Kdm6b* mutant RG cells. While we had already noted changes in Wnt-related transcripts in *Kdm6b* mutants, these changes became evident at the chromatin regulation level in *HnrnpU* mutant progenitors. Moreover, *Kdm6b* mutant RG cells also showed responses to BMP activity, which was shown to promote neural progenitor division during neurogenesis[362,363].

To gain insights into potential gene regulatory elements, we performed a motif enrichment analysis of regions with reduced differential accessibility (Fig. 13d). We found that DARs identified in *HnrnpU*$^{+/-}$ RG cells were enriched for multiple transcription factors (TF, *adj. p-value* < 0.01). Interestingly, several of the top TFs were previously described as having roles in neurodevelopment and RG lineage progression[364–367]. For example, one of the top TF identified was Sp2, previously implicated in the regulation of cell cycle lengthening in mouse neural progenitor cells at E14.5[368]. Interestingly, several of these TFs were similarly enriched in *Kdm6b* mutant samples, suggesting common underlying regulatory mechanisms.

2.7 Sex-specific gene expression alterations in ASD mutants

One open question in unraveling the complexities of ASD is its higher prevalence in males. Given that the ASD genes selected for this study were found mutated in both female and male patients, we sought to address whether their mutations manifest similarly across sexes in animal models. Beyond the differential expression of sex-chromosome genes, we observed relatively few DEGs between female and male wild-type control samples at the time points we analyzed (Extended Data Fig. 8a). Furthermore, we did not detect major differences in gene expression variability or number of transcripts between the two sexes in either control or mutant samples (Extended Data Fig. 8b, c). No distinct cell type clustering was observed between males and females (Extended Data Fig. 8d).

Next, we explored the impact of ASD-related mutations on gene transcript levels by splitting the two sexes (Fig. 14).

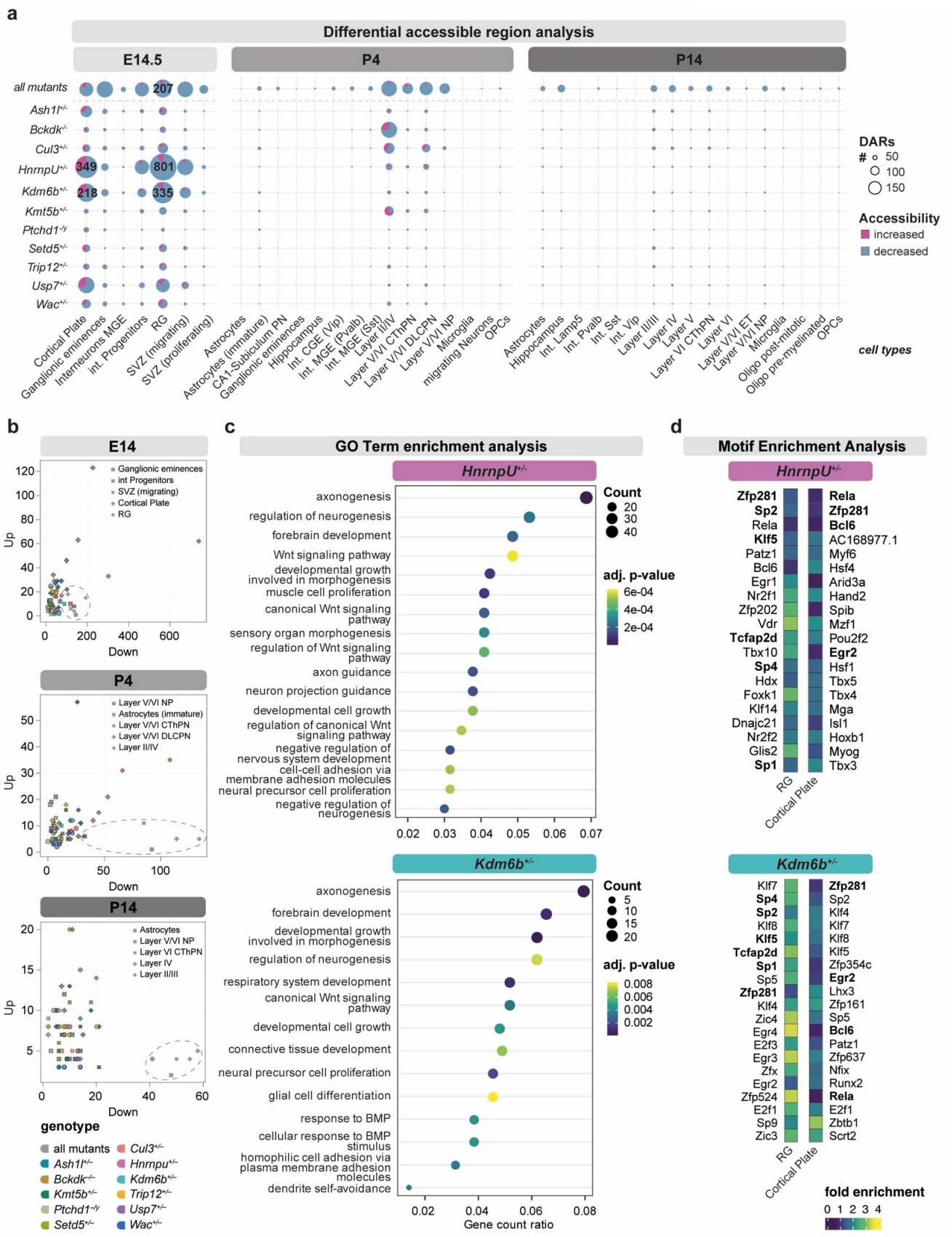


Figure 13: Chromatin differential accessibility analysis in ASD mutants.
a, Number of differentially accessible regions (DARs; *p-value* < 0.05) in individual cell types and mutants. "*All mutants*" refers to the mutants analyzed collectively compared to wild-type controls. For five comparisons, the number of DARs exceeded the scale; thus, the actual numbers are presented as

numerical values. **b**, Comparison of DARs between individual mutants and wild types reveals numerous regions with both decreased and increased accessibility, whereas the aggregate comparison of all mutants predominantly shows regions with decreased accessibility. **c**, Enriched biological processes of differential accessible genes identified in RG cells of *HnrnpU* and *Kdm6b* mutants. **d**, Heatmaps of transcription factor (TF) motif enrichment analysis of DARs identified in RG cells of *HnrnpU* and *Kdm6b* mutants (*p-adj.* < 0.05). The identified TFs suggest the involvement of regulators associated with neurogenesis and differentiation of progenitor cells. TFs are sorted according to ascending adjusted p-values.

While female and male control animals did not exhibit notable differences, the disparity of gene expression changes in female and male mutants compared to sex-matched controls was pronounced. Specifically, at P4, *Ash1l, Bckdk*, *HnrnpU*, *Trip12*, *Usp7*, and *Wac* mutants exhibited a significantly higher number of DEGs in females compared to males (Fig. 14a). In contrast, the other analyzed mutant strains showed no or mild sex-dependent effects. For example, although combined data from male and female samples indicated a comparable number of DEGs across cells for *Cul3* and *Trip12* mutants, our analysis focusing on sex differences revealed that *Trip12* haploinsufficiency predominantly affected females, while in *Cul3* mutant mice, only a minor portion of DEGs was significant in either males or females. In most cases, sex differences were less pronounced at E14.5 and P14, except for *HnrnpU* and *Trip12* mutant females, which consistently had more DEGs at E14.5 and P14, respectively. Conversely, at P14, *Bckdk* and *Kdm6b* mutants displayed enhanced responses in males.

Next, we investigated the origins of the sex differences observed at P4. Initially, we studied the transcripts that were classified as DEGs when analyzing both females and males together but not when analyzing each sex individually (approximately 61% of DEGs). We called these genes ‘merged DEGs’. While these genes did not reach statistical significance in the sex-specific analysis, they exhibited comparable trends in both sexes (Fig. 14b). This suggests that these genes undergo similar changes in both sexes, but when analyzed separately, they fail to reach statistical significance due to insufficient statistical power. These included, for example, genes identified as characteristic of specific ASD mutants, such as *Bcat1* and *Slc7a5* in *Bckdk, Ccnd2* and *Sema5a* in *HnrnpU*, *Mdh1, Mdh2,* and *Lactb* in *Trip12*.

Subsequently, we explored the overlap of the DEGs identified in females and males. In most instances, a gene significantly differentially expressed in males was also identified as a DEG in females of the same genotype and cell type (Fig. 14d), independently confirming the changes observed in these DEGs. Conversely, many of the DEGs identified in females did not significantly change in males, reflecting the generally lower number of DEGs detected in males. We categorized these genes into two groups: i) DEGs only significantly affected in females with similar expression trends in both females and males, which we termed female-biased DEGs (fbDEGs), and ii) DEGs only significantly affected in females but exhibiting no or even opposite expression changes in males, referred to as female-specific DEGs (fsDEGs) (Fig. 14c).

Next, we explored the behavior of the fbDEGs across mutants and sexes. Precisely, we compared standardized effect sizes (i.e., Cohen’s d values) between females and

males for each fbDEG (Fig. 14e). Unlike the merged DEGs, which showed similar effect sizes in both sexes, fbDEGs consistently exhibited higher effect sizes in females than males. Additionally, the average effect sizes of fbDEGs in females were higher than the average effect sizes of merged DEG in either sex, indicating that the differences between sexes stem from stronger effects in females (Fig. 14e).

Variations in Cohen's d values might be influenced by differences in either or both gene expression levels and variability in mutant as well as control samples. We thus wanted to determine whether the results were affected by slight differences among female and male control groups. Consequently, we conducted a follow-up analysis by pooling the data from female and male controls and then comparing this combined control group against either female or male mutants. This analysis revealed a consistent pattern, where several genotypes demonstrated higher numbers of DEGs in females compared to males (Extended Data Fig. 9a). These results were independently validated by a separate experiment, where we performed bulk RNAseq of *HnrnpU* E16.5 mutant and wild-type littermate brains. This analysis confirmed that not only did females show a higher number of DEGs compared to males (Extended Data Fig. 9b), but the directionality of these DEGs was also preserved (Extended Data Fig. 9c-c'').

Finally, we investigated the nature of the fsDEGs (Fig. 14f). *Wac* mutant animals showed the highest proportion of fsDEGs (Fig. 14g). *WAC* was recently identified as a female-specific candidate gene in an independent study[369], thereby suggesting that *Wac* mutations have sex-specific effects and that the larger response in females could correspond to higher disease penetrance.

Comparing all our mouse models, we found that several fsDEGs were shared across ASD mutants and cell subclasses (Fig. 14d, f). These common fsDEGs (Fig. 14f) were enriched for genes related to synaptic functions (e.g., *Grik1* and *Grik3*, *q-value* 6.5^{-7}), ion channels (e.g., *Kcnh7* and *Kcnc2*, *q-value* 4.8^{-6}) and cell adhesion (e.g., *Ncam2* and *Sema6d*, *q-value* 7.9^{-3}). Some of these fsDEGs have been previously implicated in sex-specific effects. For example, *Grik1*, a kainate-type glutamate receptor, was identified as a fsDEG in inhibitory neurons in *Bckdk* and *HnrnpU* mutants. *Grik1* participates in interneuron maturation, and its deletion in mice has been connected to distinct physiological and behavioral outcomes in female and male animals[370]. Interestingly, *Grik3,* another low-affinity kainate glutamate receptor, was identified as fsDEG in interneurons in *Cul3*, *HnrnpU*, and *Usp7* mutants. An additional example is *ApoE*, which we found to be downregulated specifically in female interneurons in *Ash1l*, *Bckdk*, *Trip12*, and *Usp7* mutants. *ApoE* is a genetic risk for Alzheimer's disease that has been associated with sex differences, even in the context of ASD[371–374].

In summary, our analysis indicates that mutations in several ASD genes elicit sex-specific effects, with generally higher effect sizes in female mutant mice.

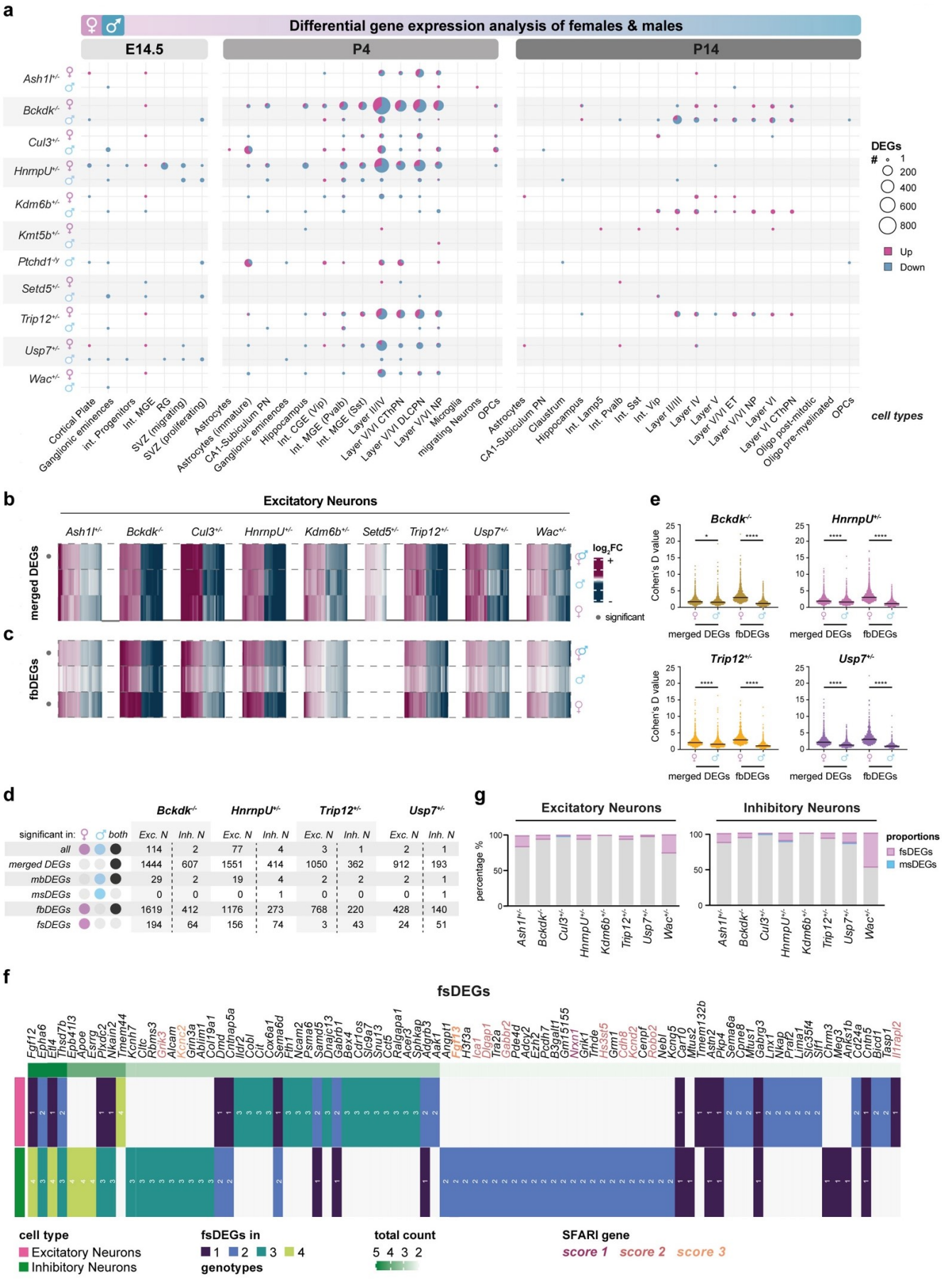


Figure 14: Sex-specific effects across ASD mutants.

a, Number of differentially expressed genes (DEGs; *p-adj.* < 0.05) in female and male mutants in comparison to sex-matched wild-type controls. **b**, **c**, Heatmaps of fold changes of a representative set of merged DEGs (**b**) and female-biased DEGs (fbDEGs) (**c**) in excitatory neurons at P4. **d**, Overlap of DEGs found in either or both females and males in selected ASD mutants at P4. Black circles indicate DEGs detected in the combined analysis, pink circles DEGs detected in females, and blue circles DEGs detected in males. **e**, Effect sizes for merged DEGs and fbDEGs in both females and males reveal that fbDEGs had larger effect sizes in females compared to males, whereas the effect sizes for merged DEGs were comparable between sexes (*P < 0.05, ****P < 0.0001; 1-way ANOVA and Sidak's multiple comparison test). **g**, Relative proportion of fsDEGs and msDEGs across all ASD mutants in excitatory and inhibitory neurons at P4. **f**, Shared fsDEGs across mutants in excitatory and inhibitory neurons at P4. ASD risk genes are highlighted with their respective SFARI gene score.

2.8 ASD mutant effects in the cerebellum are restricted to Bckdk mutant mice

To investigate whether the changes observed in the cerebral cortex were present in other brain regions, we analyzed gene expression in the cerebellum, a region associated with motor coordination as well as cognitive functions affected in autistic patients[375,376]. As a starting point, we selected a single sex (males) and time point (P4) (Fig. 15), as this stage is likely to capture a diverse array of cell types within a single sample[377].

In this dataset, we identified 16 primary cell types (Fig. 15b), with a balanced distribution of samples and genotypes across all clusters (Fig. 15c). As expected for this cerebellar stage of development[377], we primarily identified Granule cells (*Reln, Rbfox3)* and a small number of Purkinje cells (*Calb1*). We were able to differentiate between molecular cell layer interneurons (MLI; *Grm8, Nxph1*), Purkinje cell layer interneurons (PLI; *Klhl1, Chrm2*), and unipolar brush cells (UBC; *Lmx1a*). Several glial cell types were detected, including Astrocytes (*Apoe*), Bergmann Glia (*Zeb2*), Microglia (*Cxcr3*), and OPCs *(Pdgfra, Mag;* Fig. 15d*).*

Next, we assessed the abundance of each cell type to determine whether ASD mutations in the cerebellum, similar to the cerebral cortex, were associated with lineage progression issues. Comparing cell counts across clusters between mutant and wild-type specimens revealed no significant overall differences (Fig. 15e). However, analyzing individual genotypes, we found that *Cul3* mutants exhibited a trend towards increased numbers of Golgi cells and a diminished count of Granule cells (Fig. 15f).

We then investigated whether ASD gene mutations affect gene expression in the cerebellum at this developmental stage. Pseudo-bulk analysis revealed no significant uniform alterations in gene expression across the ASD mutants, whether comparing all mutants collectively against controls or each mutant individually. However, conducting this analysis separately for each mutant revealed widespread changes in gene expression in *Bckdk* mutants, affecting both glial cells, as well as excitatory and inhibitory neurons (Fig. 15g). To ensure that potential anomalies in the control group did not influence these findings, we compared each mutant against all other mutants collectively (Fig. 15g'). This analysis further highlighted *Bckdk*'s distinct profile but indicated limited changes in the other mutants. Interestingly, transcripts affected in the

cerebellum of *Bckdk* mouse mutants largely matched those altered in the cortex, suggesting consistency in impacted pathways in the two regions (Fig. 15h).
Finally, we performed a GSEA analysis to pinpoint specific alterations in biological processes. This confirmed significant shifts in amino acid and metabolic pathways in *Bckdk* mutants, particularly affecting neurons and, more specifically, Golgi cells. These findings correspond to our observations in the cerebral cortex. Conversely, other genotypes displayed only a few changes, with a minority showing variations in the expression of synaptic proteins.
Altogether, we found that ASD mutations generally do not lead to significant changes in gene expression within the cerebellum at the investigated time point, with the exception of *Bckdk* mutant mice. This gene's effects mirror those observed in the cerebral cortex, predominantly influencing metabolic and synaptic functions in neuronal cells.

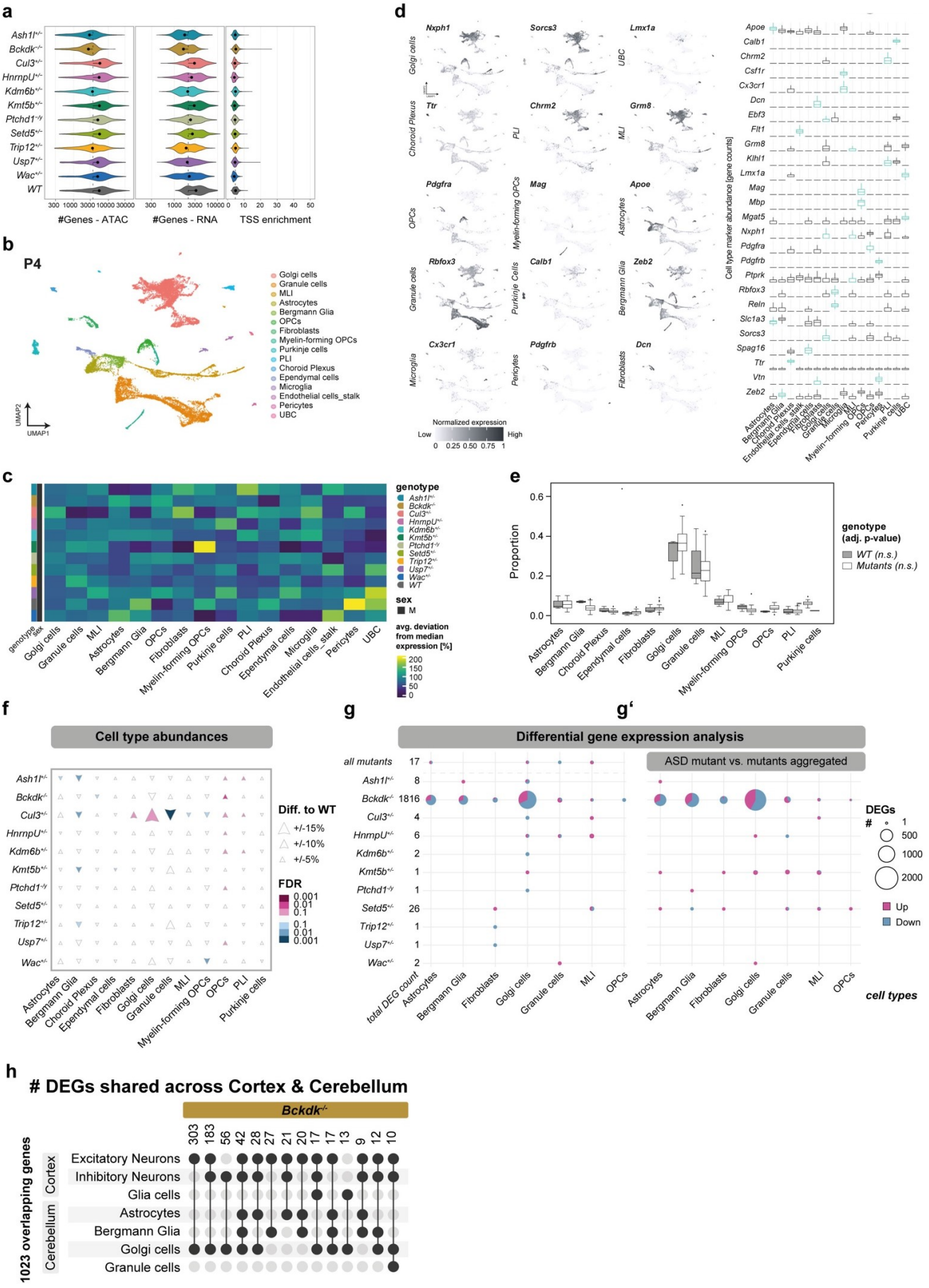


Figure 15: Multi-omics sequencing of perinatal cerebellar tissue.

a, Quality metrics of the sequenced samples. **b**, UMAP visualization of integrated snRNA- and snATAC-seq data from male cerebellar samples at P4. Cells are colored based on cell type assignment. **c**, Average deviation from the median expression of individual cell types of the ASD mutants at P4. Each tile in the heatmap shows the average expression deviation of each replicate relative to the median expression of all samples per cell type expressed as a percentage. **d**, UMAP visualization showing expression levels of canonical molecular markers. Box plots show the abundance of selected cell type markers. Centre lines represent medians, and the box limits show the 25-75% interquartile ranges. **e**, scCODA analysis indicates no significant compositional cell type changes of ASD mutants in comparison to wild-type controls. **f**, Changes in cell type abundance in individual ASD mutants. Arrows represent the relative difference in percentage compared to wild-type (WT) controls. Nominal p-values are shown. **g**, Number of differentially expressed genes (DEGs; *p-adj.* < 0.05) across mutants and cell types. "*All mutants*" refers to the mutants analyzed collectively compared to wild-type controls. Total number of DEGs summarized across cell types and per time point, with repeated DEGs counted only once. **g'**, Number of differentially expressed genes (DEGs; *p-adj.* < 0.05) across mutants and cell types when comparing each mutant with all the other ASD mutants collectively. **h**, Overlap of DEGs in *Bckdk* mutant cortex and cerebellum at P4. In total, 1023 genes overlapped between the indicated cortical and cerebellar cell types.

3 Discussion

ASD is a highly complex group of disorders, encompassing dozens of different genetically defined and idiopathic conditions. Key questions in the field are how all these different disorders evolve, the extent to which they overlap in their pathophysiology, and, consequently, whether it will be feasible to identify shared therapeutic time windows and targets. By examining the molecular profile of the brain of monogenic models of ASD across development, we uncovered dynamic changes in the cellular and molecular landscapes, highlighting the complexity of ASD trajectories.

Our study shows that ASD mutants converge on affecting the progression of the radial glia cell lineage. However, we suggest that this common phenotype is due to a developmental delay rather than a specific alteration in neural lineage specification, as in most cases, it seems to arise very early during development and resolves as the brain matures. In fact, we did not observe differences in neuronal cell numbers at P14. A lack of changes in neuronal cell numbers past developmental stages aligns with findings in human postmortem ASD samples[378]. Thus, our data combined with human postmortem studies indicate that neither monogenic nor idiopathic ASDs are generally associated with differences in neuronal cell numbers, except for developmental, transitory effects. However, by highlighting transient changes in cell numbers, our data raise questions about the implications of the observed delays for brain connectivity, particularly whether minor cell count variations could lead to significant connectivity changes later in life. Furthermore, unlike recent results in human patient samples[378], we did not observe changes in the number of microglial cells, suggesting that microglia activation might be an indirect effect appearing later in life. We independently confirmed this finding by analyzing postnatal microglial numbers in *Cul3*, *Setd5*, and *Ptchd1* mutants, which showed no significant difference in overall cell counts (data not shown). Whether microglia activation is a protective or disruptive event should be further investigated.

Despite the number of cells normalizing with time, we found that in terms of molecular changes, P4 is the most affected stage. This is intriguing since previous functional genomic studies have hypothesized that ASDs converge on a perturbation of excitatory neurons at human mid-fetal developmental stages, corresponding to early postnatal stages in mice[188,379,380]. Despite this convergence, we also found variations in how mutations in different genes manifest across development. For example, *HnrnpU* and *Kdm6b* mutant mice showed many changes at E14.5 and P4 but not P14, while *Bckdk* and *Trip12* mutations only affected P4 and P14. Other mutants showed minimal effects throughout. Given the temporal ubiquitous expression of the ASD genes we have modeled, these results suggest that the specific developmental context in which a mutated gene is expressed plays a crucial role in determining the phenotypic outcomes of these mutations. To this end, transient and milder differences could, of course, be exacerbated during particular behavioral tasks. Our data also

shows that the same mutation can affect different biological processes at distinct developmental stages. This implies that the effects of ASD mutations evolve over time, thus explaining the challenges in identifying reliable biomarkers and achieving an early diagnosis for ASDs.

Although different ASD mutants led to the deregulation of many different DEGs, our analysis identified several DEGs that are shared across mutants. Moreover, we observed a strong convergence in the biological processes affected in the different mouse models, indicating that despite the genetic diversity of ASDs, the resulting cell states are similar across these disorders. In particular, we found a consistent upregulation of processes related to cell division and neurogenesis at E14.5, along with a downregulation of synaptic functions and ion channels at later stages. The strong convergence along these functions led us to hypothesize that some of these changes may represent homeostatic adaptations programmed to compensate for the developmental delays observed in mutants. Nevertheless, the strong enrichment for ion channel-related genes among DEGs aligns with the literature indicating that ASD is associated with E/I imbalances[344].

By employing whole-cell patch-clamp electrophysiological recordings in *Bckdk* and *Usp7* mutant animals at P7, we were able to experimentally confirm the synaptic defects indicated by bioinformatics analyses. Notably, both lines primarily align on the same specific set of intrinsic property changes, including increased action potential frequencies and decreased mEPSC and mIPSC frequencies (data not shown). After birth, integration of ion channels in the neuronal membrane increases, causing cells to grow and excitability to decrease during brain development[381]. While we have not yet confirmed synaptic defects at the cellular level (e.g., differences in spine density or neuronal morphology), it is possible that these excitability defects stem from a global developmental delay. By P14, the differences in DEGs become less apparent, suggesting that both excitatory and inhibitory neurons may be balancing themselves through compensatory mechanisms.
Nevertheless, the effects on synaptic circuitry during later stages may still be impacted. Considering that we observed a consistent reduction of OPCs across all three time points, it suggests that myelination might also be developmentally delayed along with the early perinatal synaptic imbalances. Thus, even though synaptic defects may not be as prominent at P14, the implications for synaptic circuitry can still be substantial. This possibility needs to be experimentally validated and assessed at later developmental stages.

The possibility of analyzing distinct forms of ASD simultaneously also allowed us to underscore differences among them. Precisely, we found that a large fraction (on average 50%) of the DEGs detected in each mutant/cell type were unique to that particular mutant. Several of these transcripts were consistently affected in the same mutant at different developmental stages, indicating their potential role as molecular biomarkers for specific conditions. These consistent, genotype-specific changes likely

represent the most direct effects of the genetic mutations we have modeled, whereas the common changes may be downstream effects. These findings suggest that there are multiple pathways resulting in similar cellular states. For example, we identified *CamKIIa* as one of the most commonly regulated DEG. *HnrnpU* has been shown to bind to *CamKIIa* mRNA and transport it at the synapse, thus potentially directly regulating its levels[382]. Other ASD genes may, however, regulate this transcript in an indirect way. Thus, when the commonly affected processes are part of resilience, compensatory mechanisms, or are at the root of the disorder remains to be discovered. Nevertheless, we also noted slight differences in cellular states, whereby we identified different synaptic signatures and ion channel profiles in each mutant. Importantly, these distinct cell states correspond with previous independent findings from our group. We observed, for example, enrichment for metabolic amino acid-related processes in *Bckdk* mutant animals[329], while *Cul3* mutants showed an enrichment of processes linked to cell migration and cytoskeletal organization[313]. Understanding how these distinct states can determine physiological and behavioral differences remains both a challenge and an opportunity for future research.

To expand our analyses, we also investigated a different brain region, the cerebellum, given its connection to the motor and cognitive challenges observed in ASDs. We found that, at the analyzed time point, most mutations did not significantly alter cell numbers or gene expression in this region. This is particularly interesting, considering that the cerebellar samples were obtained from the same animals as the cortical samples. While this could be a limitation of the chosen time point, analysis of human samples supports this observation[383], thus suggesting that ASD mutations have a much weaker effect on the cerebellum than the cerebral cortex. Moreover, as the proportion of Purkinje cells is progressively decreasing over the course of brain development[377,384], selecting P4 as the primary time point may explain the minor changes observed. Since Granule cells outnumber the fraction of Purkinje cells at this stage, their large abundance may allow them to counterbalance potential defects. It would have been interesting to expand the cerebellar analyses to earlier, embryonic stages (e.g., E12.5 – E15.5), where the abundance between Granule and Purkinje cells is more balanced. Additionally, including female subjects in the analyses would enhance our understanding of sex-specific effects in this brain region as well.
However, where changes were noted, such as with *Bckdk* mutations, the affected transcripts in the cerebellum largely matched those altered in the cortex, suggesting shared affected pathways.

Importantly, our experimental design allowed us to identify major sex differences. Identifying the potential biological origins of the observed sex bias in autism is a very important, outstanding challenge. Although the forms of ASD we studied are associated with rare mutations mostly identified in both females and males, we found that some mutations affected the two sexes differently, with females displaying larger effect sizes than males. Interestingly, a very recent study sequencing schizophrenia, bipolar disorder, and ASD adult patient brain samples aligns with this observation[385].

It is unclear whether the larger effect size observed in females is causing stronger responses or is a resilience mechanism. However, it is interesting that several of the DEGs specifically identified in females are shared across mutants. Among them, we identified many transcripts related to synaptic functions and ion channels. Unfortunately, despite the relevance of the proteins encoded by these genes, we found very little in the literature concerning their differences between males and females. Interestingly, some of the shared fsDEGs are X-linked and have been shown to be able to escape X-inactivation[386–389], thus potentially capable of activating female-specific mechanisms. For example, *Nkap* was upregulated in excitatory neurons in females at P4 in *HnrnpU* and *Trip12,* two of the mutants that showed the highest female effect sizes. *Nkap* can escape X-inactivation and is a known activator of the transcription factor NF-κB and repressor of Notch[390], which play crucial roles in proper brain development and functioning[391–395]. Mutations in *Nkap* itself have been identified as a cause of intellectual disability, affecting only males[396]. Furthermore, it is interesting to note that our ATAC-seq analysis indicated that DARs were enriched for the TF Sp1. Sp1 is known to bind to estrogen receptors[397] and has recently been linked to sex-biased gene expression in primate brains[398].

Interestingly, our findings align with the concept of the “female protective effect” mentioned in **1.1.4.1**. Given that females are thought to require a greater mutational burden to show clinical signs of ASD, the larger number of DEGs we identified in females than in males supports this theory. While we did not perform a systematic side-by-side analysis of behavioral traits in our male and female mutant lines, *Wac* female mutants serve as a notable example.
When *Wac* mutant animals are subjected to an open-field test, female mutant mice display behavioral characteristics related to ASD, suggesting hyperactivity and anxiety, whereas males behave similarly to their wild-type counterparts (data not shown). Notably, *Wac* mutant animals also had the highest proportion of fsDEGs.
Interestingly, *Cul3* mutant animals did not exhibit a notable skewed sex ratio based on their DEGs. In fact, the differential gene expression in *Cul3* female and male mutants was relatively balanced in comparison. We have similarly demonstrated this in a previous study, showing that female and male *Cul3* mutant mice perform comparably in behavioral tasks[313]. Although *Cul3* mutants may not align with the concept of a female protective effect, other significantly affected mutant lines such as *HnrnpU*, *Trip12*, and *Usp7* could show characteristics of ASD specific to one sex when tested behaviorally.

Considering the proposed hypothesis regarding the X-chromosome's link to the skewed gender ratio (4:1) in ASD (as discussed in **1.1.4.3**), we found few very DEGs located on the X or Y chromosomes. This result contrasts with the idea that genetic risks might be encoded on sex chromosomes. Additionally, *Ptchd1* mouse mutants, which represent an X-linked form of ASD, did not show substantially more severe effects compared to the other mutant lines. Nevertheless, according to the earlier hypothesis about genetic risks encoded on sex chromosomes, we would expect to

observe more DEGs associated with X or Y chromosomes. However, studying only one X-linked mutant line is not representative and requires further research.

In conclusion, by simultaneously testing multiple genetic forms of ASD models across development, our study highlights the dynamic nature of ASD-related changes in the brain, revealing both shared and unique molecular profiles across different mutations. Altogether, our results contribute to a comprehensive overview of the cell state landscape found in ASD and underscore sex-dependent effects.

4 Concluding remarks, limitations, and future directions

Substantial progress has been made in recent years in understanding the pathogenesis of ASD, particularly monogenic ASDs. Yet, the field is encountering major difficulties in categorizing the diverse patient population into more precise subgroups. Given the challenges of patient stratification, the focus has shifted towards gene stratification, exploring which specific subsets of ASD risk genes converge on a smaller set of target genes and pathways. Several studies have highlighted functional commonalities among ASD risk genes[25,28,30,252], offering insights for more targeted interventions.

While our work presents a step forward in understanding the biology, convergence, and divergence of genetically distinct forms of ASD, it also has certain limitations. While we offer a view of the temporal evolution of the mutants, there are developmental gaps between the analyzed time points. Thus, it is plausible that some of the mutants for which we observed rather small changes might show more changes at other time points. Considering that the present work utilized wild-type C57BL6/J mice as a “unique” control mouse line, extending the analysis to include littermate controls could further strengthen the findings. Although the experimental design was carefully developed to avoid this as a confounding factor, incorporating wild-type littermates for every mutant line may still be beneficial.
In this regard, we have started to confirm initial results by investigating *HnrnpU* mutants in comparison to their wild-type littermates. Remarkably, the pronounced impact of a delay in neural lineage progression remains still apparent (data not shown).

We could show a substantial regulatory convergence among synaptic genes and ion channels. However, several of the results presented are at a bioinformatics level and require experimental validation. To experimentally explore synaptic defects, we have performed whole-cell patch-clamp recordings in P7 *Bckdk* and *Usp7* mouse mutants (data not shown). Notably, our findings demonstrate that both mutants show substantial imbalances in excitatory and inhibitory signaling, with a generally more excitable phenotype. This observation aligns with existing literature, which indicates that excitability tends to decrease over time in wild-type mice[381], suggesting that the more excitable cells in our mutant models may actually be developmentally delayed.

An unexpected finding was the differences in gene expression between females and males, along with the large overlap of fsDEGs across mutant mouse models.
While our present work represents a great step toward incorporating both female and male samples in ASD research, the lack of literature regarding neurotypical subjects and wild-type mice of both sexes highlights the need for more extensive studies. Even within a wild-type context, there is sparse information on sex differences such as temporal gene expression variations, overall proportional changes of DEGs, and alterations of chromatin accessibility between females and males

Currently, male mice are predominantly used in ASD research, which makes it difficult to compare our identified DEGs with the existing literature due to the scarcity of female subjects used. This represents a substantial gap and limitation in the field, underscoring the critical importance of investigating both sexes simultaneously to identify specific cell types and developmental stages where one or the other sex may be particularly sensitive.

Overall, based on our present findings, while some questions remain to be explored, we could greatly contribute to our understanding of convergent and divergent causal paths in ASD. By mapping the developmental dynamics of the cortical cell landscape, we could define cellular diversity and molecular patterning of ASD at single-cell resolution. This study ultimately offers a valuable multi-omics resource, encouraging further research in this area and laying the foundation for future studies.

5 Methods

**Unless specified otherwise, experiments, analyses, and data interpretations were conducted by Lena A. Schwarz.*

5.1 Generation of experimental models

Animals

All animals used in this study were approved by the Institutional Animal Care and Use Committee at ISTA and by the Bundesministerium für Bildung, Wissenschaft und Forschung, Austria (approval numbers BMWFW-66.018/0008-WF/II/3b/2014, BMWFW-66.018/0012-WF/V/3b/2015, BMWFW-66.018/0012-WF/V/3b/2017, BMWFW-66.018/0015-V/3b/2019, BMWFW-66.018/0032-V/3b/2019, BMBWF-V/3b/2020-0.342.159, BMBWF-V/3b/2020-0.148.791, BMBWF-V/3b/2021-0.291.172, BMBWF-V/3b/2021-0.291.177, BMBWF-V/3b/2022-0.292.788, BMBWF-V/3b/2022-0.121.445). All experiments were performed on mice ranging from embryonic day (E) 14.5 to postnatal day (P)4 and P14. Embryonic time points were determined by plug checks after timed matings, defining E0.5 as the morning after copulation. Animals were kept on a 12 h light/dark cycle (lights on at 7:00 am) and housed in groups of 3-4 animals per cage, with food and water available *ad libitum.* Experiments were carried out under specific pathogen-free conditions, and the health status of the mouse lines was routinely checked by a veterinarian. All transgenic mouse lines were backcrossed into *C57BL/6J* background a minimum of two times. Both females and males were used for experiments.

Generation of constitutive heterozygous mouse lines

** Electroporation and zygote transfer was performed by Satish Arcot Jayaram*

*C*onstitutive heterozygous mice (i.e., *Ash1l*$^{+/-}$*, Kdm6b*$^{+/-}$*, Kmt5b*$^{+/-}$*, Trip12*$^{+/-}$*, Usp7*$^{+/-}$*, Wac*$^{+/-}$*)* were generated within the Transgenic Unit at IST Austria in a *C57BL/6J* background by zygote electroporation of the Cas9 protein (TakaraBio #634621) and custom-made sgRNAs. To generate *Ash1l*$^{+/-}$ mice, one sgRNA (CAATCACCATTCCGCTATCC *AGG*) targeting exon 12 of *the Ash1l* gene was used. For *Kdm6b*$^{+/-}$, two sgRNAs (CCCAAGGACCCGAGGTGATA *GGG* and TACGTATGAGGAGCGAACCC *TGG*) targeting intronic regions flanking exon 19 of the *Kdm6b* gene were used. For *Kmt5b*$^{+/-}$, two sgRNAs (CCCTCACGACCCTACTACTG *TGG* and TTTACGTCTCAAGTCACACT *GGG*) targeting intronic regions flanking exon 9 of the *Kmt5b* gene were used. Similarly, to generate *Trip12*$^{+/-}$ mice, two sgRNA (AGCGTATTCTCACTTTGATC *TGG* and TAAATTTGTAGAGACAGTTA *AGG*) targeting intronic regions flanking exon 3 of the *Trip12* gene were used. Similarly, for *Usp7*$^{+/-}$, two sgRNAs (CTCTCCCGAACATTATGAAG *AGG* and TGCCACGTCTTATACACATT *AGG*) targeting intronic regions flanking exon 6 of the *Usp7* gene were used. To generate

Wac$^{+/-}$ mice, one sgRNA (ATGTCGGAGGCGCAGATGTA *GGG*) targeting exon 8 of *the Wac* gene was used.
Superovulation was performed to produce large numbers of zygotes. In brief, 3-4 weeks old donor females (in-house) were hormone primed by intraperitoneal injection of 5 IU of pregnant mare serum gonadotropin (PMSG). 5 IU of human chorionic gonadotropin (hCG) were administered at 46-48 h after PMSG treatment, followed by 1:1 mating with stud males (in-house). Zygotes were isolated from the oviduct of mated females at 0.5 d post coitum (dpc). M2 with Hyaluronidase (Sigma cat. no. #MR-051-F) was used to dissociate cumulus cells. Zygotes were then cultured in small drops of KSOM (Sigma cat. no. MR-121-D) under mineral oil (Sigma cat. no. M-5310) at 37 °C and 5% CO_2, until the electroporation. Electroporation of mouse embryos was performed similarly as described in[399] with the adaption of using Opti-MEM (Thermo Fischer #31985062) instead of PBS. Finally, F0 founder mice were genotyped using standard PCR amplification with primers 500 bp to 1 kb away from guide-RNA binding sites. F1 mice were generated by backcrossing founder mice with C57BL/6J animals. The F1 mice were again genotyped by PCR, and positive amplicons covering the deleted sequence were Sanger sequenced to confirm precise targeting. All transgenic mouse lines were back-crossed into *C57BL/6J* background a minimum of two times, and predicted off-targets were checked. A list of oligonucleotides used is provided in Supplementary Table 1). The constitutive knockout mouse line (*HnrnpU*$^{+/-}$) was obtained by mating *HnrnpU*$^{wt/flox}$ (Hnrnpu<tm1.1Tman>/J, Strain: #032187, RRID:IMSR_JAX:032187) mice with a *CMV-Cre* line (B6.C-Tg(CMV-cre)1Cgn/J, Strain #:006054, RRID:IMSR_JAX:006054) and subsequent backcrossings to C57BL/6J wild-type animals. Crossing of *HnrnpU*$^{flox/wt}$ mice with homozygous animals of the *CMV-Cre*$^{Cre/Cre}$ line results in ubiquitous deletion of one allele of *Hnrnpu* spanning exons 4 to 14.

5.2 Method details

Single-cell multi-omics profiling of gene expression (snRNA-seq) and chromatin accessibility (snATAC-seq) from the same cell (scMultiome-seq).

Sample preparation and Nuclei isolation

** Nuclei isolation was performed with the help of Sabrina Ladstätter*

Brain tissue (forebrain; cerebellum) from E14.5, P4, and P14 mice were used for scMultiome-seq experiments. Animals coming from 3 separate litters were collected to avoid potential litter-specific biases. For the embryonic time point (i.e., E14.5; *n*= 3 per genotype + sex), timed-pregnant females were decapitated, and embryos were rapidly dissected on ice. Cortical tissue was dissected in ice-cold PBS, meninges were removed, and forebrain structures were snap-frozen in liquid nitrogen and stored at -80°C until nuclei isolation.
For postnatal time points (i.e., P4, P14; n= 3 per genotype + sex + time point), mice were decapitated, the brain was rapidly dissected on ice, and subcortical structures

were removed. The remaining forebrain (cortex + hippocampus) and cerebellum were separately snap-frozen in liquid nitrogen and stored at -80°C until nuclei isolation.

Frozen tissue samples were dissociated to generate single nuclei gene expression libraries following a modified protocol from 10X Genomics (Chromium Nuclei Isolation Kit CG000505, Rev A). Buffers were supplemented with RNase inhibitors (provided by 10X Genomics and Sigma cat. no. 3335402001). In brief, 200 µl of lysis buffer was added to the sample and dissociated with pestles provided by the vendor. After adding an additional 300 µl of lysis buffer, the tissue was homogenized by pipette-mixing and incubated on ice for 10min. For the P14 forebrain, an additional 500 µl of EZ lysis buffer (Sigma cat. no. #NUC101) was added to the samples to prevent clogging of the nuclei isolation columns. Afterward, 500 µl of the cell suspension was loaded onto Nuclei Isolation Columns and centrifuged for 20s at 16,000 rcf, 4°C, followed by vortexing the flow-through for 10s and centrifugation for 3min at 500 rcf, 4°C in a swinging bucket rotor. The supernatant was removed, and the pellet was gently resuspended in 500 µl of Debris Removal Buffer before centrifugation for 10min at 700 rcf, 4°C. After removal of the supernatant, the pellet was washed with 1ml of Wash Buffer followed by centrifugation for 5min at 500 rcf, 4°C. For multiplexing, 6 samples were pooled after barcoding with cholesterol-modified oligos (CMOs; sequences of all CMOs used are provided in Supplementary Table 1). Each sample pellet was resuspended in a total of 180 µl of Wash Buffer containing 0.2 µM unique CMO Anchor-Barcode, vortexed for 3s, and incubated on ice for 5min. CMO Co-Anchor was added to all samples of a multiplexing group with a final concentration of 0.2 µM, vortexed for 3s, and incubated on ice for 5min. After adding 1ml of wash buffer, samples were centrifuged for 5min at 500 rcf, 4°C. Depending on the tissue size, one (embryonic, P4 cortex/cerebellum) or two (P14 cortex) additional washing steps were performed. After removing the remaining supernatant, the pellet was resuspended in 50 µl of resuspension buffer. Nuclei were counted by flow cytometry (BD LSRFortessa™) with Precision Count Beads™ (BioLegend cat. no. #424902), and samples were diluted to obtain approximately 4,000 nuclei per sample, resulting in a total of 20,000 nuclei per lane of a 10X Chromium Controller (PN-1000204). GEMs were generated using Chromium Next GEM Chip J Single Cell kit (PN-1000230), Chromium Next GEM Single Cell Multiome GEM Kit A (PN-1000232), Chromium Next GEM Single Cell Multiome Gel Bead Kit A (PN-1000231) as instructed by the manufacturer.

Library preparation and sequencing

Library preparation was carried out according to the manufacturer's protocol (Chromium Next GEM Single Cell Multiome ATAC + Gene Expression, CG000338 Rev F) with the following modifications regarding the multiplexing reactions: During cDNA amplification, 0.2 µM ADT additive primer (5'-CCTTGGCACCCGAGAATTCC-3') was added to the reaction. During cDNA cleanup, 120 µl of supernatant was saved to purify Hash-DNA using a 2.0x ratio of SPRIselect bead volume (Beckman Coulter, B23319) to sample volume. Hashtag libraries were generated using 5ng of Hash-DNA,

1X KAPA2G Fast HotStart Readymix (Roche cat. no. #7958935001), and unique combinations of 0.4 µM i5 and i7 indices (sequences are provided in Supplementary Table 1). Following amplification (98°C 2min, 10x [98°C 20s, 54°C 30s, 72°C 20s], 72°C 5min, 4°C ∞), libraries were cleaned up using a 1.2x ratio of SPRIselect bead volume (Beckman Coulter, B23319) to sample volume. Library quality and size were assessed with the High Sensitivity DNA Analysis Kit (Agilent Technologies #5067-4626) and the Bioanalyzer 2100. Libraries were sequenced by the Biomedical Sequencing Facility at the CeMM Research Center for Molecular Medicine of the Austrian Academy of Sciences, using the Illumina NovaSeq 6000 platform. For gene expression, libraries were pooled in a ratio of 83% RNA; 17% HTO and sequenced on Illumina NovaSeq6000 systems using the sequencing format: read 1: 28 cycles, i7: 10 cycles, i5: 10 cycles, read 2: 90 cycles. For snATAC-seq, libraries were sequenced on Illumina NovaSeq6000 systems using the sequencing format: read 1N: 50 cycles; i7: 8 cycles; i5: 24 cycles; read 2N: 49 cycles.

Single-cell muli-omics data analysis

Pre-processing and demultiplexing, initial analysis and clustering

* *performed by Biomedical Sequencing Facility, Christoph Dotter and Christoph Büschl*

Samples were de-multiplexed, and the raw sequencing data was converted to FASTQ format using bcl2fastq (version 2.20.0.422). Joint processing of the gene expression and ATAC modalities was performed using the cellranger-arc software (version 2.0.0). The mm10 reference genome was used for the alignment *(refdata-cellranger-arc-mm10-2020-A-2.0.0, obtained from https://cf.10xgenomics.com/supp/cell-arc/refdata-cellranger-arc-mm10-2020-A-2.0.0.tar.gz).* To capture CMO reads, the gene expression modality was separately processed using the cellranger count pipeline (version 7.0.0 and version 7.1.0), aligning it against the mm10 reference genome *(refdata-gex-mm10-2020-A, obtained from https://cf.10xgenomics.com/supp/cell-exp/refdata-gex-mm10-2020-A.tar.gz)*. Each nucleus was assigned to the sample of origin as part of further demultiplexing, for which a Gaussian mixture model was fitted to the CMO count distributions. The probability that a given CMO read count was derived from background or positive signal was then inferred (as described in[400]). The resulting multiome data was further analyzed in R (version 4.3.0) using Seurat[401] (version 4.3.0.9012) and Signac[402] (version 1.10.0). For reproducibility, the analysis was implemented as targets[403] (version 1.2.2) pipeline using renv (version 1.0.2).
Pre-processing was done per 10X lane (i.e., per multiplexing group of 4-6 samples). Peaks for the snATAC-seq modality were called for each run separately using MACS2 (version 2.2.7.1) within Signac. A set of consensus peaks for the snATAC-seq analysis was created according to Signac. CMO demultiplexing information was taken from Cellranger output and added as metadata.

Doublets were identified using scDblFinder[404] (version 1.14.0), separately for snRNA-seq and snATAC-seq modality. snRNA-seq parameters for the scDblFinder function were dims = 50, cluster = TRUE, knownUse = “discard”. snATAC-seq features were first aggregated (aggregateFeatures function, k = 500) and parameters for

scDblFinder were dims = 50, aggegateFeatures = TRUE. Cells identified as doublets based on CMO data were included as known doublets (knownDoublets parameter). Quality control metrics such as the percentage of mitochondrial reads, nucleosome signal, and transcription start site (TSS) enrichment were calculated per run. After removing known and estimated doublets outlier thresholds for snRNA-seq read counts (nCount_RNA) or snATAC-seq read counts (nCount_ATAC) were derived using the isOutlier function from the scuttle package[405] (version 1.10.2) with parameters nmads = 3, type = "both", log = TRUE. Nuclei falling outside these thresholds or with more than 5% of mitochondrial reads were removed.

Integration into combined analysis

* *performed by Christoph Dotter and Christoph Büschl*

Complete datasets for each time point/tissue were created by integrating individual Seurat objects representing separate 10X lanes (i.e., multiplexing groups). snRNA-seq data were normalized using SCTransform[406,407] from Seurat with parameter vst.flavor = "v2". Integration of normalized snRNA-seq data was performed according to Seurat using the reciprocal PCA method with the following non-default parameters: SelectIntegrationFeatures(nfeatures = 2500), FindIntegrationAnchors(reduction = "rpca"), IntegrateData(dims = 1:50). Integration of snATAC-seq data was performed at the level of the LSI embedding using IntegrateEmbeddings(dims.to.integrate = 1:50) function with the integration anchors derived from snRNA-seq data. Identification of cell types was performed using the combination of both modalities, snRNA-seq and snATAC-seq. A PCA embedding was derived for the integrated snRNA-seq data, weighted nearest neighbor (WNN) graph was calculated using the FindMultimodalNeighbors function with the integrated LSI and integrated PCA reductions as input and dims_atac = 2:50, dims_rna = 1:50. The resulting WNN graph was used for UMAP visualization of the dataset and identification of clusters using the FindClusters function with parameters algorithm = 3 (smart local moving (SLM) algorithm), resolution = 0.5 (forebrain/cortex) or 0.3 (cerebellum). Cells designated as outliers per cell cluster were designated as such and removed using the Mahalanobis distance (> 100) calculated from genes expressed in > 80% of the cells.

Label-transfer and cell type annotation

To support cluster annotation, reference datasets for each tissue and time point were used (list of respective references used is provided in Supplementary Table 1). Seurat objects were created from all datasets except where data was provided in this form. Normalization and dimensionality reduction were performed in alignment with the published studies where possible. Cell type annotation of clusters was done in multiple steps. Label transfer from multiple published datasets (see above) was used for automated annotation of clusters using Seurat. Seurat's FindMarkers was used to determine marker genes for each cluster. Cluster annotations were manually validated afterward. Here, information from different reference data sets, in addition to the expression of canonical marker genes, was validated. Clusters annotated as striatal cell types were excluded from further analyses due to sample preparation variabilities,

i.e., brain region adjacent to forebrain, and the presence or absence thereof is highly variable. To reduce the complexity of downstream analyses, clusters belonging to the same cell type annotation were merged. To avoid merging disparate clusters, differential expression (using FindMarkers of subgroups of clusters) was used as a reference.

Cell variability

** performed by Christoph Büschl*

Single-cell gene expression heterogeneity within each cell type cluster and mutant was tested and visualized using coefficient of variation (CV) histogram plots and permutation testing. Permutation testing refers to the number of genes designated as significantly different between i) cells of the same transgenic mouse line or the *C57BL/6J* wild-type mice or ii) cells of different transgenic mouse line or the *C57BL/6J* wild-type mice. 12 cells were randomly sampled from the respective population(s) two times, and differences in expression values were obtained. Any difference value that was obtained from less than 10 cells with an expression value was discarded. Then, two such differences in expression value sets (either for i) or ii)) were compared with a t-test and deemed to have a high variability when their p-value was below 0.05. This was repeated 10 times. Furthermore, differences were also calculated between cell type clusters of one transgenic mouse line and the *C57BL/6J* wild-type mice.

Differential abundance analysis

* *performed by Christoph Dotter, Christoph Büschl and Sergey Isaev*

Differential compositional analysis of cell abundances between all ASD mutants collectively and wild-type mice was conducted using the scCODA Python package[408] (version 0.1.8), employing Hamiltonian Monte Carlo sampling. The reference cell types used were as follows: Layer I (Cajal-Retzius) neurons for the cerebral cortex at E14.5, caudal-ganglionic eminence interneurons (Int. CGE (Vip)) for the cerebral cortex at P4, Int. Sncg (Vip) for the cerebral cortex at P14 and Choroid Plexus cells for the cerebellum at P4. The credibility of the effects was evaluated at two false discovery rate (FDR) thresholds, 0.05 and 0.01. Differential abundance of cell type clusters across individual ASD mutants was also tested with edgeR[409] (version 3.42.4) using absolute cluster abundances in cells/sample as input. For cortical time points, the model included sex as a covariate.

Pseudo-time analysis

** coding performed by Sergey Isaev*

To reconstruct the differentiation trajectory from radial glia (RG) to the cortical plate cells at E14.5, we created an embedding based on the transcriptomic profiles using the Python package Harmony[410] (harmonypy, version 0.0.5) for batch correction. After that, Palantir[411] (version 1.0.1) was used to generate a latent representation that preserves the pseudo-time ordering of cells. Utilizing the first five components of this representation, the SimplePPT algorithm[412,413] was applied to learn the principal tree that captures the differentiation process. Subsequently, the scFates tool[414] (version

1.0.6) was employed to map this principal tree back onto the constructed UMAP using Harmony-corrected PCA coordinates. Pseudo-time values for each cell were assigned by projecting the cells onto the principal tree.

Pseudo-bulk differential gene expression analysis

** coding performed by Christoph Dotter and Christoph Büschl*

Differential gene expression between genotypes within cell type clusters was performed on pseudo-bulk data. Either i) all female mice only, ii) all male mice only, or iii) all female and male mice without sex indicators were used for testing between one transgenic mouse line and the *C57BL/6J* wild-type mice.

Pseudo-bulk profiles per cluster and per sample were derived using the Libra package (version 1.0.0). Mitochondrial genes were removed, and only genes with at least 15 counts in at least two samples (single sex) or 30 counts in at least two samples (pooled sexes) were included. DESeq2[415] (version 1.40.2) was used to test for differential gene expression using test = “Wald”, fitType = “local” and an adjusted p-value threshold of 0.05. The model included sex as a covariate for the analysis of the forebrain. Shrunk fold changes for downstream rank-based analyses were calculated using the lfcShrink function. The tests involved three comparison types: a) comparing each single mutant genotype to wild-type controls, b) comparing each of the single mutant genotypes to all other mutant genotypes (excluding wild-type controls), and c) comparing the wild-type mice to all mutants collectively. Composite differential expression analysis was carried out by comparing gene names designated as differently expressed (DESeq2) and organizing these as Venn diagrams. Furthermore, a leave-one-out cross-validation strategy, which systematically removed one of the *C57BL/6J* wild-type mice from the DESeq2 comparison, was employed to investigate if any of the wild-type mice were a strong outlier. In order to assess differences between female and male wild-type controls, wild-type controls were also compared with a similar statistical setup as described above employing pseudo-bulk differential gene expression analysis. Here, instead of adjusted p-values, nominal p-values were used to assess the extent of the sex differences with a critical α threshold of 0.05.

Gene Ontology (GO) analysis and gene set enrichment analysis (GSEA)

** coding performed by Christoph Dotter and Christoph Büschl*

GO term analysis was performed using the enrichGO function from the clusterProfiler package[416] (version 4.8.2) using the list of differentially expressed genes (DEGs) using a p-value cut-off < 0.01 and q-value cut-off < 0.05.

GSEA was performed using the gseGO function from the clusterProfiler package[416] (version 4.8.2) with default parameters except minGSSize = 100 and ont = “ALL” using a p-value cut-off of < 0.05. All genes were used as input for clusterProfiler, the list of genes was sorted by $\log_2$FC using shrunk fold changes using the lfcShrink function. Benjamini-Hochberg FDR correction of p-values was used for both analyses.

In order to remove redundancy in enriched gene ontologies, the simplify-method function from clusterProfiler was used to visualize enriched gene sets (Fig. 11c).

Constructing Enrichment Maps using Cytoscape

To visualize the results of enriched gene sets and pathways for ASD mutants, the EnrichmentMap plugin[417] (version 3.4.0) for Cytoscape (version 3.10.1) was used. Enriched gene sets for excitatory neurons were loaded into the EnrichmentMap plugin with an FDR cut-off value of 0.1. Gene sets were filtered to include only those biological pathways with a minimum of 50% of experiments showing positive results. The resulting network maps grouped functionally related gene sets together (Fig. 11d). Alternatively, gene sets were not filtered to resolve converging pathways, setting no minimum experimental cut-off (Extended Data Figure 4).

Summarizing of GO terms employing REVIGO

REVIGO[418] was used to consolidate GSEA terms into a reduced set of parent terms. For this, a comprehensive list of all GSEA terms, irrespective of time point or genotype, was constructed and uploaded. The parameters “small (0.5)” and “remove obsolete GO terms” were used, resulting in robust and comprehensive clustering. Subsequently, all detected GSEA terms were mapped to their new parents. The parent terms were organized in subclusters of circular heatmaps, which were implemented with the circos R-package[419]. Representative terms were highlighted in the corresponding figures showing circular heatmaps.

Synaptic function and localization analysis using Synaptic Gene Ontology (SynGO)

SynGO[420] (v1.2) was used to identify types of known synaptic proteins (in pre- and post-synaptic compartments) and different functional classes. Lists of DEGs of the respective ASD mutants of P4 and P14 excitatory neurons were used as input to investigate overrepresented synaptic terms. Biological processes (BP) were selected for enrichment.

Differential accessibility

** coding performed by Sergey Isaev*

We conducted pseudo-bulk testing using the DESeq2 R package[415] (version 1.34.0) to identify peaks that differ between ASD mutant and wild-type mice. Given the low signal-to-noise ratio in scATAC-seq experiments[421] and the high number of comparisons, we employed an uncorrected p-value threshold of 0.001 to include peaks in the list of differentially accessible regions. Motif enrichment analysis was performed on a set of down-regulated peaks using the SnapATAC2 Python package (version 2.3.0), with binomial testing and Benjamini-Hochberg FDR correction of p-values.

Bulk RNA-sequencing

** performed by Barbara Oliveira*

Sample preparation

Brain tissue from E16.5 *HnrnpU* and wild-type littermate mice (*n*= 3 per sex + genotype) were used for the bulk RNA-seq experiment. Animals coming from 3 separate litters were collected to avoid potential litter-specific biases. Timed-pregnant

females were decapitated, and embryos were rapidly dissected on ice. Cortical tissue was dissected in ice-cold PBS, meninges were removed, and the whole brain was snap-frozen in liquid nitrogen and stored at -80°C.RNA extraction was performed as described in the Methods section for RNA isolation. One µg of RNA obtained was used for cDNA library preparation using the NEBNext Ultra II Directional RNA Library Prep kit (NEB #E7765) with unique dual indexing primers (NEBNext Multiplex Oligos for Illumina, NEB #E6440S) and poly(A) selection with the NEBNext Poly(A) mRNA Magnetic Isolation Module (NEB #E7490), according to the manufacturer's protocol. Library quality and size were assessed with the High Sensitivity DNA Analysis Kit (Agilent Technologies #5067-4626) and the Bioanalyzer 2100. Libraries were sequenced on the Illumina NextSeq 2000 platform by the Vienna Bio Center NGS facility.

Pre-processing and analysis of RNA-seq

** coding performed by Christoph Büschl*

Demultiplexed FASTQ files were filtered and trimmed using Cutadapt[422] (version 4.1) and aligned to the mm10 reference genome using STAR[423]. Similarly, this method was employed to obtain read counts. All further downstream analyses were performed in R. The same pipeline used for pseudo-bulk differential gene expression analysis of the snRNA dataset as described above was employed. However, the pseudo-bulking step was omitted, and only the mutant genotype was compared to wild-type littermate mice. One sample (HET genotype, female) was removed due to an increased number (~10%) of duplicated sequences.

RNA isolation and quantitative real-time PCR (qRT-PCR) analysis

** RNA isolation was performed with the help of Matteo Barel, Real-Time PCR was performed by Matteo Barel*

Brain tissue from male and female *Ash1l*$^{+/-}$, *HnrnpU*$^{+/-}$, *Kdm6b*$^{+/-}$, *Kmt5b*$^{+/-}$, *Trip12*$^{+/-}$, *Usp7*$^{+/-}$ and *Wac*$^{+/-}$ and their wild-type littermates were used to validate the expression of targeted genes. For RNA extraction of cortical samples, 700 µl Trizol (Invitrogen) and 150 µl chloroform (Sigma) were used for homogenization, followed by centrifugation at 12,000 × *g* for 15 min at 4 °C. For cerebellar samples, 600 µl Trizol and 130 µl chloroform were used.

The upper aqueous phase was transferred to a new tube, and 1.5 volumes of 100% ethanol (EtOH) were added. RNA was extracted using Zymo-Spin™ IC columns (Zymo Research). The aqueous phase/ethanol mixture was loaded onto the column and washed with 400 µl of 70% EtOH following treatment with RQ1 DNAseI (Promega, 5 µl + 5 µl reaction buffer + 40 µl 70% EtOH) for 15 min at RT. After two washes with 70% EtOH the sample was eluted from the column with DEPC-treated H_2O. RNA concentration was measured using the NanoDrop spectrophotometer (Thermo Scientific). 1 µg of RNA was used for cDNA preparation with the RevertAid First Strand cDNA Synthesis Kit (ThermoFisher). cDNA was diluted 1:5 and used for qPCR analysis with Lightcycler 480 Sybr green master mix (Roche) on a Real-Time PCR Roche Lightcycler 480 machine. Samples were run in triplicates for target genes, a list

of all oligonucleotides used is provided in Supplementary Table 1. ΔCq expression levels (relative mRNA) were calculated upon normalization to housekeeper genes and plotted.

Illustrations and Figures

Illustrations were created with Adobe Illustrator and BioRender (BioRender.com). If any illustrations were adapted from existing literature, the primary source is cited in the figure legend title.

6 Supplementary Information

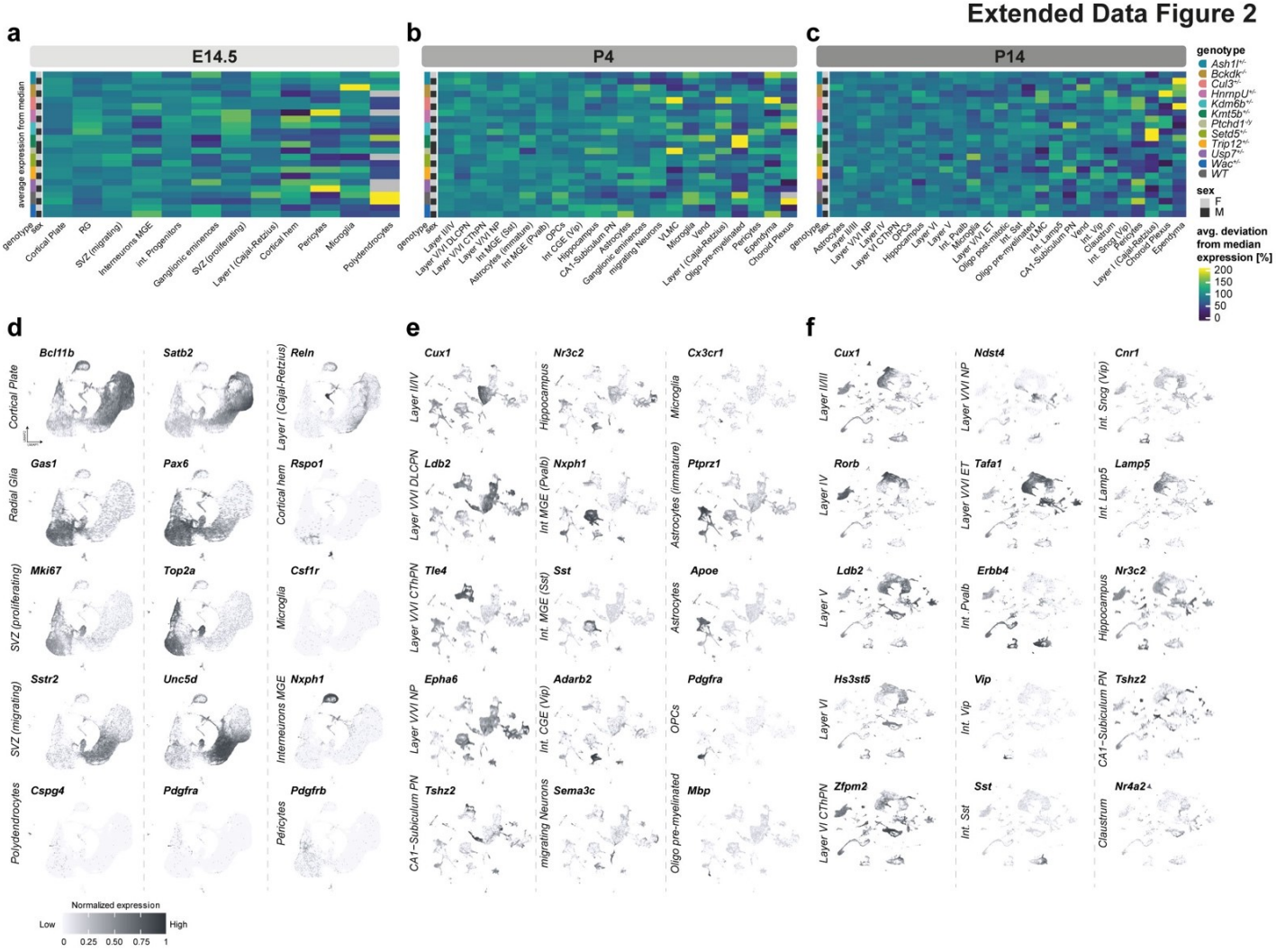
6.1 Extended Data Figures



Extended Data Fig. 1: Expression of the selected ASD risk genes and sequencing quality statistics.

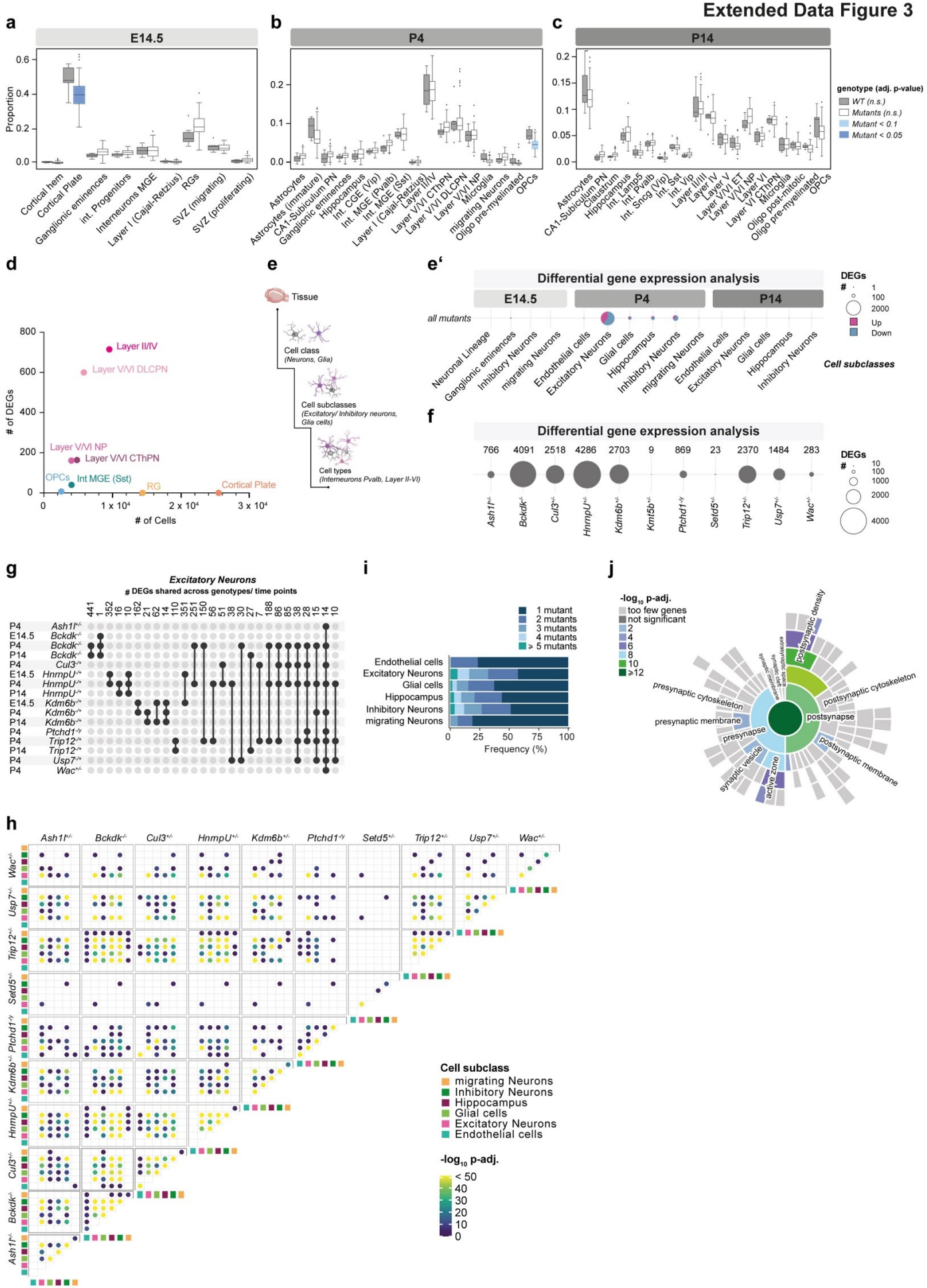
a, Quantitative real-time PCR analysis of mRNA levels for each ASD risk gene in their respective mutants. mRNA levels were normalized to *Gapdh* and *Pgk1* (ΔCq expression values; *n* (wild-types) = 3-7 per condition, *n* (mutants) = 2-8; **P* < 0.05, ***P* < 0.01, *****P* < 0.0001, n.s. not significant; 1-way ANOVA and Sidak's multiple comparison test). **b**, Expression levels of the selected high-risk ASD genes in the murine cortex during perinatal development (E16, E18, P1, and P4) based on single-cell RNA sequencing data[334] (AP, apical progenitor; IP, intermediate progenitor; MN, migrating neuron; UL, upper layer excitatory neurons; L4, layer IV excitatory neurons; DL, deeper layer excitatory neurons; A,

astrocytes; O, oligodendrocytes). **c**, Expression of the selected high-risk ASD genes in excitatory neurons of different cortical layers during postnatal development (P1, P7, and P21) based on single-cell RNA sequencing data[424] (L2/L3, layer II/III excitatory neurons; L4, layer IV excitatory neurons; L5, LV excitatory neurons; L6, layer VI excitatory neurons). Error bars presented in (**b**, **c**) depict SEM. **d**, Quality metrics for the number of genes sequenced in snRNA- and snATAC-seq and transcription starting site (TSS) enrichment per time point. The dotted lines represent the median values.



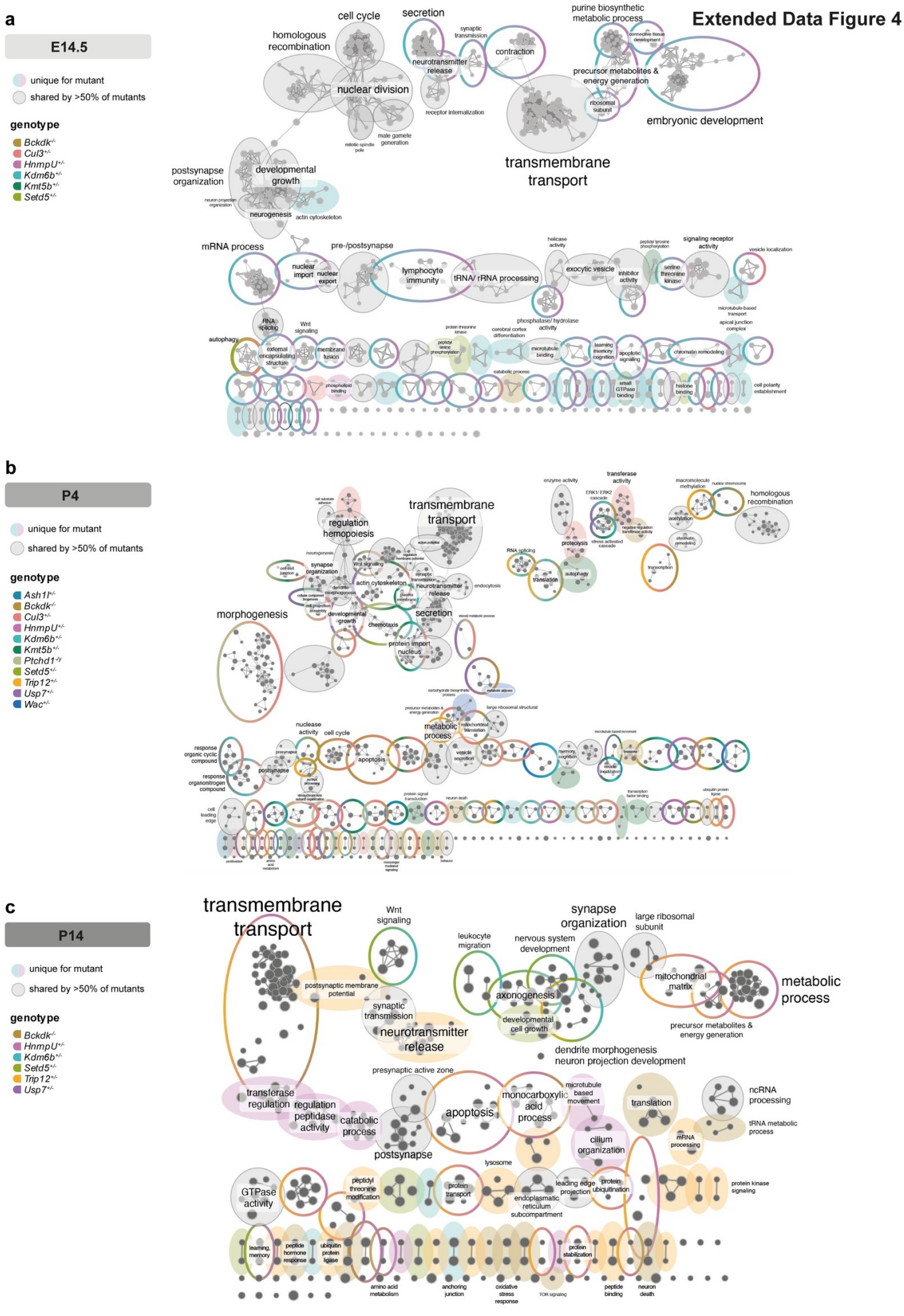
Extended Data Fig. 2: Cell type classifications and distribution across individual time points. **a-c**, Average deviation from the median expression of individual cell types of the ASD mutants across time points. Each tile in the heatmap shows the average expression deviation of each replicate relative to the median expression of all samples per cell type expressed as a percentage. **d-f**, UMAP visualization of cells collected at each time point, showing expression levels of canonical molecular markers. **g**, Box plots show marker abundance of selected cell type markers across time points. Centre lines represent medians, and the box limits show the 25-75% interquartile range.

Extended Data Figure 3



Extended Data Fig. 3: Analysis of the cellular composition and transcriptome correlations across mutants.

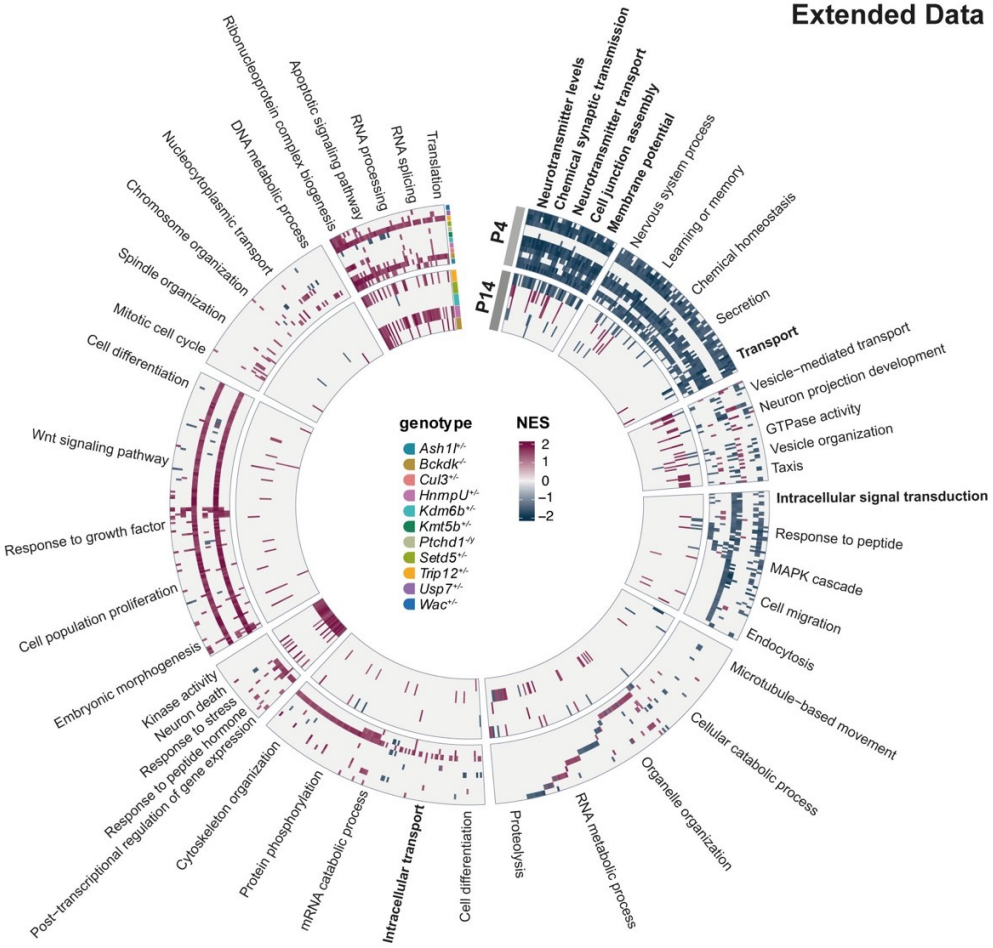
a-c, scCODA analysis from individual time points quantifying compositional cell type changes in the aggregated ASD mutants compared to wild-type controls. Center lines represent medians, the box limits show the 25-75% interquartile range (IQR), whiskers extend to 1.5 the range of the IQR, and data points outside this range are represented as dots. **d**, The relationship between the total number of cells sequenced and the number of DEGs shows no linearity. Representative cell types of E14.5 and P4 are shown. **e**, Scheme of the hierarchy between cell classes, subclasses, and types with examples. **e'**, Number of differentially expressed genes (*p-adj.* < 0.05) of cell subclasses highlights excitatory neurons at P4 as the main cell subclass sharing DEGs across mutants. "*All mutants*" refers to the mutants analyzed collectively compared to wild-type controls. **f**, Overview of the number of DEGs combined across cell subclasses and time points, with repeated DEGs counted only once. **g**, UpSet R plot showing the number of DEGs identified in the excitatory neuron lineage across time points and mutants showing that many DEGs are identified multiple times over time. Representative overlaps are shown. **h**, Correlation analysis of DEGs identified in each mutant and cell subclass at P4 revealing a high overlap among neuronal cells. **i**, Proportion of DEGs identified at P4 overlapping across a given number of mutants. **j**, SynGO analysis of DEGs found in the highest number of ASD mutants, affecting at least one cell type, reveals enrichment for genes encoding synaptic-related proteins at P4.


a
E14.5
unique for mutant
shared by >50% of mutants
genotype
Bckdk-/-
Cul3+/-
HnmpU+/-
Kdm6b+/-
Kmt5b+/-
Setd5+/-
cell cycle
secretion
homologous recombination
synaptic transmission
contraction
neurotransmitter release
nuclear division
receptor internalization
purine biosynthetic metabolic process
connective tissue development
precursor metabolites & energy generation
ribosomal subunit
embryonic development
transmembrane transport
male gamete generation
mitotic spindle pole
postsynapse organization
developmental growth
neuron projection organization
neurogenesis
actin cytoskeleton
mRNA process
pre-/postsynapse
nuclear import
nuclear export
lymphocyte immunity
tRNA/ rRNA processing
helicase activity
exocytic vesicle
inhibitor activity
peptidyl tyrosine phosphorylation
signaling receptor activity
serine threonine kinase
vesicle localization
microtubule-based transport
apical junction complex
RNA splicing
Wnt signaling
autophagy
external encapsulating structure
membrane fusion
protein threonine kinase
peptidyl serine phosphorylation
cerebral cortex differentiation
phosphatase/ hydrolase activity
microtubule binding
learning memory cognition
apoptotic signaling
chromatin remodeling
catabolic process
phospholipid binding
small GTPase binding
histone binding
cell polarity establishment
b
P4
unique for mutant
shared by >50% of mutants
genotype
Ash1l-/-
Bckdk-/-
Cul3+/-
HnmpU+/-
Kdm6b+/-
Kmt5b+/-
Ptchd1-/y
Setd5+/-
Trip12+/-
Usp7+/-
Wac+/-
transmembrane transport
regulation hemopoiesis
enzyme activity
transferase activity
ERK1/ ERK2 cascade
macromolecule methylation
homologous recombination
acetylation
proteolysis
stress activated cascade
RNA splicing
translation
autophagy
chromatin remodeling
transcription
synapse organization
Wnt signaling
actin cytoskeleton
synaptic transmission
neurotransmitter release
endocytosis
morphogenesis
developmental growth
chemotaxis
secretion
protein import
nucleus
metabolic process
nuclease activity
cell cycle
apoptosis
vesicle secretion
memory cognition
response organic cyclic compound
postsynapse
response organonitrogen compound
cell leading edge
c
P14
unique for mutant
shared by >50% of mutants
genotype
Bckdk-/-
HnmpU+/-
Kdm6b+/-
Setd5+/-
Trip12+/-
Usp7+/-
transmembrane transport
Wnt signaling
postsynaptic membrane potential
synaptic transmission
neurotransmitter release
synapse organization
large ribosomal subunit
leukocyte migration
nervous system development
axonogenesis
developmental cell growth
mitochondrial matrix
metabolic process
precursor metabolites & energy generation
dendrite morphogenesis
neuron projection development
presynaptic active zone
transferase regulation
regulation peptidase activity
catabolic process
apoptosis
monocarboxylic acid process
microtubule based movement
translation
ncRNA processing
tRNA metabolic process
mRNA processing
cilium organization
postsynapse
lysosome
GTPase activity
peptidyl threonine modification
protein transport
endoplasmatic reticulum subcompartment
leading edge projection
protein ubiquitination
protein kinase signaling
learning, memory
peptide hormone response
ubiquitin protein ligase
protein stabilization
amino acid metabolism
anchoring junction
oxidative stress response
TOR signaling
peptide binding
neuron death

Extended Data Fig. 4: Network of the biological processes affected in ASD mutant mice.
a-c, Networks of GO terms identified in the excitatory neuronal lineage at E14.5 (**a**), P4 (**b**), and P14 (**c**). GO terms were automatically clustered using the EnrichmentMap plugin of Cytoscape. Nodes represent functionally related gene sets. Cluster size (circles) corresponds to the total number of gene sets. Cluster in grey indicate processes shared by at least 50% of the mutants. Clusters are colored to match the color of an ASD mutant and to indicate processes unique to that mutant. Shared processes are highlighted by colored contours representing the respective ASD mutants.

a

P4 & P14 - Excitatory neurons

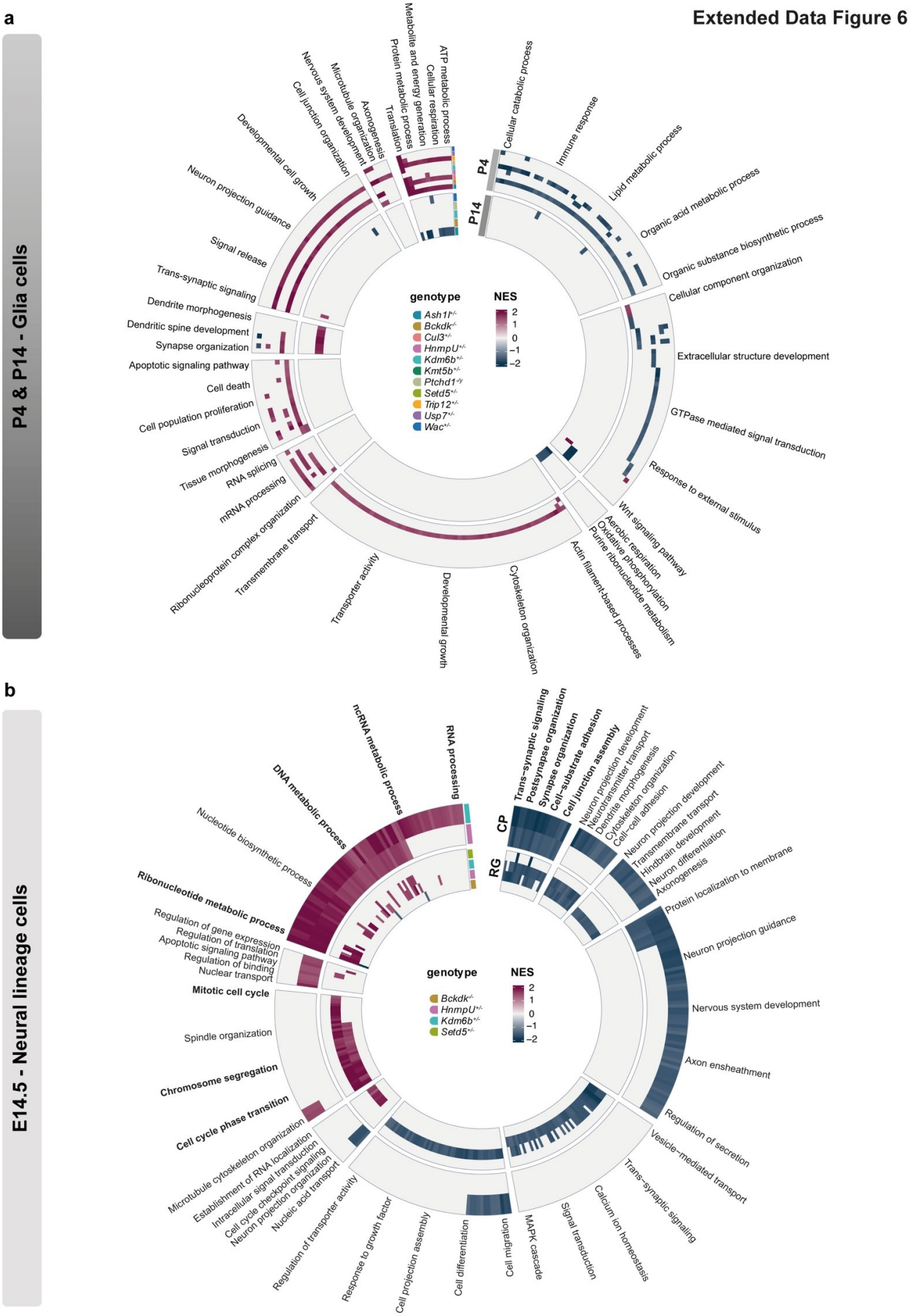


b

P4 & P14 - Inhibitory neurons

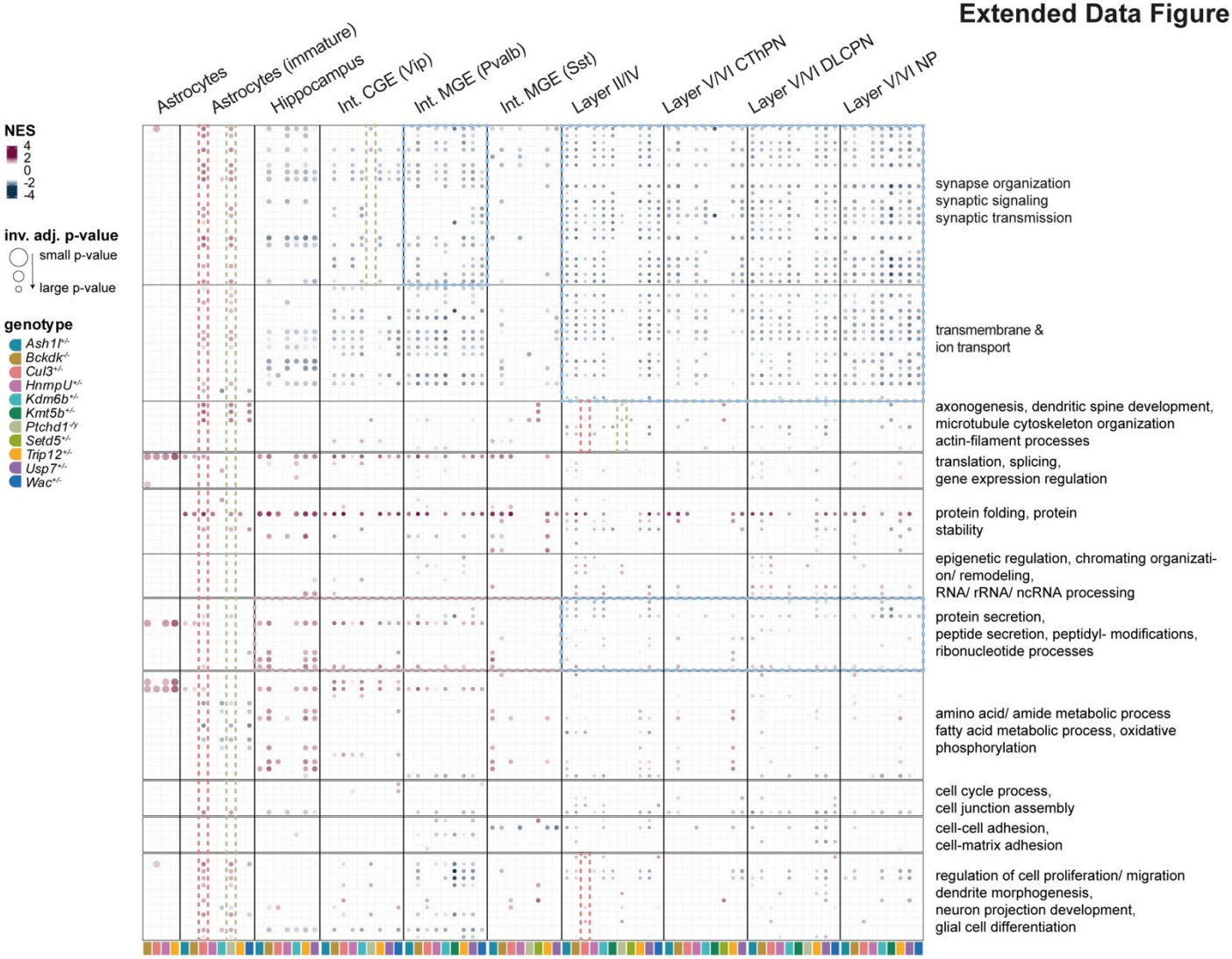


Extended Data Fig. 5: Biological processes impacted in excitatory cells and inhibitory neurons at postnatal stages.
a, **b**, Circular heatmap of enriched biological processes at P4 and P14 in excitatory (**a**) and inhibitory neurons (**b**). Representative terms have been selected, and processes mentioned in the results are highlighted in bold.

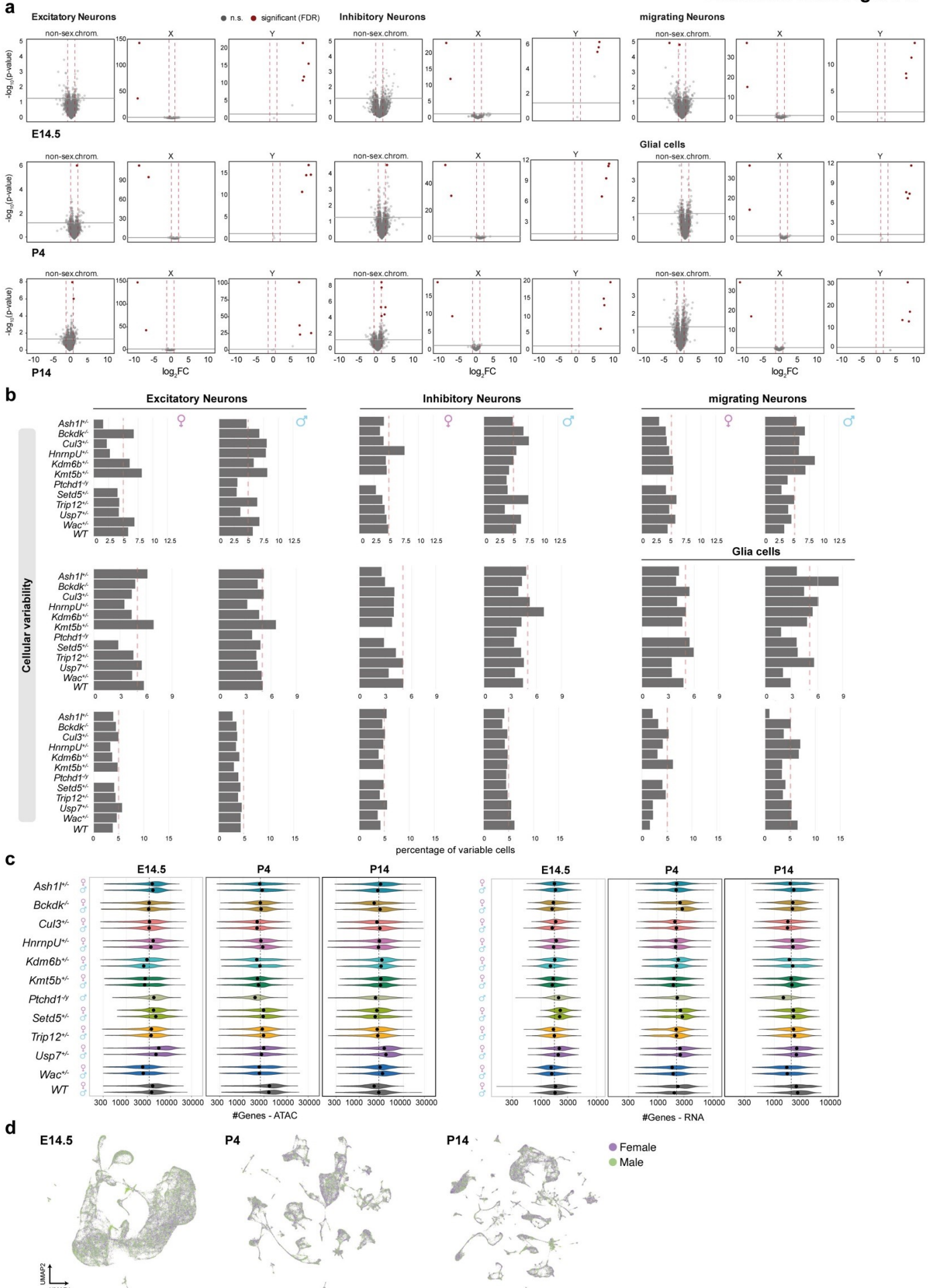

a
P4 & P14 - Glia cells
P4
P14
Cellular catabolic process
Immune response
Lipid metabolic process
Organic acid metabolic process
Organic substance biosynthetic process
Cellular component organization
Extracellular structure development
GTPase mediated signal transduction
Response to external stimulus
Wnt signaling pathway
Aerobic respiration
Oxidative phosphorylation
Purine ribonucleotide metabolism
Actin filament-based processes
Cytoskeleton organization
Developmental growth
Transporter activity
Transmembrane transport
Ribonucleoprotein complex organization
mRNA processing
RNA splicing
Tissue morphogenesis
Signal transduction
Cell population proliferation
Cell death
Apoptotic signaling pathway
Synapse organization
Dendritic spine development
Dendrite morphogenesis
Trans-synaptic signaling
Signal release
Neuron projection guidance
Developmental cell growth
Cell junction organization
Nervous system development
Microtubule organization
Axonogenesis
Translation
Protein metabolic process
Metabolite and energy generation
Cellular respiration
ATP metabolic process
genotype
Ash1l+/-
Bckdk+/-
Cul3+/-
HnmpU+/-
Kdm6b+/-
Kmt5b+/-
Ptchd1-/y
Setd5+/-
Trip12+/-
Usp7+/-
Wac+/-
NES
2
1
0
−1
−2
b
E14.5 - Neural lineage cells
CP
RG
Trans−synaptic signaling
Postsynapse organization
Synapse organization
Cell−substrate adhesion
Cell junction assembly
Neuron projection development
Neurotransmitter transport
Dendrite morphogenesis
Cytoskeleton organization
Cell−cell adhesion
Neuron projection development
Transmembrane transport
Hindbrain development
Neuron differentiation
Axonogenesis
Protein localization to membrane
Neuron projection guidance
Nervous system development
Axon ensheathment
Regulation of secretion
Vesicle−mediated transport
Trans−synaptic signaling
Calcium ion homeostasis
Signal transduction
MAPK cascade
Cell migration
Cell differentiation
Cell projection assembly
Response to growth factor
Regulation of transporter activity
Nucleic acid transport
Neuron projection organization
Cell cycle checkpoint signaling
Intracellular signal transduction
Establishment of RNA localization
Microtubule cytoskeleton organization
Cell cycle phase transition
Chromosome segregation
Spindle organization
Mitotic cell cycle
Nuclear transport
Regulation of binding
Apoptotic signaling pathway
Regulation of translation
Regulation of gene expression
Ribonucleotide metabolic process
Nucleotide biosynthetic process
DNA metabolic process
ncRNA metabolic process
RNA processing
genotype
Bckdk+/-
HnmpU+/-
Kdm6b+/-
Setd5+/-
NES
2
1
0
−1
−2

Extended Data Fig. 6: Biological processes affected in neural lineage cells at E14.5, and glial cells at postnatal stages.
a, **b**, Circular heatmap of enriched biological processes at P4 and P14 in glial cells (**a**) and neural lineage cells, including RG and CP cells at E14.5 (**b**). Representative terms have been selected, and processes mentioned in the results are highlighted in bold.

Extended Data Figure 7

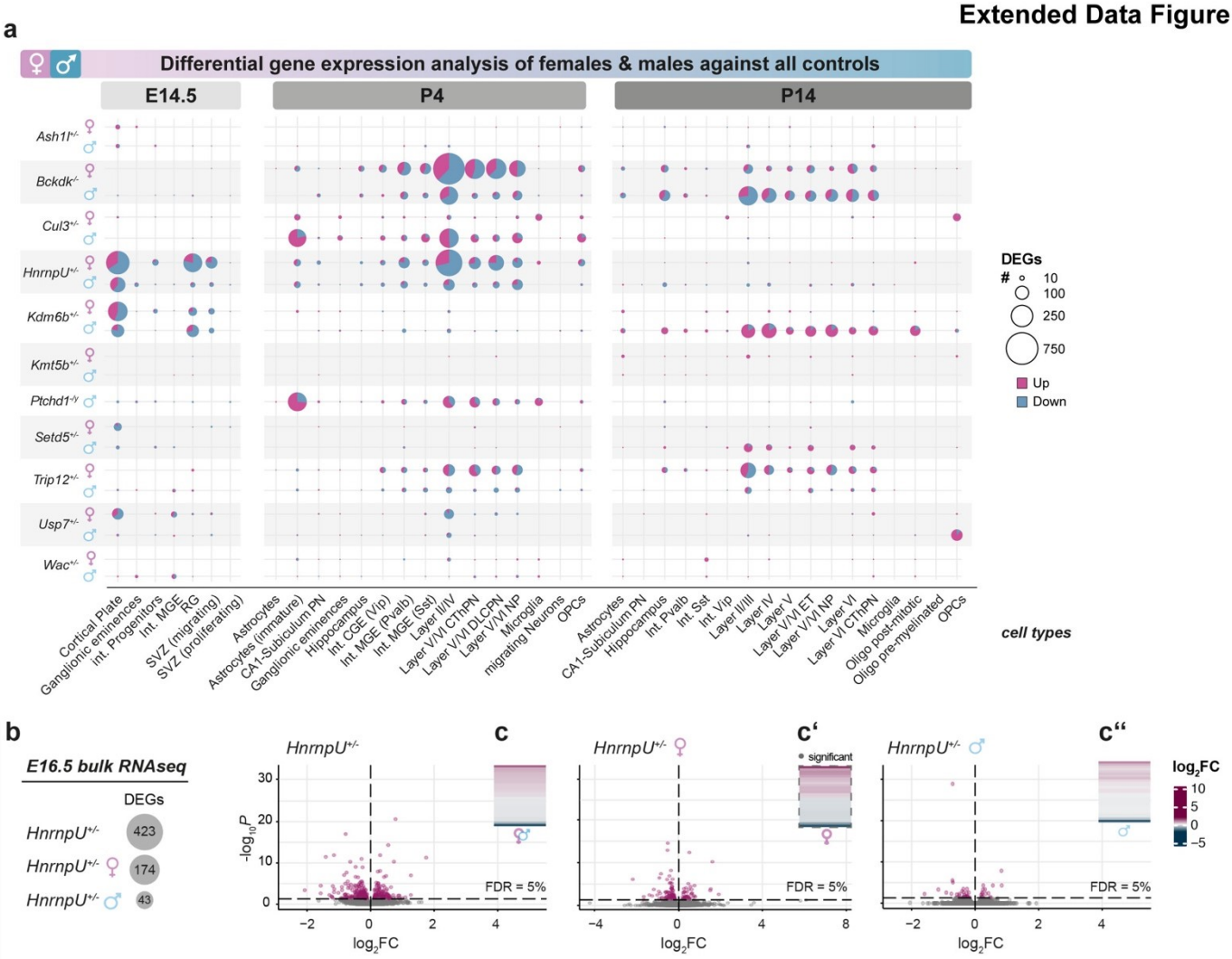


Extended Data Fig. 7: Gene Set Enrichment Analysis of individual cell types at P4.
a, Heatmap showing the gene set enriched in different cell types at P4. Processes mentioned in the results are highlighted (dashed rectangles).


a
Excitatory Neurons
n.s.
significant (FDR)
Inhibitory Neurons
migrating Neurons
Glial cells
non-sex.chrom.
X
Y
-log10(p-value)
log2FC
E14.5
P4
P14
b
Excitatory Neurons
Inhibitory Neurons
migrating Neurons
Glia cells
Cellular variability
Ash1l+/-
Bckdk+/-
Cul3+/-
HnrnpU+/-
Kdm6b+/-
Kmt5b+/-
Ptchd1-/y
Setd5+/-
Trip12+/-
Usp7+/-
Wac+/-
WT
percentage of variable cells
c
E14.5
P4
P14
#Genes - ATAC
#Genes - RNA
d
E14.5
P4
P14
Female
Male
UMAP2
UMAP1

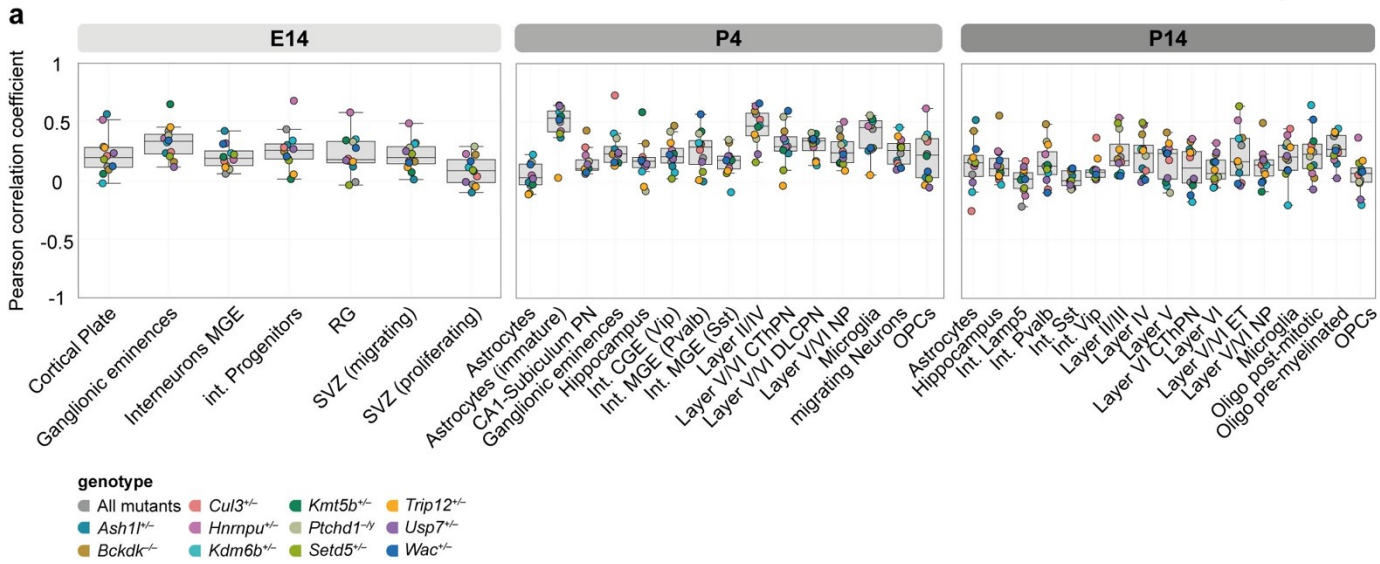
Extended Data Fig. 8: Differential gene expression analysis and quality control of female and male mice.

a, Differential gene expression analysis of wild-type female and male mice exhibits very little transcriptional differences. DEGs with a nominal *p-value* < 0.05 are shown. **b**, The fraction of gene expression differences observed through pairwise comparison of random cells between females and males of the same genotype suggests minimal variability in gene expression across cells. **c**, Quality metrics for number of genes sequenced in snRNA- and snATAC-seq in females and males across time points. The dotted lines represent the median values. **d**, UMAP visualization of integrated snRNA- and snATAC-seq data from individual time points. Cells are colored based on sex.



Extended Data Fig. 9: Gene expression analysis of female and male ASD mutants, bulk RNA-seq results confirm sex-specific gene expression changes.

a, Number of differentially expressed genes (*p-adj.* < 0.05) in cell types across female and male ASD mutants in comparison to all (female & male) wild types collectively. **b**, Independent bulk RNA-seq analysis of E16.5 *HnrnpU* brains reveals that females exhibit a higher number of DEGs compared to males. **c-c’’**, Heatmaps of the fold changes of a representative subset of DEGs significant in females show that the directionality of changes was similar in males.



Extended Data Fig. 10: Correlation of snRNA- and snATAC-seq.
a, Pearson correlation between fold changes of genes (*p-value* < 0.1) of pseudo-bulk chromatin accessibility and gene expression across cell types and time points. Center lines represent medians, the box limits show the 25-75% interquartile range (IQR), whiskers extend to 1.5 the range of the IQR.

6.2 Supplementary Tables

Supplementary Table 1: List of barcodes used for sequencing, oligonucleotides, and cell type references used (related to Methods section)
Sequences of i5 and i7 indices, List of CMO barcodes, Sequences and purpose of all oligonucleotides used, List of reference datasets used for label-transfer in cell type annotations

oligo_ID	Full Sequence
10xMULTIseq_501	AATGATACGGCGACCACCGAGATCTACACTCGTGGAGCGACACTCTTTCCCTACACGACGC*T*C
10xMULTIseq_502	AATGATACGGCGACCACCGAGATCTACACCTACAAGATAACACTCTTTCCCTACACGACGC*T*C
10xMULTIseq_503	AATGATACGGCGACCACCGAGATCTACACTATAGTAGCTACACTCTTTCCCTACACGACGC*T*C
10xMULTIseq_504	AATGATACGGCGACCACCGAGATCTACACTGCCTGGTGGACACTCTTTCCCTACACGACGC*T*C
10xMULTIseq_505	AATGATACGGCGACCACCGAGATCTACACACATTATCCTACACTCTTTCCCTACACGACGC*T*C
10xMULTIseq_506	AATGATACGGCGACCACCGAGATCTACACGTCCACTTGTACACTCTTTCCCTACACGACGC*T*C
10xMULTIseq_507	AATGATACGGCGACCACCGAGATCTACACTGGAACAGTAACACTCTTTCCCTACACGACGC*T*C
10xMULTIseq_508	AATGATACGGCGACCACCGAGATCTACACCCTTGTTAATACACTCTTTCCCTACACGACGC*T*C
10xMULTIseq_509	AATGATACGGCGACCACCGAGATCTACACGTTGATAGTGACACTCTTTCCCTACACGACGC*T*C
10xMULTIseq_510	AATGATACGGCGACCACCGAGATCTACACACCAGCGACAACACTCTTTCCCTACACGACGC*T*C
10xMULTIseq_701	CAAGCAGAAGACGGCATACGAGATCGCTCAGTTCGTGACTGGAGTTCCTTGGCACCCGAGAATTC*C*A
10xMULTIseq_702	CAAGCAGAAGACGGCATACGAGATTATCTGACCTGTGACTGGAGTTCCTTGGCACCCGAGAATTC*C*A
10xMULTIseq_703	CAAGCAGAAGACGGCATACGAGATATATGAGACGGTGACTGGAGTTCCTTGGCACCCGAGAATTC*C*A
10xMULTIseq_704	CAAGCAGAAGACGGCATACGAGATCTTATGGAATGTGACTGGAGTTCCTTGGCACCCGAGAATTC*C*A
10xMULTIseq_705	CAAGCAGAAGACGGCATACGAGATTAATCTCGTCGTGACTGGAGTTCCTTGGCACCCGAGAATTC*C*A
10xMULTIseq_706	CAAGCAGAAGACGGCATACGAGATGCGCGATGTTGTGACTGGAGTTCCTTGGCACCCGAGAATTC*C*A
10xMULTIseq_707	CAAGCAGAAGACGGCATACGAGATAGAGCACTAGGTGACTGGAGTTCCTTGGCACCCGAGAATTC*C*A
10xMULTIseq_708	CAAGCAGAAGACGGCATACGAGATTGCCTTGATCGTGACTGGAGTTCCTTGGCACCCGAGAATTC*C*A
10xMULTIseq_709	CAAGCAGAAGACGGCATACGAGATCTACTCAGTCGTGACTGGAGTTCCTTGGCACCCGAGAATTC*C*A
10xMULTIseq_710	CAAGCAGAAGACGGCATACGAGATTCGTCTGACTGTGACTGGAGTTCCTTGGCACCCGAGAATTC*C*A

CMO class	Full Sequence
CMO Co-Anchor	TGGAATTCTCGGGTGCCAAGGTAGTGA/3CholTEG/
CMO Anchor-Barcode_1	/5Chol-TEG/TCACTACCTTGGCACCCGAGAATTCCAACCCACCAGTAAGACBAAAAAAAAAAAAAAAAAAAAAAAAAA*A*A

CMO Anchor-Barcode_2	/5Chol-TEG/TCACTACCTTGGCACCCGAGAATTCCAGGTCGAGAGCATTCABAAAAAAAAAAAAAAAAAAAAAAAAA*A*A
CMO Anchor-Barcode_3	/5Chol-TEG/TCACTACCTTGGCACCCGAGAATTCCACTTGCCGCATGTCATBAAAAAAAAAAAAAAAAAAAAAAAAA*A*A
CMO Anchor-Barcode_4	/5Chol-TEG/TCACTACCTTGGCACCCGAGAATTCCAAAAGCATTCTTCACGBAAAAAAAAAAAAAAAAAAAAAAAAA*A*A
CMO Anchor-Barcode_5	/5Chol-TEG/TCACTACCTTGGCACCCGAGAATTCCACTTTGTCTTTGTGAGBAAAAAAAAAAAAAAAAAAAAAAAAA*A*A
CMO Anchor-Barcode_6	/5Chol-TEG/TCACTACCTTGGCACCCGAGAATTCCATATGCTGCCACGGTABAAAAAAAAAAAAAAAAAAAAAAAAA*A*A

Oligonucleotides	
Sequence	***Purpose***
5' ACCTAGGGGAAGTTGTCAGC 3'	Genotyping & Sanger sequencing primer: *Ash1l* mouse forward
5' CCGATTCACGGTTTCATGC 3'	Genotyping primer: *Ash1l* mouse reverse
5' AAGTGGAATAACTCACAGTAACTCAC 3'	Genotyping primer: *Bckdk* mouse forward
5' CCTCGAGGATGCAGACGTGCTCAGC 3'	Genotyping primer: *Bckdk* mouse reverse
5' AAATGGCGTTACTTAAGCTAGCTTGC 3'	Genotyping primer: *Bckdk* mouse reverse
5' GGAAACCTAAAGTTTTTATGCATG 3'	Genotyping primer: *Cul3* mouse forward
5' TTTGTCTGGACCAAATATGGCAGCCCAAACC 3'	Genotyping primer: *Cul3* mouse reverse
5' TCAATGGCAGCACTGTAAATATGC 3'	Gentoyping primer: *HnrnpU* mouse forward
5' CAGCAGGAAATCAAAGTGTAGCAA 3'	Gentoyping primer: *HnrnpU* mouse reverse
5' GCCCTTCTACATACACTCCATCTT 3'	Gentoyping primer: *HnrnpU* mouse reverse
5' ACTGCTCTAGCACCACCACG 3'	Gentoyping primer: *Kdm6b* forward
5' CTGAGCCTCTGACCTGACTGAC 3'	Gentoyping primer: *Kdm6b* reverse
5' TGGCTCTGGTGTTGCACATG 3'	Gentoyping primer: *Kmt5b* forward
5' GGGCAGGGTCAATACCACAC 3'	Gentoyping primer: *Kmt5b* reverse
5′-GTAGGGCTGGAATCATGAGG-3′	Gentoyping primer: *Ptchd1* forward
5′-CACATCCTTTGGTGTGATGC-3′	Gentoyping primer: *Ptchd1* reverse
5' CATGTCCTTGGTGGATGAGA 3'	Gentoyping primer: *Setd5* forward
5' TGAGGTCAGCCATGTAAACAA 3'	Gentoyping primer: *Setd5* reverse
5' GGATGTGGCTCACTGTTCTCTC 3'	Gentoyping primer: *Trip12* forward
5' ACCCTGGTCCTCAGCCAAAG 3'	Gentoyping primer: *Trip12* reverse
5' TATGAAGCCGAGGCAGGAGG 3'	Gentoyping primer: *Usp7* forward
5' TGGCTAGTGGTGGGTCTTGG 3'	Gentoyping primer: *Usp7* reverse
5' TAGCACACAGATGATGTTGCT 3'	Gentoyping primer: *Wac* forward
5' AACCAAGCACATTGGAGGT 3'	Gentoyping primer: *Wac* reverse
5' GAAGAAGAGACAAGTTTTGGGACTG 3'	Gentoyping primer: Y-Chromosome forward
5' GGATATCAACAGGCTGCCAATAAAA 3'	Gentoyping primer: Y-Chromosome reverse
forward AAAGTCAGCCATGTGAGCACT	qPCR primer for *Pgk1* (housekeeping gene)
reverse ACTTAGGAGCACAGGAACCAAA	qPCR primer for *Pgk1* (housekeeping gene)

forward AACGGGAAGCTCACTGGCAT	qPCR primer for *Gapdh* (housekeeping gene)
reverse GCTTCACCACCTTCTTGATG	qPCR primer for *Gapdh (*housekeeping gene)
forward AGCACTACCTTTGTGAGCAGT	qPCR primer for *Ash1l* forward
reverse ACACACAATCACCCTGACGA	qPCR primer for *Ash1l* reverse
forward TCAATGGCAGCACTGTAAATATGC	qPCR primer for *HnrnpU* forward
reverse CAGCAGGAAATCAAAGTGTAGCAA	qPCR primer for *HnrnpU* reverse_1
reverse GCCCTTCTACATACACTCCATCTT	qPCR primer for *HnrnpU* reverse_2
forward GTACAGACCCCCGGAACC	qPCR primer for *Kdm6b* forward
reverse TGGTGGAGAAAAGGCCTAAG	qPCR primer for *Kdm6b* reverse
forward TGCGGATGTTTGCAACTGAC	qPCR primer for *Kmt5b* forward
reverse TTCGGCAATACAACCCACCA	qPCR primer for *Kmt5b* reverse
forward TTGATTGGGCTGCTCGCTT	qPCR primer for *Trip12* forward
reverse TGCGTTTCTTGGTGGACTTTC	qPCR primer for *Trip12* reverse
forward GACCCTCAGACGGACCAAAA	qPCR primer for *Usp7* forward
reverse TTGCAGGGTCCTTAGGGTCT	qPCR primer for *Usp7* reverse
forward CTCCCGTTCCACAATCAACA	qPCR primer for *Wac* forward
forward CAGCTGCTGTAAGAACTTCATTT	qPCR primer for *Wac* reverse

Timepoint	***Reference dataset used for label transfer***
E14.5 forebrain	Loo, L. *et al.* (2019) 'Single-cell transcriptomic analysis of mouse neocortical development', *Nature Communications*, 10(1), p. 134. Available at: https://doi.org/10.1038/s41467-018-08079-9. (E14.5 datset was used)
	Di Bella, D.J. *et al.* (2021) 'Molecular logic of cellular diversification in the mouse cerebral cortex', *Nature*, 595(7868), pp. 554–559. Available at: https://doi.org/10.1038/s41586-021-03670-5. (E14.5 datset was used)
P4 cortex	Zeisel, A. *et al.* (2015) 'Cell types in the mouse cortex and hippocampus revealed by single-cell RNA-seq', *Science*, 347(6226), pp. 1138–1142. Available at: https://doi.org/10.1126/science.aaa1934.
	Loo, L. *et al.* (2019) 'Single-cell transcriptomic analysis of mouse neocortical development', *Nature Communications*, 10(1), p. 134. Available at: https://doi.org/10.1038/s41467-018-08079-9. (P0 dataset was used)
	Di Bella, D.J. *et al.* (2021) 'Molecular logic of cellular diversification in the mouse cerebral cortex', *Nature*, 595(7868), pp. 554–559. Available at: https://doi.org/10.1038/s41586-021-03670-5. (P4 dataset was used)
	Yao, Z. *et al.* (2021) 'A taxonomy of transcriptomic cell types across the isocortex and hippocampal formation', *Cell*, 184(12), pp. 3222-3241.e26. Available at: https://doi.org/10.1016/j.cell.2021.04.021.
P14 cortex	Zeisel, A. et al. (2015) 'Cell types in the mouse cortex and hippocampus revealed by single-cell RNA-seq', Science, 347(6226), pp. 1138–1142. Available at: https://doi.org/10.1126/science.aaa1934.
	Bakken, T.E. *et al.* (2021) 'Comparative cellular analysis of motor cortex in human, marmoset and mouse', *Nature*, 598(7879), pp. 111–119. Available at: https://doi.org/10.1038/s41586-021-03465-8.
P4 cerebellum	Kozareva, V. *et al.* (2021) 'A transcriptomic atlas of mouse cerebellar cortex comprehensively defines cell types', *Nature*, 598(7879), pp. 214–219. Available at: https://doi.org/10.1038/s41586-021-03220-z.

References

1. Maenner, M. J. *et al.* Prevalence and Characteristics of Autism Spectrum Disorder Among Children Aged 8 Years - Autism and Developmental Disabilities Monitoring Network, 11 Sites, United States, 2018. *Morb. Mortal. Wkly. Rep. Surveill. Summ. Wash. DC 2002* **70**, 1–16 (2021).
2. Chen, J. A., Peñagarikano, O., Belgard, T. G., Swarup, V. & Geschwind, D. H. The Emerging Picture of Autism Spectrum Disorder: Genetics and Pathology. *Annu. Rev. Pathol. Mech. Dis.* **10**, 111–144 (2015).
3. Penney, A. M., Greenson, J., Schwartz, I. S. & Estes, A. M. "On-Time Autism Intervention": A Diagnostic Practice Framework to Accelerate Access. *Front. Psychiatry* **13**, (2022).
4. Zuckerman, K., Lindly, O. J. & Chavez, A. E. Timeliness of Autism Spectrum Disorder Diagnosis and Use of Services among U.S. Elementary School-Aged Children. *Psychiatr. Serv. Wash. DC* **68**, 33–40 (2017).
5. Khachadourian, V. *et al.* Comorbidities in autism spectrum disorder and their etiologies. *Transl. Psychiatry* **13**, 1–7 (2023).
6. Lundström, S. *et al.* Autism spectrum disorders and coexisting disorders in a nationwide Swedish twin study. *J. Child Psychol. Psychiatry* **56**, 702–710 (2015).
7. Zeidan, J. *et al.* Global prevalence of autism: A systematic review update. *Autism Res.* **15**, 778–790 (2022).
8. Hansen, S. N., Schendel, D. E. & Parner, E. T. Explaining the Increase in the Prevalence of Autism Spectrum Disorders: The Proportion Attributable to Changes in Reporting Practices. *JAMA Pediatr.* **169**, 56–62 (2015).
9. Sandin, S. *et al.* The Heritability of Autism Spectrum Disorder. *JAMA* **318**, 1182–1184 (2017).
10. Gaugler, T. *et al.* Most genetic risk for autism resides with common variation. *Nat. Genet.* **46**, 881–885 (2014).
11. Cirnigliaro, M. *et al.* The contributions of rare inherited and polygenic risk to ASD in multiplex families. *Proc. Natl. Acad. Sci.* **120**, e2215632120 (2023).
12. Grove, J. *et al.* Identification of common genetic risk variants for autism spectrum disorder. *Nat. Genet.* **51**, 431–444 (2019).

13. Modabbernia, A., Velthorst, E. & Reichenberg, A. Environmental risk factors for autism: an evidence-based review of systematic reviews and meta-analyses. *Mol. Autism* **8**, 13 (2017).
14. Meredith, R. M. Sensitive and critical periods during neurotypical and aberrant neurodevelopment: a framework for neurodevelopmental disorders. *PubMed* (2015).
15. Basilico, B., Morandell, J. & Novarino, G. Molecular mechanisms for targeted ASD treatments. *Curr. Opin. Genet. Dev.* **65**, 126–137 (2020).
16. Parenti, I., Rabaneda, L. G., Schoen, H. & Novarino, G. Neurodevelopmental Disorders: From Genetics to Functional Pathways. *Trends Neurosci.* **43**, 608–621 (2020).
17. Velmeshev, D. *et al. Single-Cell Analysis of Prenatal and Postnatal Human Cortical Development*. http://biorxiv.org/lookup/doi/10.1101/2022.10.24.513555 (2022) doi:10.1101/2022.10.24.513555.
18. Wamsley, B. *et al.* Molecular cascades and cell type–specific signatures in ASD revealed by single-cell genomics. *Science* **384**, eadh2602 (2024).
19. Satterstrom, F. K. *et al.* Large-Scale Exome Sequencing Study Implicates Both Developmental and Functional Changes in the Neurobiology of Autism. *Cell* **180**, 568-584.e23 (2020).
20. De La Torre-Ubieta, L., Won, H., Stein, J. L. & Geschwind, D. H. Advancing the understanding of autism disease mechanisms through genetics. *Nat. Med.* **22**, 345–361 (2016).
21. Abrahams, B. S. *et al.* SFARI Gene 2.0: a community-driven knowledgebase for the autism spectrum disorders (ASDs). *Mol. Autism* **4**, 36 (2013).
22. Dantuma, N. P. & Bott, L. C. The ubiquitin-proteasome system in neurodegenerative diseases: Precipitating factor, yet part of the solution. *Front. Mol. Neurosci.* **7**, 1–18 (2014).
23. Hamilton, A. M. & Zito, K. Breaking it down: the ubiquitin proteasome system in neuronal morphogenesis. *Neural Plast.* **2013**, 196848 (2013).
24. Wu, S. *et al.* Advanced parental age and autism risk in children: a systematic review and meta-analysis. *Acta Psychiatr. Scand.* **135**, 29–41 (2017).
25. Iossifov, I. *et al.* The contribution of de novo coding mutations to autism spectrum disorder. *Nature* **515**, 216–221 (2014).

26. Neale, B. M. *et al.* Patterns and rates of exonic de novo mutations in autism spectrum disorders. *Nature* **485**, 242–245 (2012).
27. Kong, A. *et al.* Rate of de novo mutations and the importance of father's age to disease risk. *Nature* **488**, 471–475 (2012).
28. O'Roak, B. J. *et al.* Sporadic autism exomes reveal a highly interconnected protein network of de novo mutations. *Nature* **485**, 246–250 (2012).
29. Iossifov, I. *et al.* De Novo Gene Disruptions in Children on the Autistic Spectrum. *Neuron* **74**, 285–299 (2012).
30. De Rubeis, S. *et al.* Synaptic, transcriptional and chromatin genes disrupted in autism. *Nature* **515**, 209–215 (2014).
31. Zhou, X. *et al.* Integrating de novo and inherited variants in 42,607 autism cases identifies mutations in new moderate-risk genes. *Nat. Genet.* **54**, 1305–1319 (2022).
32. Reichard, J. & Zimmer-Bensch, G. Frontiers | The Epigenome in Neurodevelopmental Disorders. doi:10.3389/fnins.2021.776809.
33. Zahir, F. R. & Brown, C. J. Epigenetic Impacts on Neurodevelopment: Pathophysiological Mechanisms and Genetic Modes of Action. *Pediatr. Res.* **69**, 92–100 (2011).
34. Salinas, R. D., Connolly, D. R. & Song, H. Epigenetics in Neurodevelopment. *Neuropathol. Appl. Neurobiol.* **46**, 6–27 (2020).
35. Schanen, N. C. Epigenetics of autism spectrum disorders. *Hum. Mol. Genet.* **15**, R138–R150 (2006).
36. Keil, K. P. & Lein, P. J. DNA methylation: a mechanism linking environmental chemical exposures to risk of autism spectrum disorders? *Environ. Epigenetics* **2**, dvv012 (2016).
37. Rangasamy, S., D'Mello, S. R. & Narayanan, V. Epigenetics, Autism Spectrum, and Neurodevelopmental Disorders. *Neurotherapeutics* **10**, 742–756 (2013).
38. LaSalle, J. M. Epigenomic signatures reveal mechanistic clues and predictive markers for autism spectrum disorder. *Mol. Psychiatry* **28**, 1890–1901 (2023).
39. Loke, Y. J., Hannan, A. J. & Craig, J. M. Frontiers | The Role of Epigenetic Change in Autism Spectrum Disorders.
40. Lasser, M. *et al.* Pleiotropy of autism-associated chromatin regulators. *Development* **150**, dev201515 (2023).
41. Fu, J. M. *et al.* Rare coding variation provides insight into the genetic architecture and phenotypic context of autism. *Nat. Genet.* **54**, 1320–1331 (2022).

42. Schaafsma, S. M. & Pfaff, D. W. Etiologies underlying sex differences in Autism Spectrum Disorders. *Front. Neuroendocrinol.* **35**, 255–271 (2014).
43. Werling, D. M. & Geschwind, D. H. Sex differences in autism spectrum disorders. *Curr. Opin. Neurol.* **26**, 146–153 (2013).
44. Werling, D. M. The role of sex-differential biology in risk for autism spectrum disorder. *Biol. Sex Differ.* **7**, 1–18 (2016).
45. Loomes, R., Hull, L. & Mandy, W. P. L. What Is the Male-to-Female Ratio in Autism Spectrum Disorder? A Systematic Review and Meta-Analysis. *J. Am. Acad. Child Adolesc. Psychiatry* **56**, 466–474 (2017).
46. Wigdor, E. M. *et al.* The female protective effect against autism spectrum disorder. *Cell Genomics* **2**, 100134 (2022).
47. Dougherty, J. D. *et al.* Can the “female protective effect” liability threshold model explain sex differences in autism spectrum disorder? **110**, P3243-3262 (2022).
48. Zhang, Y. *et al.* Genetic evidence of gender difference in autism spectrum disorder supports the female-protective effect. *Transl. Psychiatry* **10**, 1–10 (2020).
49. Lai, M.-C. *et al.* Quantifying and exploring camouflaging in men and women with autism. *Autism* **21**, 690–702 (2017).
50. Hull, L., Petrides, K. V. & Mandy, W. The Female Autism Phenotype and Camouflaging: a Narrative Review. *Rev. J. Autism Dev. Disord.* **7**, 306–317 (2020).
51. Alaghband-rad, J., Hajikarim-Hamedani, A. & Motamed, M. Camouflage and masking behavior in adult autism. *Front. Psychiatry* **14**, 1108110 (2023).
52. Corbett, B. A. *et al.* Camouflaging in Autism: Examining Sex-Based and Compensatory Models in Social Cognition and Communication. *Autism Res. Off. J. Int. Soc. Autism Res.* **14**, 127–142 (2021).
53. Baron-Cohen, S. *et al.* Why Are Autism Spectrum Conditions More Prevalent in Males? doi:10.1371/journal.pbio.1001081.
54. Baron-Cohen, S. *et al.* Elevated fetal steroidogenic activity in autism. *Mol. Psychiatry* **20**, 369–376 (2015).
55. Mitra, I. *et al.* Pleiotropic Mechanisms Indicated for Sex Differences in Autism. (2016) doi:10.1371/journal.pgen.1006425.
56. Werling, D. M. & Geschwind, D. H. Recurrence rates provide evidence for sex-differential, familial genetic liability for autism spectrum disorders in multiplex families and twins. *Mol. Autism* **6**, 27 (2015).

57. Robinson, E. B., Lichtenstein, P., Anckarsäter, H., Happé, F. & Ronald, A. Examining and interpreting the female protective effect against autistic behavior. *Proc. Natl. Acad. Sci.* **110**, 5258–5262 (2013).
58. Jacquemont, S. *et al.* A Higher Mutational Burden in Females Supports a "Female Protective Model" in Neurodevelopmental Disorders. *Am. J. Hum. Genet.* **94**, 415–425 (2014).
59. He, X. *et al.* Integrated Model of De Novo and Inherited Genetic Variants Yields Greater Power to Identify Risk Genes. (2013) doi:10.1371/journal.pgen.1003671.
60. Mattila, M.-L. *et al.* Autism Spectrum Disorders According to *DSM-IV-TR* and Comparison With *DSM-5* Draft Criteria: An Epidemiological Study. *J. Am. Acad. Child Adolesc. Psychiatry* **50**, 583-592.e11 (2011).
61. Kopp, S. & Gillberg, C. The Autism Spectrum Screening Questionnaire (ASSQ)-Revised Extended Version (ASSQ-REV): An instrument for better capturing the autism phenotype in girls? A preliminary study involving 191 clinical cases and community controls. *Res. Dev. Disabil.* **32**, 2875–2888 (2011).
62. Van Wijngaarden-Cremers, P. J. M. *et al.* Gender and Age Differences in the Core Triad of Impairments in Autism Spectrum Disorders: A Systematic Review and Meta-analysis. *J. Autism Dev. Disord.* **44**, 627–635 (2013).
63. Wood-Downie, H., Wong, B., Kovshoff, H., Cortese, S. & Hadwin, J. A. Research Review: A systematic review and meta-analysis of sex/gender differences in social interaction and communication in autistic and nonautistic children and adolescents. *J. Child Psychol. Psychiatry* **62**, 922–936 (2021).
64. Wood-Downie, H. *et al.* Sex/Gender Differences in Camouflaging in Children and Adolescents with Autism. *J. Autism Dev. Disord.* **51**, 1353–1364 (2020).
65. Frazier, T. W., Georgiades, S., Bishop, S. L. & Hardan, A. Y. Behavioral and Cognitive Characteristics of Females and Males With Autism in the Simons Simplex Collection. **53**, P329-340.e3 (2013).
66. Lai, M.-C. *et al.* A Behavioral Comparison of Male and Female Adults with High Functioning Autism Spectrum Conditions. (2011) doi:10.1371/journal.pone.0020835.
67. Backer van Ommeren, T., Koot, H. M., Scheeren, A. M. & Begeer, S. Sex differences in the reciprocal behaviour of children with autism. *Autism* **21**, 795–803 (2017).

68. Mandy, W. *et al.* Sex Differences in Autism Spectrum Disorder: Evidence from a Large Sample of Children and Adolescents. *J. Autism Dev. Disord.* **42**, 1304–1313 (2011).
69. Rea, H. M., Øien, R. A., Shic, F., Webb, S. J. & Ratto, A. B. Sex Differences on the ADOS-2. *J. Autism Dev. Disord.* **53**, 2878–2890 (2022).
70. Hiller, R. M., Young, R. L. & Weber, N. Sex differences in pre-diagnosis concerns for children later diagnosed with autism spectrum disorder. *Autism* **20**, 75–84 (2016).
71. Harrop, C. *et al.* Social and Object Attention Is Influenced by Biological Sex and Toy Gender-Congruence in Children with and Without Autism. *Autism Res. Off. J. Int. Soc. Autism Res.* **13**, 763–776 (2020).
72. Tubío-Fungueiriño, M., Cruz, S., Sampaio, A., Carracedo, A. & Fernández-Prieto, M. Social Camouflaging in Females with Autism Spectrum Disorder: A Systematic Review. *J. Autism Dev. Disord.* **51**, 2190–2199 (2020).
73. Cook, J., Hull, L., Crane, L. & Mandy, W. Camouflaging in autism: A systematic review. *Clin. Psychol. Rev.* **89**, 102080 (2021).
74. Dean, M., Harwood, R. & Kasari, C. The art of camouflage: Gender differences in the social behaviors of girls and boys with autism spectrum disorder. *Autism* **21**, 678–689 (2017).
75. Hull, L. *et al.* "Putting on My Best Normal": Social Camouflaging in Adults with Autism Spectrum Conditions. *J. Autism Dev. Disord.* **47**, 2519–2534 (2017).
76. Cruz, S. *et al.* Is There a Bias Towards Males in the Diagnosis of Autism? A Systematic Review and Meta-Analysis. *Neuropsychol. Rev.* 1–24 (2024) doi:10.1007/s11065-023-09630-2.
77. Auyeung, B., Lombardo, M. V. & Baron-Cohen, S. Prenatal and postnatal hormone effects on the human brain and cognition. *Pflüg. Arch. - Eur. J. Physiol.* **465**, 557–571 (2013).
78. Ocañas, S. R. *et al.* Chromosomal and gonadal factors regulate microglial sex effects in the aging brain. *Brain Res. Bull.* **195**, 157–171 (2023).
79. Geschwind, N. & Galaburda, A. M. Cerebral Lateralization: Biological Mechanisms, Associations, and Pathology: I. A Hypothesis and a Program for Research. *Arch. Neurol.* **42**, 428–459 (1985).
80. Baron-Cohen, S., Knickmeyer, R. C. & Belmonte, M. K. Sex Differences in the Brain: Implications for Explaining Autism. *Science* **310**, 819–823 (2005).

81. Auyeung, B. *et al.* Fetal testosterone and autistic traits. *Br. J. Psychol.* **100**, 1–22 (2010).
82. Knickmeyer, R., Baron-Cohen, S., Raggatt, P. & Taylor, K. Foetal testosterone, social relationships, and restricted interests in children. *J. Child Psychol. Psychiatry* **46**, 198–210 (2005).
83. Auyeung, B. *et al.* Prenatal versus postnatal sex steroid hormone effects on autistic traits in children at 18 to 24 months of age. *Mol. Autism* **3**, 17 (2010).
84. Chapman, E. *et al.* Fetal testosterone and empathy: Evidence from the Empathy Quotient (EQ) and the “Reading the Mind in the Eyes” Test. *Soc. Neurosci.* **1**, 135–148 (2007).
85. Marco, E. J. & Skuse, D. H. Autism-lessons from the X chromosome. *Soc. Cogn. Affect. Neurosci.* **1**, 183–193 (2006).
86. Jamain, S. *et al.* Y chromosome haplogroups in autistic subjects. *Mol. Psychiatry* **7**, 217–219 (2002).
87. Skuse, D. H. Imprinting, the X-Chromosome, and the Male Brain: Explaining Sex Differences in the Liability to Autism. *Pediatr. Res.* **47**, 9–9 (2000).
88. Azevedo, F. A. C. *et al.* Equal numbers of neuronal and nonneuronal cells make the human brain an isometrically scaled-up primate brain. *J. Comp. Neurol.* **513**, 532–541 (2009).
89. Herculano-Houzel, S., Mota, B. & Lent, R. Cellular scaling rules for rodent brains. (2006) doi:10.1073/pnas.0604911103.
90. Lui, J. H., Hansen, D. V. & Kriegstein, A. R. Development and Evolution of the Human Neocortex. *Cell* **146**, 18–36 (2011).
91. Lodato, S. & Arlotta, P. Generating Neuronal Diversity in the Mammalian Cerebral Cortex. *Annu. Rev. Cell Dev. Biol.* **31**, 699–720 (2015).
92. Stiles, J. & Jernigan, T. L. The Basics of Brain Development. *Neuropsychol. Rev.* **20**, 327–348 (2010).
93. Kempermann, G. *et al.* Human Adult Neurogenesis: Evidence and Remaining Questions. *Cell Stem Cell* **23**, 25–30 (2018).
94. Kumar, A., Pareek, V., Faiq, M. A., Ghosh, S. K. & Kumari, C. ADULT NEUROGENESIS IN HUMANS: A Review of Basic Concepts, History, Current Research, and Clinical Implications. *Innov. Clin. Neurosci.* **16**, 30–37 (2019).

95. Silva, C. G., Peyre, E. & Nguyen, L. Cell migration promotes dynamic cellular interactions to control cerebral cortex morphogenesis. *Nat. Rev. Neurosci.* **20**, 318–318 (2019).

96. Vanderhaeghen, P. & Polleux, F. Developmental mechanisms underlying the evolution of human cortical circuits. *Nat. Rev. Neurosci.* **24**, 213–232 (2023).

97. Dwyer, N. D. *et al.* Neural Stem Cells to Cerebral Cortex: Emerging Mechanisms Regulating Progenitor Behavior and Productivity. *J. Neurosci.* **36**, 11394–11401 (2016).

98. Zeiss, C. J. Comparative Milestones in Rodent and Human Postnatal Central Nervous System Development. *Toxicol. Pathol.* **49**, 1368–1373 (2021).

99. Molnár, Z., Luhmann, H. J. & Kanold, P. O. Transient cortical circuits match spontaneous and sensory-driven activity during development. *Science* **370**, eabb2153 (2020).

100. Ameele, J. van den, Tiberi, L., Vanderhaeghen, P. & Espuny-Camacho, I. Thinking out of the dish: what to learn about cortical development using pluripotent stem cells. **37**, P334-34 (2014).

101. Akula, S. K., Exposito-Alonso, D. & Walsh, C. A. Shaping the brain: The emergence of cortical structure and folding. **58**, P2836-2849 (2023).

102. Hansen, D. V., Lui, J. H., Parker, P. R. L. & Kriegstein, A. R. Neurogenic radial glia in the outer subventricular zone of human neocortex. *Nature* **464**, 554–561 (2010).

103. Pollen, A. A. *et al.* Molecular Identity of Human Outer Radial Glia during Cortical Development. *Cell* **163**, 55–67 (2015).

104. Nowakowski, T. J., Pollen, A. A., Sandoval-Espinosa, C. & Kriegstein, A. R. Transformation of the Radial Glia Scaffold Demarcates Two Stages of Human Cerebral Cortex Development. *Neuron* **91**, 1219–1227 (2016).

105. Betizeau, M. *et al.* Precursor Diversity and Complexity of Lineage Relationships in the Outer Subventricular Zone of the Primate. **80**, p442-457 (2013).

106. Tau, G. Z. & Peterson, B. S. Normal Development of Brain Circuits. *Neuropsychopharmacology* **35**, 147–168 (2010).

107. Schepanski, S., Buss, C., Hanganu-Opatz, I. L. & Arck, P. C. Frontiers | Prenatal Immune and Endocrine Modulators of Offspring's Brain Development and Cognitive Functions Later in Life. **9**, (2018).

108. Miller, F. D. & Gauthier, A. S. Timing Is Everything: Making Neurons versus Glia in the Developing Cortex. *Neuron* **54**, 357–369 (2007).
109. Diniz, L. P., Matias, I., Siqueira, M., Stipursky, J. & Gomes, F. C. A. Astrocytes and the TGF-β1 Pathway in the Healthy and Diseased Brain: a Double-Edged Sword. *Mol. Neurobiol.* **56**, 4653–4679 (2018).
110. Métin, C., Baudoin, J.-P., Rakić, S. & Parnavelas, J. G. Cell and molecular mechanisms involved in the migration of cortical interneurons. *Eur. J. Neurosci.* **23**, 894–900 (2006).
111. Yu, Y. *et al.* Interneuron origin and molecular diversity in the human fetal brain. *Nat. Neurosci.* **24**, 1745–1756 (2021).
112. Zhao, Z. *et al.* Evolutionarily conservative and non-conservative regulatory networks during primate interneuron development revealed by single-cell RNA and ATAC sequencing. *Cell Res.* **32**, 425–436 (2022).
113. Guo, J. & Anton, E. S. Decision making during interneuron migration in the developing cerebral cortex. *Trends Cell Biol.* **24**, 342–351 (2014).
114. Lim, L. *et al.* Optimization of interneuron function by direct coupling of cell migration and axonal targeting. *Nat. Neurosci.* **21**, 920–931 (2018).
115. Bakken, T. E. *et al.* Comparative cellular analysis of motor cortex in human, marmoset and mouse. *Nature* **598**, 111–119 (2021).
116. Hodge, R. D. *et al.* Conserved cell types with divergent features in human versus mouse cortex. *Nature* **573**, 61–68 (2019).
117. Hattori, Y. Frontiers | The multifaceted roles of embryonic microglia in the developing brain. **17**, (2023).
118. Ginhoux, F. & Prinz, M. Origin of Microglia: Current Concepts and Past Controversies. *Cold Spring Harb. Perspect. Biol.* **7**, a020537 (2015).
119. Herculano-Houzel, S. The glia/neuron ratio: How it varies uniformly across brain structures and species and what that means for brain physiology and evolution. *Glia* **62**, 1377–1391 (2014).
120. Gradisnik, L. & Velnar, T. Astrocytes in the central nervous system and their functions in health and disease: A review. *World J. Clin. Cases* **11**, 3385–3394 (2023).
121. Schober, A. L., Wicki-Stordeur, L. E., Murai, K. K. & Swayne, L. A. Foundations and implications of astrocyte heterogeneity during brain development and disease. **45**, p692-703 (2022).

122. Clavreul, S. *et al.* Cortical astrocytes develop in a plastic manner at both clonal and cellular levels. *Nat. Commun.* **10**, 4884 (2019).
123. Yang, L., Li, Z., Liu, G., Li, X. & Yang, Z. Developmental Origins of Human Cortical Oligodendrocytes and Astrocytes. *Neurosci. Bull.* **38**, 47–68 (2021).
124. Degl'Innocenti, E. & Dell'Anno, M. T. Frontiers | Human and mouse cortical astrocytes: a comparative view from development to morphological and functional characterization. **17**, (2023).
125. Tan, C. X., Burrus Lane, C. J. & Eroglu, C. Chapter Nine - Role of astrocytes in synapse formation and maturation. in *Current Topics in Developmental Biology* (ed. Bashaw, G. J.) vol. 142 371–407 (Academic Press, 2021).
126. Goldman, S. A. & Kuypers, N. J. How to make an oligodendrocyte. *Development* **142**, 3983–3995 (2015).
127. Motavaf, M. & Piao, X. Frontiers | Oligodendrocyte Development and Implication in Perinatal White Matter Injury. **15**, (2021).
128. de Faria, O. *et al.* Periods of synchronized myelin changes shape brain function and plasticity. *Nat. Neurosci.* **24**, 1508–1521 (2021).
129. Fletcher, J. L., Makowiecki, K., Cullen, C. L. & Young, K. M. Oligodendrogenesis and myelination regulate cortical development, plasticity and circuit function. *Semin. Cell Dev. Biol.* **118**, 14–23 (2021).
130. Jakovcevski, I., Filipovic, R., Mo, Z., Rakic, S. & Zecevic, N. Frontiers | Oligodendrocyte development and the onset of myelination in the human fetal brain. **3**, (2009).
131. Zeisel, A. *et al.* Cell types in the mouse cortex and hippocampus revealed by single-cell RNA-seq. *Science* **347**, 1138–1142 (2015).
132. Kuhn, S., Gritti, L., Crooks, D. & Dombrowski, Y. Oligodendrocytes in Development, Myelin Generation and Beyond. *Cells* **8**, 1424 (2019).
133. Wurm, J., Konttinen, H., Andressen, C., Malm, T. & Spittau, B. Microglia Development and Maturation and Its Implications for Induction of Microglia-Like Cells from Human iPSCs. *Int. J. Mol. Sci.* **22**, 3088 (2021).
134. Matcovitch-Natan, O. *et al.* Microglia development follows a stepwise program to regulate brain homeostasis. *Science* **353**, aad8670 (2016).
135. Mosser, C.-A., Baptista, S., Arnoux, I. & Audinat, E. Microglia in CNS development: Shaping the brain for the future. *Prog. Neurobiol.* **149–150**, 1–20 (2017).

136. Lenz, K. M. & Nelson, L. H. Microglia and Beyond: Innate Immune Cells As Regulators of Brain Development and Behavioral Function. *Front. Immunol.* **9**, 698 (2018).
137. Thion, M. S., Ginhoux, F. & Garel, S. Microglia and early brain development: An intimate journey. *Science* **362**, 185–189 (2018).
138. Koziol, L. F. *et al.* Consensus Paper: The Cerebellum's Role in Movement and Cognition. *The Cerebellum* **13**, 151–177 (2013).
139. Wagner, M. J., Kim, T. H., Savall, J., Schnitzer, M. J. & Luo, L. Cerebellar granule cells encode the expectation of reward. *Nature* **544**, 96–100 (2017).
140. Bing, Y.-H., Zhang, G.-J., Sun, L., Chu, C.-P. & Qiu, D.-L. Dynamic properties of sensory stimulation evoked responses in mouse cerebellar granule cell layer and molecular layer. *Neurosci. Lett.* **585**, 114–118 (2015).
141. Ishikawa, T., Shimuta, M. & Häusser, M. Multimodal sensory integration in single cerebellar granule cells in vivo. *eLife* https://elifesciences.org/articles/12916 (2015) doi:10.7554/eLife.12916.
142. Haldipur, P. *et al.* Spatiotemporal expansion of primary progenitor zones in the developing human cerebellum. *Science* **366**, 454–460 (2019).
143. Sathyanesan, A. *et al.* Emerging connections between cerebellar development, behaviour and complex brain disorders. *Nat. Rev. Neurosci.* **20**, 298–313 (2019).
144. Rahimi-Balaei, M., Bergen, H., Kong, J. & Marzban, H. Frontiers | Neuronal Migration During Development of the Cerebellum. **12**, (2018).
145. Leto, K. *et al.* Consensus Paper: Cerebellar Development. *The Cerebellum* **15**, 789–828 (2015).
146. Essen, M. J. van, Nayler, S., Becker, E. B. E. & Jacob, J. Deconstructing cerebellar development cell by cell. (2020) doi:10.1371/journal.pgen.1008630.
147. Consalez, G. G., Goldowitz, D., Casoni, F. & Hawkes, R. Origins, Development, and Compartmentation of the Granule Cells of the Cerebellum. *Front. Neural Circuits* **14**, 611841 (2020).
148. Hibi, M., Matsuda, K., Takeuchi, M., Shimizu, T. & Murakami, Y. Evolutionary mechanisms that generate morphology and neural-circuit diversity of the cerebellum. *Dev. Growth Differ.* **59**, 228–243 (2017).
149. Amore, G. *et al.* Frontiers | A Focus on the Cerebellum: From Embryogenesis to an Age-Related Clinical Perspective. **15**, (2021).

150. Yang, F. *et al.* Single-cell multi-omics analysis of lineage development and spatial organization in the human fetal cerebellum. *Cell Discov.* **10**, 1–16 (2024).
151. Fombonne, E., Rogé, B., Claverie, J., Courty, S. & Frémolle, J. Microcephaly and Macrocephaly in Autism. *J. Autism Dev. Disord.* **29**, 113–119 (1999).
152. Sacco, R., Gabriele, S. & Persico, A. M. Head circumference and brain size in autism spectrum disorder: A systematic review and meta-analysis. *Psychiatry Res. Neuroimaging* **234**, 239–251 (2015).
153. Juric-Sekhar, G. & Hevner, R. F. Malformations of Cerebral Cortex Development: Molecules and Mechanisms. *Annu. Rev. Pathol.* **14**, 293–318 (2019).
154. Klein, S., Sharifi-Hannauer, P. & Martinez-Agosto, J. A. Macrocephaly as a Clinical Indicator of Genetic Subtypes in Autism. *Autism Res. Off. J. Int. Soc. Autism Res.* **6**, 51–56 (2013).
155. Garcia-Forn, M., Boitnott, A., Akpinar, Z. & De Rubeis, S. Linking Autism Risk Genes to Disruption of Cortical Development. *Cells* **9**, 2500 (2020).
156. Mensen, V. T. *et al.* Development of cortical thickness and surface area in autism spectrum disorder. *NeuroImage Clin.* **13**, 215–222 (2017).
157. DeSilva, M. *et al.* Congenital microcephaly: Case definition & guidelines for data collection, analysis, and presentation of safety data after maternal immunisation. *Vaccine* **35**, 6472–6482 (2017).
158. Kortüm, F. *et al.* The core FOXG1 syndrome phenotype consists of postnatal microcephaly, severe mental retardation, absent language, dyskinesia, and corpus callosum hypogenesis. (2011) doi:10.1136/jmg.2010.087528.
159. Knaus, L. S. *et al.* Large neutral amino acid levels tune perinatal neuronal excitability and survival. *Cell* **186**, 1950-1967 e25 (2023).
160. Tărlungeanu, D. C. *et al.* Impaired Amino Acid Transport at the Blood Brain Barrier Is a Cause of Autism Spectrum Disorder. *Cell* **167**, 1481-1494.e18 (2016).
161. Wu, H. *et al.* Phenotype-to-genotype approach reveals head-circumference-associated genes in an autism spectrum disorder cohort. *Clin. Genet.* **97**, 338–346 (2020).
162. Barkovich, A. J., Guerrini, R., Kuzniecky, R. I., Jackson, G. D. & Dobyns, W. B. A developmental and genetic classification for malformations of cortical development: update 2012. *Brain* **135**, 1348–1369 (2012).
163. Accogli, A. *et al.* Diagnostic Approach to Macrocephaly in Children. *Front. Pediatr.* **9**, 794069 (2022).

164. Mirzaa, G. M. & Poduri, A. Megalencephaly and hemimegalencephaly: Breakthroughs in molecular etiology. *Am. J. Med. Genet. C Semin. Med. Genet.* **166**, 156–172 (2014).

165. Winden, K. D., Yuskaitis, C. J. & Poduri, A. Megalencephaly and Macrocephaly. *Semin. Neurol.* **35**, 277–287 (2015).

166. Watrin, F., Manent, J., Cardoso, C. & Represa, A. Causes and Consequences of Gray Matter Heterotopia. *CNS Neurosci. Ther.* **21**, 112–122 (2014).

167. Klingler, E., Francis, F., Jabaudon, D. & Cappello, S. Mapping the molecular and cellular complexity of cortical malformations. *Science* **371**, eaba4517 (2021).

168. Lasser, M., Tiber, J. & Lowery, L. A. Frontiers | The Role of the Microtubule Cytoskeleton in Neurodevelopmental Disorders. **12**, (2018).

169. Guerrini, R. & Dobyns, W. B. Malformations of cortical development: clinical features and genetic causes. *Lancet Neurol.* **13**, 710–726 (2014).

170. Chakraborti, S., Natarajan, K., Curiel, J., Janke, C. & Liu, J. The emerging role of the tubulin code: From the tubulin molecule to neuronal function and disease. *Cytoskeleton* **73**, 521–550 (2016).

171. Keays, D. A. *et al.* Mutations in α-Tubulin Cause Abnormal Neuronal Migration in Mice and Lissencephaly in Humans.

172. Jaglin, X. H. *et al.* Mutations in the β-tubulin gene TUBB2B result in asymmetrical polymicrogyria. *Nat. Genet.* **41**, 746–752 (2009).

173. Bahi-Buisson, N. *et al.* The wide spectrum of tubulinopathies: what are the key features for the diagnosis? *Brain* **137**, 1676–1700 (2014).

174. Poirier, K. *et al.* Mutations in the neuronal β-tubulin subunit TUBB3 result in malformation of cortical development and neuronal migration defects. *Hum. Mol. Genet.* **19**, 4462–4473 (2010).

175. Delatycki, M. B. & Leventer, R. J. Listen carefully: LIS1 and DCX MLPA in lissencephaly and subcortical band heterotopia. *Eur. J. Hum. Genet.* **17**, 701–702 (2009).

176. Leventer, R. J., Cardoso, C., Ledbetter, D. H. & Dobyns, W. B. LIS1: from cortical malformation to essential protein of cellular dynamics. *Trends Neurosci.* **24**, 489–492 (2001).

177. Guerrini, R. & Filippi, T. Topical Review: Neuronal Migration Disorders, Genetics, and Epileptogenesis. *J. Child Neurol.* **20**, 287–299 (2005).

178. Sisodiya, S. M., Fauser, S., Cross, J. H. & Thom, M. Focal cortical dysplasia type II: biological features and clinical perspectives. *Lancet Neurol.* **8**, 830–843 (2009).
179. Jung, E.-M. *et al.* Arid1b haploinsufficiency disrupts cortical interneuron development and mouse behavior. *Nat. Neurosci.* **20**, 1694–1707 (2017).
180. Edwards, T. J., Sherr, E. H., Barkovich, A. J. & Richards, L. J. Clinical, genetic and imaging findings identify new causes for corpus callosum development syndromes. *Brain* **137**, 1579–1613 (2014).
181. Subramanian, L., Calcagnotto, M. E. & Paredes, M. F. Frontiers | Cortical Malformations: Lessons in Human Brain Development. **13**, (2020).
182. Nelson, A. D. & Bender, K. J. Dendritic Integration Dysfunction in Neurodevelopmental Disorders. *Dev. Neurosci.* **43**, 201–221 (2021).
183. Bonsi, P., De Jaco, A., Fasano, L. & Gubellini, P. Postsynaptic autism spectrum disorder genes and synaptic dysfunction. *Neurobiol. Dis.* **162**, 105564 (2022).
184. Sullivan, J. M., De Rubeis, S. & Schaefer, A. Convergence of spectrums: neuronal gene network states in autism spectrum disorder. *Curr. Opin. Neurobiol.* **59**, 102–111 (2019).
185. Pinto, D. *et al.* Convergence of genes and cellular pathways dysregulated in autism spectrum disorders. *Am. J. Hum. Genet.* **94**, 677–694 (2014).
186. Berg, J. M. & Geschwind, D. H. Autism genetics: searching for specificity and convergence. *Genome Biol.* **13**, 247–247 (2012).
187. Louros, S. R. & Osterweil, E. K. Perturbed proteostasis in autism spectrum disorders. *J. Neurochem.* **139**, 1081–1092 (2016).
188. Parikshak, N. N. *et al.* Integrative functional genomic analyses implicate specific molecular pathways and circuits in autism. *Cell* **155**, 1008–1021 (2014).
189. Krishnan, A. *et al.* Genome-wide prediction and functional characterization of the genetic basis of autism spectrum disorder. *Nat. Neurosci.* **19**, 1454–1462 (2016).
190. Bourgeron, T. From the genetic architecture to synaptic plasticity in autism spectrum disorder. *Nat. Rev. Neurosci.* **16**, 551–563 (2015).
191. Kwan, V., Unda, B. K. & Singh, K. K. Wnt signaling networks in autism spectrum disorder and intellectual disability. *J. Neurodev. Disord.* **8**, 1–10 (2016).
192. Südhof, T. C. Neuroligins and neurexins link synaptic function to cognitive disease. *Nature* **455**, 903–911 (2008).

193. Canitano, R. & Palumbi, R. Frontiers | Excitation/Inhibition Modulators in Autism Spectrum Disorder: Current Clinical Research. *Front Neurosci* **15**, (2021).
194. Culotta, L. & Penzes, P. Exploring the mechanisms underlying excitation/inhibition imbalance in human iPSC-derived models of ASD. *Mol. Autism* **11**, 32 (2020).
195. Auerbach, B. D., Osterweil, E. K. & Bear, M. F. Mutations causing syndromic autism define an axis of synaptic pathophysiology. *Nature* **480**, 63–68 (2011).
196. Ebert, D. H. & Greenberg, M. E. Activity-dependent neuronal signalling and autism spectrum disorder. *Nature* **493**, 327–337 (2013).
197. Chen, J. A., Peñagarikano, O., Belgard, T. G., Swarup, V. & Geschwind, D. H. The Emerging Picture of Autism Spectrum Disorder: Genetics and Pathology. *Annu. Rev. Pathol. Mech. Dis.* **10**, 111–144 (2015).
198. Trobiani, L. *et al.* The neuroligins and the synaptic pathway in Autism Spectrum Disorder. *Neurosci. Biobehav. Rev.* **119**, 37–51 (2020).
199. Tabuchi, K. *et al.* A Neuroligin-3 Mutation Implicated in Autism Increases Inhibitory Synaptic Transmission in Mice. *Science* **318**, 71–76 (2007).
200. Kalbassi, S., Bachmann, S. O., Cross, E., Roberton, V. H. & Baudouin, S. J. Male and Female Mice Lacking Neuroligin-3 Modify the Behavior of Their Wild-Type Littermates. (2017) doi:10.1523/ENEURO.0145-17.2017.
201. Baudouin, S. J. *et al.* Shared Synaptic Pathophysiology in Syndromic and Nonsyndromic Rodent Models of Autism. *Science* **338**, 128–132 (2012).
202. Cao, W. *et al.* Gamma Oscillation Dysfunction in mPFC Leads to Social Deficits in Neuroligin 3 R451C Knockin Mice. *Neuron* **97**, 1253-1260.e7 (2018).
203. Rabaneda, L. G., Robles-Lanuza, E., Nieto-González, J. L. & Scholl, F. G. Neurexin Dysfunction in Adult Neurons Results in Autistic-like Behavior in Mice. **8**, p338-346 (2014).
204. Huang, M., Qi, Q. & Xu, T. Targeting Shank3 deficiency and paresthesia in autism spectrum disorder: A brief review. **16**, (2023).
205. Monteiro, P. & Feng, G. SHANK proteins: roles at the synapse and in autism spectrum disorder. *Nat. Rev. Neurosci.* **18**, 147–157 (2017).
206. Hung, A. Y. *et al.* Smaller Dendritic Spines, Weaker Synaptic Transmission, but Enhanced Spatial Learning in Mice Lacking Shank1. *J. Neurosci.* **28**, 1697–1708 (2008).

207. Silverman, J. L. *et al.* Sociability and motor functions in *Shank1* mutant mice. *Brain Res.* **1380**, 120–137 (2011).
208. Jiang, Y. & Ehlers, M. D. Modeling Autism by SHANK Gene Mutations in Mice. *Neuron* **78**, 8–27 (2013).
209. Schmeisser, M. J. *et al.* Autistic-like behaviours and hyperactivity in mice lacking ProSAP1/Shank2. *Nature* **486**, 256–260 (2012).
210. Won, H. *et al.* Autistic-like social behaviour in Shank2-mutant mice improved by restoring NMDA receptor function. *Nature* **486**, 261–265 (2012).
211. Wilson, H. L. *et al.* Molecular characterisation of the 22q13 deletion syndrome supports the role of haploinsufficiency of SHANK3/PROSAP2 in the major neurological symptoms. (2003) doi:10.1136/jmg.40.8.575.
212. Phelan, M. C. *et al.* 22q13 deletion syndrome. *Am. J. Med. Genet.* **101**, 91–99 (2001).
213. Bozdagi, O. *et al.* Haploinsufficiency of the autism-associated Shank3 gene leads to deficits in synaptic function, social interaction, and social communication. *Mol. Autism* **1**, 1–15 (2010).
214. Peça, J. *et al.* Shank3 mutant mice display autistic-like behaviours and striatal dysfunction. *Nature* **472**, 437–442 (2011).
215. Wang, X. *et al.* Synaptic dysfunction and abnormal behaviors in mice lacking major isoforms of Shank3. *Hum. Mol. Genet.* **20**, 3093–3108 (2011).
216. Jaramillo, T. C. *et al.* Novel Shank3 mutant exhibits behaviors with face validity for autism and altered striatal and hippocampal function. *Autism Res.* **10**, 42–65 (2017).
217. Yang, M. *et al.* Reduced Excitatory Neurotransmission and Mild Autism-Relevant Phenotypes in Adolescent Shank3 Null Mutant Mice. *J. Neurosci.* **32**, 6525–6541 (2012).
218. Guo, B. *et al.* Anterior cingulate cortex dysfunction underlies social deficits in Shank3 mutant mice. *Nat. Neurosci.* **22**, 1223–1234 (2019).
219. Mei, Y. *et al.* Adult restoration of Shank3 expression rescues selective autistic-like phenotypes. *Nature* **530**, 481–484 (2016).
220. Jaramillo, T. C. *et al.* Early Restoration of Shank3 Expression in Shank3 Knock-Out Mice Prevents Core ASD-Like Behavioral Phenotypes. (2020) doi:10.1523/ENEURO.0332-19.2020.

221. Shcheglovitov, A. *et al.* SHANK3 and IGF1 restore synaptic deficits in neurons from 22q13 deletion syndrome patients. *Nature* **503**, 267–271 (2013).
222. Orefice, L. L. *et al.* Targeting Peripheral Somatosensory Neurons to Improve Tactile-Related Phenotypes in ASD Models. **178**, p867-886.e24 (2019).
223. Rhine, M. A., Parrott, J. M., Schultz, M. N., Kazdoba, T. M. & Crawley, J. N. Hypothesis-driven investigations of diverse pharmacological targets in two mouse models of autism. *Autism Res.* **12**, 401–421 (2019).
224. Bozdagi, O., Tavassoli, T. & Buxbaum, J. D. Insulin-like growth factor-1 rescues synaptic and motor deficits in a mouse model of autism and developmental delay. *Mol. Autism* **4**, 1–4 (2013).
225. Kolevzon, A. *et al.* Clinical trial of insulin-like growth factor-1 in Phelan-McDermid syndrome. *Mol. Autism* **13**, 17 (2022).
226. Sanders, S. J. *et al.* De novo mutations revealed by whole-exome sequencing are strongly associated with autism. *Nature* **485**, 237–241 (2012).
227. Meisler, M. H., Hill, S. F. & Yu, W. Sodium channelopathies in neurodevelopmental disorders. *Nat. Rev. Neurosci.* **22**, 152–166 (2021).
228. Ding, J. *et al.* SCN1A Mutation—Beyond Dravet Syndrome: A Systematic Review and Narrative Synthesis. *Front. Neurol.* **12**, 743726 (2021).
229. Scheffer, I. E. & Nabbout, R. SCN1A-related phenotypes: Epilepsy and beyond. *Epilepsia* **60**, S17–S24 (2019).
230. Han, S. *et al.* Autistic behavior in Scn1a+/− mice and rescue by enhanced GABAergic transmission. *Nature* **489**, 385–390 (2012).
231. Ogiwara, I. *et al.* Nav1.2 haplodeficiency in excitatory neurons causes absence-like seizures in mice. *Commun. Biol.* **1**, 1–16 (2018).
232. Spratt, P. W. E. *et al.* The Autism-Associated Gene *Scn2a* Contributes to Dendritic Excitability and Synaptic Function in the Prefrontal Cortex. *Neuron* **103**, 673-685.e5 (2019).
233. Gallegos, D. A., Chan, U., Chen, L.-F. & West, A. E. Chromatin Regulation of Neuronal Maturation and Plasticity. *Trends Neurosci.* **41**, (2018).
234. LaSalle, J. M. Autism genes keep turning up chromatin. *OA Autism* **1**, 14 (2013).
235. Suzuki, M. M. & Bird, A. DNA methylation landscapes: provocative insights from epigenomics. *Nat. Rev. Genet.* **9**, 465–476 (2008).

236. Kreibich, E., Kleinendorst, R., Barzaghi, G., Kaspar, S. & Krebs, A. R. Single-molecule footprinting identifies context-dependent regulation of enhancers by DNA methylation. *Mol. Cell* **83**, 787-802.e9 (2023).
237. Bannister, A. J. & Kouzarides, T. Regulation of chromatin by histone modifications. *Cell Res.* **21**, 381–395 (2011).
238. Ladd-Acosta, C. *et al.* Common DNA methylation alterations in multiple brain regions in autism. *Mol. Psychiatry* **19**, 862–871 (2014).
239. Sun, W. *et al.* Histone Acetylome-wide Association Study of Autism Spectrum Disorder. *Cell* **167**, p1385-1397.e11 (2016).
240. Rylaarsdam, L. & Guemez-Gamboa, A. Frontiers | Genetic Causes and Modifiers of Autism Spectrum Disorder. *Front. Cell. Neurosci.* **13**, (2019).
241. Corley, M. J. *et al.* Frontiers | Epigenetic Delay in the Neurodevelopmental Trajectory of DNA Methylation States in Autism Spectrum Disorders. **10**, (2019).
242. Gabriele, M., Lopez Tobon, A., D'Agostino, G. & Testa, G. The chromatin basis of neurodevelopmental disorders: Rethinking dysfunction along the molecular and temporal axes. *Prog. Neuropsychopharmacol. Biol. Psychiatry* **84**, 306–327 (2018).
243. Good, K. V., Vincent, J. B. & Ausió, J. Frontiers | MeCP2: The Genetic Driver of Rett Syndrome Epigenetics. *Front. Genet.* **12**, (2021).
244. Chahrour, M. & Zoghbi, H. Y. The Story of Rett Syndrome: From Clinic to Neurobiology. *Neuron* **56**, 422–437 (2007).
245. Jung, B. P. *et al.* The expression of methyl CpG binding factor MeCP2 correlates with cellular differentiation in the developing rat brain and in cultured cells. *J. Neurobiol.* **55**, 86–96 (2003).
246. Shahbazian, M. D., Antalffy, B., Armstrong, D. L. & Zoghbi, H. Y. Insight into Rett syndrome: MeCP2 levels display tissue- and cell-specific differences and correlate with neuronal maturation. *Hum. Mol. Genet.* **11**, 115–124 (2002).
247. McGraw, C. M., Samaco, R. C. & Zoghbi, H. Y. Adult Neural Function Requires MeCP2. *Science* **333**, 186–186 (2011).
248. Guy, J., Gan, J., Selfridge, J., Cobb, S. & Bird, A. Reversal of Neurological Defects in a Mouse Model of Rett Syndrome. *Science* **315**, 1143–1147 (2007).
249. Matagne, V. *et al.* Severe offtarget effects following intravenous delivery of AAV9-MECP2 in a female mouse model of Rett syndrome. *Neurobiol. Dis.* **149**, 105235 (2021).

250. Palmieri, M., Pozzer, D. & Landsberger, N. Frontiers | Advanced genetic therapies for the treatment of Rett syndrome: state of the art and future perspectives. **17**, (2023).
251. Bracha, S. *et al.* Engineering Toxoplasma gondii secretion systems for intracellular delivery of multiple large therapeutic proteins to neurons. *Nat. Microbiol.* **9**, 2051–2072 (2024).
252. O'Roak, B. J. *et al.* Multiplex Targeted Sequencing Identifies Recurrently Mutated Genes in Autism Spectrum Disorders. *Science* **338**, 1619–1622 (2012).
253. Bernier, R. *et al.* Disruptive CHD8 Mutations Define a Subtype of Autism Early in Development. *Cell* **158**, 263–276 (2014).
254. Marfella, C. G. A. & Imbalzano, A. N. The Chd family of chromatin remodelers. *Mutat. Res. Mol. Mech. Mutagen.* **618**, 30–40 (2007).
255. Thompson, B. A., Tremblay, V., Lin, G. & Bochar, D. A. CHD8 Is an ATP-Dependent Chromatin Remodeling Factor That Regulates β-Catenin Target Genes. *Mol. Cell. Biol.* **28**, 3894–3904 (2008).
256. Douzgou, S. *et al.* The clinical presentation caused by truncating CHD8 variants. *Clin. Genet.* **96**, 72–84 (2019).
257. Nishiyama, M. *et al.* CHD8 suppresses p53-mediated apoptosis through histone H1 recruitment during early embryogenesis. *Nat. Cell Biol.* **11**, 172–182 (2009).
258. Katayama, Y. *et al.* CHD8 haploinsufficiency results in autistic-like phenotypes in mice. *Nature* **537**, 675–679 (2016).
259. Suetterlin, P. *et al.* Altered Neocortical Gene Expression, Brain Overgrowth and Functional Over-Connectivity in Chd8 Haploinsufficient Mice. *Cereb. Cortex* **28**, 2192–2206 (2018).
260. Gompers, A. L. *et al.* Germline Chd8 haploinsufficiency alters brain development in mouse. *Nat. Neurosci.* **20**, 1062–1073 (2017).
261. Durak, O. *et al.* Chd8 mediates cortical neurogenesis via transcriptional regulation of cell cycle and Wnt signaling. *Nat. Neurosci.* **19**, 1477–1488 (2016).
262. Ayhan, F. & Konopka, G. Regulatory genes and pathways disrupted in autism spectrum disorders. *Prog. Neuropsychopharmacol. Biol. Psychiatry* **89**, 57–64 (2019).
263. Fernandes, I. R. *et al.* Genetic variations on SETD5 underlying autistic conditions. *Dev. Neurobiol.* **78**, 500–518 (2018).

264. Grozeva, D. *et al.* De Novo Loss-of-Function Mutations in *SETD5*, Encoding a Methyltransferase in a 3p25 Microdeletion Syndrome Critical Region, Cause Intellectual Disability. *Am. J. Hum. Genet.* **94**, 618–624 (2014).

265. Kuechler, A. *et al.* Loss-of-function variants of SETD5 cause intellectual disability and the core phenotype of microdeletion 3p25.3 syndrome. *Eur. J. Hum. Genet.* **23**, 753–760 (2015).

266. Osipovich, A. B., Gangula, R., Vianna, P. G. & Magnuson, M. A. Setd5 is essential for mammalian development and the co-transcriptional regulation of histone acetylation. *Development* **143**, 4595–4607 (2016).

267. Deliu, E. *et al.* Haploinsufficiency of the intellectual disability gene SETD5 disturbs developmental gene expression and cognition. *Nat. Neurosci.* **21**, 1717–1727 (2018).

268. Sessa, A. *et al.* SETD5 Regulates Chromatin Methylation State and Preserves Global Transcriptional Fidelity during Brain Development and Neuronal Wiring. *Neuron* **104**, 271-289.e13 (2019).

269. Moore, S. M. *et al.* Setd5 haploinsufficiency alters neuronal network connectivity and leads to autistic-like behaviors in mice. *Transl. Psychiatry* **9**, 1–12 (2019).

270. Herz, H.-M., Garruss, A. & Shilatifard, A. SET for life: biochemical activities and biological functions of SET domain-containing proteins. *Trends Biochem. Sci.* **38**, 621–639 (2013).

271. Mas-y-Mas, S. *et al.* The Human Mixed Lineage Leukemia 5 (MLL5), a Sequentially and Structurally Divergent SET Domain-Containing Protein with No Intrinsic Catalytic Activity. (2016) doi:10.1371/journal.pone.0165139.

272. Li, M. *et al.* Frontiers | Structure, activity and function of the lysine methyltransferase SETD5. **14**, (2023).

273. Van Oss, S. B., Cucinotta, C. E. & Arndt, K. M. Emerging Insights into the Roles of the Paf1 Complex in Gene Regulation. *Trends Biochem. Sci.* **42**, 788–798 (2017).

274. Bhaskara, S. *et al.* Hdac3 is essential for the maintenance of chromatin structure and genome stability. *Cancer Cell* **18**, 436–447 (2010).

275. McQuown, S. C. *et al.* HDAC3 Is a Critical Negative Regulator of Long-Term Memory Formation. *J. Neurosci.* **31**, 764–774 (2011).

276. Brehme, M., Sverchkova, A. & Voisine, C. Proteostasis network deregulation signatures as biomarkers for pharmacological disease intervention. *Curr. Opin. Syst. Biol.* **15**, 74–81 (2019).
277. Narayan, P., Ehsani, S. & Lindquist, S. Combating neurodegenerative disease with chemical probes and model systems. *Nat. Chem. Biol.* **10**, 911–920 (2014).
278. Kasherman, M. A., Premarathne, S., Burne, T. H. J., Piper, M. & Wood, S. A. The Ubiquitin System : a Regulatory Hub for Intellectual Disability and Autism Spectrum Disorder. *Mol. Neurobiol.* (2020).
279. Wang, L. W., Berry-Kravis, E. & Hagerman, R. J. Fragile X: Leading the Way for Targeted Treatments in Autism. *Neurotherapeutics* **7**, 264–274 (2010).
280. Kelleher, R. J. & Bear, M. F. The Autistic Neuron: Troubled Translation? **135**, (2008).
281. Fyke, W. & Velinov, M. FMR1 and Autism, an Intriguing Connection Revisited. *Genes* **12**, 1218 (2021).
282. Brown, V. *et al.* Microarray Identification of FMRP-Associated Brain mRNAs and Altered mRNA Translational Profiles in Fragile X Syndrome. **107**, (2011).
283. Darnell, J. C. & Klann, E. The translation of translational control by FMRP: therapeutic targets for FXS. *Nat. Neurosci.* **16**, 1530–1536 (2013).
284. Darnell, J. C. *et al.* FMRP Stalls Ribosomal Translocation on mRNAs Linked to Synaptic Function and Autism. *Cell* **146**, 247–261 (2011).
285. Khatri, N. & Man, H. Y. The autism and Angelman syndrome protein Ube3A/E6AP: The gene, E3 ligase ubiquitination targets and neurobiological functions. *Front. Mol. Neurosci.* **12**, 1–12 (2019).
286. Rao, G., Croft, B., Teng, C. & Awasthi, V. Ubiquitin-Proteasome System in Neurodegenerative Disorders. *J. Drug Metab. Toxicol.* **6**, (2015).
287. Sowa, M. E., Bennett, E. J., Gygi, S. P. & Harper, J. W. Defining the Human Deubiquitinating Enzyme Interaction Landscape. *Cell* **138**, 389–403 (2009).
288. Hormaechea-Agulla, D., Kim, Y., Song, M. S. & Song, S. J. New insights into the role of E2s in the pathogenesis of diseases: Lessons learned from UBE2O. *Mol. Cells* **41**, 168–178 (2018).
289. Naujokat, C. & Šarić, T. Concise Review: Role and Function of the Ubiquitin-Proteasome System in Mammalian Stem and Progenitor Cells. *Stem Cells* **25**, 2408–2418 (2007).

290. Djagaeva, I. & Doronkin, S. COP9 Limits Dendritic Branching via Cullin3-Dependent Degradation of the Actin-Crosslinking BTB-Domain Protein Kelch. *PLoS ONE* **4**, (2009).
291. Kawabe, H. *et al.* Regulation of Rap2A by the Ubiquitin Ligase Nedd4-1 Controls Neurite Development. *Neuron* **65**, 358–372 (2010).
292. Ikeuchi, Y. *et al.* A SnoN-Ccd1 pathway promotes axonal morphogenesis in the mammalian brain. *J. Neurosci.* **29**, 4312–4321 (2009).
293. Lasorella, A. *et al.* Degradation of Id2 by the anaphase-promoting complex couples cell cycle exit and axonal growth. *Nature* **442**, 471–474 (2006).
294. Hamilton, A. M. & Zito, K. Breaking it down: the ubiquitin proteasome system in neuronal morphogenesis. *Neural Plast.* **2013**, 196848 (2013).
295. Vatsa, N. & Jana, N. R. UBE3A and its link with autism. *Front. Mol. Neurosci.* **11**, 1–8 (2018).
296. Dantuma, N. P. & Bott, L. C. The ubiquitin-proteasome system in neurodegenerative diseases: Precipitating factor, yet part of the solution. *Front. Mol. Neurosci.* **7**, 1–18 (2014).
297. Neri, G., Schwartz, C. E., Lubs, H. A. & Stevenson, R. E. X-linked intellectual disability update 2017. *Am. J. Med. Genet. A.* **176**, 1375–1388 (2018).
298. Sell, G. L. & Margolis, S. S. From UBE3A to Angelman syndrome: A substrate perspective. *Front. Neurosci.* **9**, 1–6 (2015).
299. Smith, S. E. P. *et al.* Increased Gene Dosage of Ube3a Results in Autism Traits and Decreased Glutamate Synaptic Transmission in Mice. *Sci. Transl. Med.* **3**, (2011).
300. Elgersma, Y. & Sonzogni, M. UBE3A reinstatement as a disease-modifying therapy for Angelman syndrome. *Dev. Med. Child Neurol.* **63**, 802–807 (2021).
301. Rotaru, D. C., Mientjes, E. J. & Elgersma, Y. Angelman Syndrome: From Mouse Models to Therapy. *Neuroscience* **445**, 172–189 (2020).
302. O'Geen, H. *et al.* Transcriptional reprogramming restores UBE3A brain-wide and rescues behavioral phenotypes in an Angelman syndrome mouse model. *Mol. Ther.* **31**, 1088–1105 (2023).
303. Meng, L. *et al.* Towards a therapy for Angelman syndrome by targeting a long non-coding RNA. *Nature* **518**, 409–412 (2015).
304. Wolter, J. M. *et al.* Cas9 gene therapy for Angelman syndrome traps Ube3a-ATS long non-coding RNA. *Nature* **587**, 281–284 (2020).

305. Silva-Santos, S. *et al.* Ube3a reinstatement identifies distinct developmental windows in a murine Angelman syndrome model. *J. Clin. Invest.* **125**, 2069–2076 (2015).
306. Zhang, J. *et al.* Haploinsufficiency of the E3 ubiquitin-protein ligase gene TRIP12 causes intellectual disability with or without autism spectrum disorders, speech delay, and dysmorphic features. *Hum. Genet.* **136**, 377–386 (2017).
307. Bramswig, N. C. *et al.* Identification of new TRIP12 variants and detailed clinical evaluation of individuals with non-syndromic intellectual disability with or without autism. *Hum. Genet.* **136**, 179–192 (2017).
308. Kajiro, M. *et al.* The E3 ubiquitin ligase activity of Trip12 is essential for mouse embryogenesis. *PLoS ONE* **6**, 6–13 (2011).
309. Sluimer, J. & Distel, B. Regulating the human HECT E3 ligases. *Cell. Mol. Life Sci.* **75**, 3121–3141 (2018).
310. Genschik, P., Sumara, I. & Lechner, E. The emerging family of CULLIN3-RING ubiquitin ligases (CRL3s): cellular functions and disease implications. *EMBO J.* **32**, 2307–2320 (2013).
311. Liu, X. *et al.* Trip12 is an E3 ubiquitin ligase for USP7/HAUSP involved in the DNA damage response. *FEBS Lett.* **590**, 4213–4222 (2016).
312. Georges, A., Marcon, E., Greenblatt, J. & Frappier, L. Identification and Characterization of USP7 Targets in Cancer Cells. *Sci. Rep.* **8**, 1–12 (2018).
313. Morandell, J. *et al.* Cul3 regulates cytoskeleton protein homeostasis and cell migration during a critical window of brain development. *Nat. Commun.* **12**, (2021).
314. Amar, M. *et al.* Autism-linked Cullin3 germline haploinsufficiency impacts cytoskeletal dynamics and cortical neurogenesis through RhoA signaling. *Mol. Psychiatry* (2021) doi:10.1038/s41380-021-01052-x.
315. Rapanelli, M. *et al.* Behavioral , circuitry , and molecular aberrations by region-speci fi c de fi ciency of the high-risk autism gene Cul3. *Mol. Psychiatry* (2019) doi:10.1038/s41380-019-0498-x.
316. Lin, P. *et al.* Current trends of high-risk gene Cul3 in neurodevelopmental disorders. *Front. Psychiatry* **14**, 1215110 (2023).
317. Velmeshev, D. *et al.* Single-cell genomics identifies cell type–specific molecular changes in autism. *Science* **364**, 685–689 (2019).

318. Yap, C. X. *et al.* Brain cell-type shifts in Alzheimer's disease, autism, and schizophrenia interrogated using methylomics and genetics. *Sci. Adv.* **10**, eadn7655 (2024).

319. Gandal, M. J. *et al.* Transcriptome-wide isoform-level dysregulation in ASD, schizophrenia, and bipolar disorder. *Science* **362**, eaat8127 (2018).

320. Li, M. *et al.* Integrative functional genomic analysis of human brain development and neuropsychiatric risks. *Science* **362**, eaat7615 (2018).

321. Dixit, A. *et al.* Perturb-Seq: Dissecting Molecular Circuits with Scalable Single-Cell RNA Profiling of Pooled Genetic Screens. doi:10.1016/j.cell.2016.11.038.

322. Li, C. *et al.* Single-cell brain organoid screening identifies developmental defects in autism. *Nature* **621**, 373–380 (2023).

323. Shen, W., Krautscheid, P., Rutz, A. M., Bayrak-Toydemir, P. & Dugan, S. L. *De novo* loss-of-function variants of *ASH1L* are associated with an emergent neurodevelopmental disorder. *Eur. J. Med. Genet.* **62**, 55–60 (2019).

324. Stolerman, E. S. *et al.* Genetic variants in the KDM6B gene are associated with neurodevelopmental delays and dysmorphic features. *Am. J. Med. Genet. A.* **179**, 1276–1286 (2019).

325. Faundes, V. *et al.* Histone Lysine Methylases and Demethylases in the Landscape of Human Developmental Disorders. doi:10.1016/j.ajhg.2017.11.013.

326. Hao, Y.-H. *et al.* USP7 acts as a molecular rheostat to promote WASH-dependent endosomal protein recycling and is mutated in a human neurodevelopmental disorder. *Mol. Cell* (2015) doi:10.1016/j.molcel.2015.07.033.

327. Fountain, M. D. *et al.* Pathogenic variants in USP7 cause a neurodevelopmental disorder with speech delays, altered behavior, and neurologic anomalies.

328. DeSanto, C. *et al.* WAC loss-of-function mutations cause a recognisable syndrome characterised by dysmorphic features, developmental delay and hypotonia and recapitulate 10p11.23 microdeletion syndrome. (2015) doi:10.1136/jmedgenet-2015-103069.

329. Novarino, G. *et al.* Mutations in BCKD-kinase Lead to a Potentially Treatable Form of Autism with Epilepsy. *Science* **338**, 394–397 (2012).

330. García-Cazorla, A. *et al.* Two Novel Mutations in the (Branched-Chain Keto-Acid Dehydrogenase Kinase) Gene Are Responsible for a Neurobehavioral Deficit in Two Pediatric Unrelated Patients. *Hum. Mutat.* **35**, 470–477 (2014).

331. Noor, A. *et al.* Disruption at the PTCHD1 Locus on Xp22.11 in Autism Spectrum Disorder and Intellectual Disability. *Sci. Transl. Med.* **2**, 49ra68-49ra68 (2010).
332. Chaudhry, A. *et al.* Phenotypic spectrum associated with PTCHD1 deletions and truncating mutations includes intellectual disability and autism spectrum disorder. *Clin. Genet.* **88**, 224–233 (2015).
333. McGinnis, C. S. *et al.* MULTI-seq: sample multiplexing for single-cell RNA sequencing using lipid-tagged indices. *Nat. Methods* **16**, 619–626 (2019).
334. Di Bella, D. J. *et al.* Molecular logic of cellular diversification in the mouse cerebral cortex. *Nature* **595**, 554–559 (2021).
335. Yao, Z. *et al.* A taxonomy of transcriptomic cell types across the isocortex and hippocampal formation. *Cell* **184**, 3222-3241.e26 (2021).
336. Loo, L. *et al.* Single-cell transcriptomic analysis of mouse neocortical development. *Nat. Commun.* **10**, 134 (2019).
337. Ma, S. *et al.* Chromatin Potential Identified by Shared Single-Cell Profiling of RNA and Chromatin. *Cell* **183**, 1103-1116.e20 (2020).
338. Li, Y. *et al.* Spliceosome-regulated RSRP1-dependent NF-κB activation promotes the glioblastoma mesenchymal phenotype. *Neuro-Oncol.* **23**, 1693–1708 (2021).
339. Chen, C.-Y. *et al. Galnt17* loss-of-function leads to developmental delay and abnormal coordination, activity, and social interactions with cerebellar vermis pathology. *Dev. Biol.* **490**, 155–171 (2022).
340. Cardo, L. F., de la Fuente, D. C. & Li, M. Impaired neurogenesis and neural progenitor fate choice in a human stem cell model of SETBP1 disorder. *Mol. Autism* **14**, 8 (2023).
341. Kurolap, A. *et al.* Bi-allelic variants in neuronal cell adhesion molecule cause a neurodevelopmental disorder characterized by developmental delay, hypotonia, neuropathy/spasticity. doi:10.1016/j.ajhg.2022.01.004.
342. Keays, D. A. *et al.* Mutations in α-Tubulin Cause Abnormal Neuronal Migration in Mice and Lissencephaly in Humans.
343. Zocchi, R., Compagnucci, C., Bertini, E. & Sferra, A. Deciphering the Tubulin Language: Molecular Determinants and Readout Mechanisms of the Tubulin Code in Neurons. *Int. J. Mol. Sci.* **24**, 2781 (2023).
344. Rubenstein, J. L. R. & Merzenich, M. M. Model of autism: increased ratio of excitation/inhibition in key neural systems. *Genes Brain Behav.* **2**, 255–267 (2003).

345. Oliveira, B., Mitjans, M., Nitsche, M. A., Kuo, M.-F. & Ehrenreich, H. Excitation-inhibition dysbalance as predictor of autistic phenotypes. *J. Psychiatr. Res.* **104**, 96–99 (2018).

346. Howell, B. W. & Smith, K. M. Synaptic structural protein dysfunction leads to altered excitation inhibition ratios in models of autism spectrum disorder. *Pharmacol. Res.* **139**, 207–214 (2019).

347. Sohal, V. S. & Rubenstein, J. L. R. Excitation-inhibition balance as a framework for investigating mechanisms in neuropsychiatric disorders. *Mol. Psychiatry* **24**, 1248–1257 (2019).

348. Catterall, W. A. Dravet Syndrome: A Sodium Channel Interneuronopathy. *Curr. Opin. Physiol.* **2**, 42–50 (2018).

349. Singh, N. A. *et al.* A Role of SCN9A in Human Epilepsies, As a Cause of Febrile Seizures and As a Potential Modifier of Dravet Syndrome. *PLoS Genet.* **5**, e1000649 (2009).

350. Guerrini, R. *et al.* Variable epilepsy phenotypes associated with a familial intragenic deletion of the SCN1A gene. *Epilepsia* **51**, 2474–2477 (2010).

351. Charlier, C. *et al.* A pore mutation in a novel KQT-like potassium channel gene in an idiopathic epilepsy family. *Nat. Genet.* **18**, 53–55 (1998).

352. Miceli, F. *et al.* A novel KCNQ3 mutation in familial epilepsy with focal seizures and intellectual disability. *Epilepsia* **56**, e15–e20 (2015).

353. Fister, P., Soltirovska-Salamon, A., Debeljak, M. & Paro-Panjan, D. Benign familial neonatal convulsions caused by mutation in KCNQ3, exon 6: A European case.

354. Park, Y., Yoon, S. K. & Yoon, J.-B. TRIP12 functions as an E3 ubiquitin ligase of APP-BP1. *Biochem. Biophys. Res. Commun.* **374**, 294–298 (2008).

355. Biswas, D. *et al.* Inhibiting BCKDK in triple negative breast cancer suppresses protein translation, impairs mitochondrial function, and potentiates doxorubicin cytotoxicity. *Cell Death Discov.* **7**, 1–12 (2021).

356. Kumar, R. *et al.* Homozygous mutation of STXBP5L explains an autosomal recessive infantile-onset neurodegenerative disorder. *Hum. Mol. Genet.* **24**, 2000–2010 (2015).

357. Mastropasqua, F. *et al.* Deficiency of the Heterogeneous Nuclear Ribonucleoprotein U locus leads to delayed hindbrain neurogenesis. *Biol. Open* **12**, bio060113 (2023).

358. Caracci, M. O. *et al.* Frontiers | Wnt/β-Catenin-Dependent Transcription in Autism Spectrum Disorders. doi:10.3389/fnmol.2021.764756.

359. Kalkman, H. O. A review of the evidence for the canonical Wnt pathway in autism spectrum disorders. *Mol. Autism* **3**, 10 (2012).

360. Gulati, G. S. *et al.* Single-cell transcriptional diversity is a hallmark of developmental potential. *Science* **367**, 405–411 (2020).

361. Meléndez-Ramírez, C. *et al.* Dynamic landscape of chromatin accessibility and transcriptomic changes during differentiation of human embryonic stem cells into dopaminergic neurons. *Sci. Rep.* **11**, 16977 (2021).

362. Bond, A. M., Bhalala, O. G. & Kessler, J. A. The dynamic role of bone morphogenetic proteins in neural stem cell fate and maturation. *Dev. Neurobiol.* **72**, 1068–1084 (2012).

363. Segklia, A. *et al.* Bmp7 Regulates the Survival, Proliferation, and Neurogenic Properties of Neural Progenitor Cells during Corticogenesis in the Mouse. doi:10.1371/journal.pone.0034088.

364. Qin, S. & Zhang, C.-L. Role of Krüppel-Like Factor 4 in Neurogenesis and Radial Neuronal Migration in the Developing Cerebral Cortex. *Mol. Cell. Biol.* **32**, 4297–4305 (2012).

365. Luo, Z. *et al.* Zic2 Is an Enhancer-Binding Factor Required for Embryonic Stem Cell Specification. doi:10.1016/j.molcel.2015.01.007.

366. Hong, W. *et al.* Krüppel-like factor 7 deficiency disrupts corpus callosum development and neuronal migration in the developing mouse cerebral cortex. *Brain Pathol.* **33**, e13186 (2023).

367. Inoue, T., Ota, M., Ogawa, M., Mikoshiba, K. & Aruga, J. Zic1 and Zic3 Regulate Medial Forebrain Development through Expansion of Neuronal Progenitors. *J. Neurosci.* **27**, 5461–5473 (2007).

368. Johnson, C. A. & Ghashghaei, H. T. Sp2 regulates late neurogenic but not early expansive divisions of neural stem cells underlying population growth in the mouse cortex. *Development* **147**, dev186056 (2020).

369. Zhang, Y. *et al.* Genetic evidence of gender difference in autism spectrum disorder supports the female-protective effect. *Transl. Psychiatry* **10**, 1–10 (2020).

370. Ojanen, S. *et al.* Interneuronal GluK1 kainate receptors control maturation of GABAergic transmission and network synchrony in the hippocampus. *Mol. Brain* **16**, 43 (2023).

371. Kissel, L. T. & Werling, D. M. Neural Transcriptomic Analysis of Sex Differences in Autism Spectrum Disorder: Current Insights and Future Directions. *Biol. Psychiatry* **91**, 53–60 (2022).
372. Hsu, M., Dedhia, M., Crusio, W. E. & Delprato, A. Sex differences in gene expression patterns associated with the *APOE4* allele. Preprint at https://doi.org/10.12688/f1000research.18671.2 (2019).
373. Altmann, A., Tian, L., Henderson, V. W., Greicius, M. D. & Investigators, A. D. N. I. Sex modifies the APOE-related risk of developing Alzheimer disease. *Ann. Neurol.* **75**, 563–573 (2014).
374. Holland, D., Desikan, R. S., Dale, A. M. & McEvoy, L. K. Higher Rates of Decline for Women and Apolipoprotein E ε4 Carriers. *AJNR Am. J. Neuroradiol.* **34**, 2287–2293 (2013).
375. Marko, M. K. *et al.* Behavioural and neural basis of anomalous motor learning in children with autism. *Brain* **138**, 784–797 (2015).
376. Mosconi, M. W., Wang, Z., Schmitt, L. M., Tsai, P. & Sweeney, J. A. Frontiers | The role of cerebellar circuitry alterations in the pathophysiology of autism spectrum disorders. doi:10.3389/fnins.2015.00296.
377. Sarropoulos, I. *et al.* Developmental and evolutionary dynamics of cis-regulatory elements in mouse cerebellar cells. *Science* **373**, eabg4696 (2021).
378. Wamsley, B. *et al.* Molecular cascades and cell type–specific signatures in ASD revealed by single-cell genomics. *Science* **384**, eadh2602 (2024).
379. Willsey, A. J. *et al.* Coexpression Networks Implicate Human Midfetal Deep Cortical Projection Neurons in the Pathogenesis of Autism. doi:10.1016/j.cell.2013.10.020.
380. Geschwind, D. H. & State, M. W. Gene hunting in autism spectrum disorder: on the path to precision medicine. *Lancet Neurol.* **14**, 1109–1120 (2015).
381. Koppensteiner, P. *et al.* Age-dependent sensitivity to glucocorticoids in the developing mouse basolateral nucleus of the amygdala. *Psychoneuroendocrinology* **46**, 64–77 (2014).
382. Kanai, Y., Dohmae, N. & Hirokawa, N. Kinesin Transports RNA: Isolation and Characterization of an RNA-Transporting Granule. *Neuron* **43**, 513–525 (2004).
383. Parikshak, N. N. *et al.* Genome-wide changes in lncRNA, splicing, and regional gene expression patterns in autism. *Nature* **540**, 423–427 (2016).

384. Carter, R. A. *et al.* A Single-Cell Transcriptional Atlas of the Developing Murine Cerebellum. *Curr. Biol. CB* **28**, 2910-2920.e2 (2018).

385. Xia, Y. *et al.* Transcriptomic sex differences in postmortem brain samples from patients with psychiatric disorders. *Sci. Transl. Med.* **16**, eadh9974 (2024).

386. Sauteraud, R. *et al.* Inferring genes that escape X-Chromosome inactivation reveals important contribution of variable escape genes to sex-biased diseases. *Genome Res.* **31**, 1629–1637 (2021).

387. Wainer Katsir, K. & Linial, M. Human genes escaping X-inactivation revealed by single cell expression data. *BMC Genomics* **20**, 201 (2019).

388. Garieri, M. *et al.* Extensive cellular heterogeneity of X inactivation revealed by single-cell allele-specific expression in human fibroblasts. *Proc. Natl. Acad. Sci.* **115**, 13015–13020 (2018).

389. Marks, H. *et al.* Dynamics of gene silencing during X inactivation using allele-specific RNA-seq. *Genome Biol.* **16**, 149 (2015).

390. Pajerowski, A. G., Nguyen, C., Aghajanian, H., Shapiro, M. J. & Shapiro, V. S. NKAP Is a Transcriptional Repressor of Notch Signaling and Is Required for T Cell Development.

391. Mattson, M. P. & Meffert, M. K. Roles for NF-κB in nerve cell survival, plasticity, and disease. *Cell Death Differ.* **13**, 852–860 (2006).

392. Carlén, M. *et al.* Forebrain ependymal cells are Notch-dependent and generate neuroblasts and astrocytes after stroke. *Nat. Neurosci.* **12**, 259–267 (2009).

393. Gutierrez, H. & Davies, A. M. Regulation of neural process growth, elaboration and structural plasticity by NF-κB.

394. Yoon, K. & Gaiano, N. Notch signaling in the mammalian central nervous system: insights from mouse mutants. *Nat. Neurosci.* **8**, 709–715 (2005).

395. Lathia, J. D., Mattson, M. P. & Cheng, A. Notch: from neural development to neurological disorders. *J. Neurochem.* **107**, 1471–1481 (2008).

396. Fiordaliso, S. K. *et al.* Missense Mutations in NKAP Cause a Disorder of Transcriptional Regulation Characterized by Marfanoid Habitus and Cognitive Impairment. doi:10.1016/j.ajhg.2019.09.009.

397. Nilsson, S. *et al.* Mechanisms of Estrogen Action. *Physiol. Rev.* **81**, 1535–1565 (2001).

398. DeCasien, A. R. *et al.* Evolutionary and biomedical implications of sex differences in the primate brain transcriptome. doi:10.1016/j.xgen.2024.100589.

399. Remy, S. *et al.* Generation of gene-edited rats by delivery of CRISPR/Cas9 protein and donor DNA into intact zygotes using electroporation. *Sci. Rep.* **7**, 16554 (2017).
400. Krausgruber, T. *et al.* Single-cell and spatial transcriptomics reveal aberrant lymphoid developmental programs driving granuloma formation. doi:10.1016/j.immuni.2023.01.014.
401. Hao, Y. *et al.* Integrated analysis of multimodal single-cell data. *Cell* **184**, 3573-3587.e29 (2021).
402. Stuart, T., Srivastava, A., Madad, S., Lareau, C. & Satija, R. Single-cell chromatin state analysis with Signac. *Nat. Methods* (2021) doi:10.1038/s41592-021-01282-5.
403. Landau, W. M. The targets R package: a dynamic Make-like function-oriented pipeline toolkit for reproducibility and high-performance computing. *J. Open Source Softw.* **6**, 2959 (2021).
404. Germain, P.-L., Lun, A., Macnair, W. & Robinson, M. D. Doublet identification in single-cell sequencing data using scDblFinder. *f1000research* (2021) doi:10.12688/f1000research.73600.1.
405. McCarthy, D. J., Campbell, K. R., Lun, A. T. L. & Willis, Q. F. Scater: pre-processing, quality control, normalisation and visualisation of single-cell RNA-seq data in R. *Bioinformatics* **33**, 1179–1186 (2017).
406. Hafemeister, C. & Satija, R. Normalization and variance stabilization of single-cell RNA-seq data using regularized negative binomial regression. *Genome Biol.* **20**, 296 (2019).
407. Choudhary, S. & Satija, R. Comparison and evaluation of statistical error models for scRNA-seq. *Genome Biol.* **23**, 27 (2022).
408. Büttner, M., Ostner, J., Müller, C. L., Theis, F. J. & Schubert, B. scCODA is a Bayesian model for compositional single-cell data analysis. *Nat. Commun.* **12**, 6876 (2021).
409. Robinson, M. D., McCarthy, D. J. & Smyth, G. K. edgeR: a Bioconductor package for differential expression analysis of digital gene expression data. *Bioinformatics* **26**, 139–140 (2010).
410. Korsunsky, I. *et al.* Fast, sensitive and accurate integration of single-cell data with Harmony. *Nat. Methods* **16**, 1289–1296 (2019).

411. Setty, M. *et al.* Characterization of cell fate probabilities in single-cell data with Palantir. *Nat. Biotechnol.* **37**, 451–460 (2019).

412. Mao, Q., Yang, L., Wang, L., Goodison, S. & Sun, Y. SimplePPT: A Simple Principal Tree Algorithm. in *Proceedings of the 2015 SIAM International Conference on Data Mining (SDM)* 792–800 (Society for Industrial and Applied Mathematics, 2015). doi:10.1137/1.9781611974010.89.

413. Soldatov, R. *et al.* Spatiotemporal structure of cell fate decisions in murine neural crest. *Science* **364**, eaas9536 (2019).

414. Faure, L., Soldatov, R., Kharchenko, P. V. & Adameyko, I. scFates: a scalable python package for advanced pseudotime and bifurcation analysis from single-cell data. *Bioinformatics* **39**, btac746 (2023).

415. Love, M. I., Huber, W. & Anders, S. Moderated estimation of fold change and dispersion for RNA-seq data with DESeq2. *Genome Biol.* **15**, 550 (2014).

416. Yu, G., Wang, L.-G., Han, Y. & He, Q.-Y. clusterProfiler: an R Package for Comparing Biological Themes Among Gene Clusters. *OMICS J. Integr. Biol.* **16**, 284–287 (2012).

417. Merico, D., Isserlin, R., Stueker, O., Emili, A. & Bader, G. D. Enrichment Map: A Network-Based Method for Gene-Set Enrichment Visualization and Interpretation. doi:10.1371/journal.pone.0013984.

418. Supek, F., Bošnjak, M., Škunca, N. & Šmuc, T. REVIGO Summarizes and Visualizes Long Lists of Gene Ontology Terms. doi:10.1371/journal.pone.0021800.

419. Gu, Z., Gu, L., Eils, R., Schlesner, M. & Brors, B. circlize implements and enhances circular visualization in R. *Bioinformatics* **30**, 2811–2812 (2014).

420. Koopmans, F. *et al.* SynGO: An Evidence-Based, Expert-Curated Knowledge Base for the Synapse. doi:10.1016/j.neuron.2019.05.002.

421. Heumos, L. *et al.* Best practices for single-cell analysis across modalities. *Nat. Rev. Genet.* **24**, 550–572 (2023).

422. Martin, M. Cutadapt removes adapter sequences from high-throughput sequencing reads. *EMBnet.journal* **17**, 10–12 (2011).

423. Dobin, A. *et al.* STAR: ultrafast universal RNA-seq aligner. *Bioinformatics* **29**, 15–21 (2013).

424. Yuan, W. *et al.* Temporally divergent regulatory mechanisms govern neuronal diversification and maturation in the mouse and marmoset neocortex. *Nat. Neurosci.* **25**, 1049–1058 (2022).